Novel Strategies in Cocaine Esterase Modification for Treatment of Cocaine Intoxication

by

Tien-Yi Lee

A dissertation submitted in partial fulfillment
of the requirements for the degree of
Doctor of Philosophy
(Pharmaceutical Sciences)
in The University of Michigan
2011

Doctoral Committee:

Professor Victor Chi-Min Yang, Chair
Professor David E. Smith
Associate Professor George A. Garcia
Associate Professor Gustavo Rosania

Acknowledgement

I would like to thank my advisor, Dr. Victor Yang, for all the support and opportunities he provided. He made me want to be better, tougher, and more independent, both intellectually and personally.

I would also like to thank all the members of my dissertation committee, Dr. George Garcia, Dr. Gus Rosania, and Dr. David Smith, for their valuable time, suggestions, and support. I especially thank Dr. Garcia for graciously providing guidance and the reagents crucial for the breakthrough in my recombinant work. In addition, I would like to thank Dr. Rosania for his honest and unbiased input into my research, and generously letting me use the fluorescence microscope in his laboratory. I also want to thank Dr. Smith for lighting my way when I had difficulties during my graduate studies.

I would like to acknowledge early input on my work from Dr. Woods and Dr. Sunaraha. In addition, I would like to express my gratitude to those who have collaborated with me to enhance the strength of my research, especially Dr. M.C. Holden Ko for his support and friendship. I also wish to extend my thanks to Dr. Chris Feak for graciously providing feedback and suggestions on my dissertation.

I wish to acknowledge all the members of the Yang lab, past and present, especially Dr. Allan David, Dr. Yoon Shin Park, Dr. Jun-Beom Park, Dr. Hee Sun Chung, Dr. Yongzhuo Huang, Dr. Cheol Moon, Meong Cheol Shin, and Lindsay White. Thanks for their help and suggestions on the work pertinent to my research, as well as making the lab a friendly environment.

I also received many help from friends, peer students, and alumni of the College of Pharmacy. I would especially like to thank Dr. Xinyuan Zhang, Dr. Haili Ping, Dr. Pei-Hua Yang, Jason Baik, Kyoung-Ah Min, Yi-Chen Chen, Suman Gill, and Dr. Hsien-Chang Lin, for their friendship and support. In addition, I would also like to acknowledge the NIH grant R01DA021416, as well as the College of Pharmacy (Schering-Plough and Lilly Endowment Fellowship), for the partial financial support of my research.

I cannot overstate my appreciation of my parents, Hsian-Fu Lee and Su-Chen Cheng, as well as my brother Chieh-Yu Lee, for their never-ending encouragement. They support me, love me, and always believe that I could accomplish anything.

Lastly, and most importantly, I am ever grateful for my husband Dr. Galen Chen for all his companionship, love, and support, for giving me the strength to complete my degree, and for all the little things he does to make my life better in numerous ways. I learned from him the ways and attitude of being honest, brave, and having a high EQ. I would not be here today without him. He means everything to me.

Table of Contents

List of Figures

List of Tables

List of Abbreviations

ANOVA	Analysis of variance
BBB	Blood-brain barrier
BchE	Serum butyryl-cholinesterase
CPP	Cell penetrating peptides
CNS	Central nervous system
CocE	Bacterial cocaine esterase
DMCocE	CocE-T172R/G172Q
DIC	Differential interference contrast
DMSO	Dimethyl sulfoxide
DTT	Dithiothreitol
ELISA	Enzyme-linked immunosorbent assay
FPLC	Fast protein liquid chromatography
FBS	Fetal bovine serum
FITC	Fluorescein isothiocyanate
HBSS	Hank's balanced salt solution
hCE	Liver carboxylesterase
IPTG	Isopropyl-β-thiogalactopyranoside
hCE-1	Liver carboxylesterase-1
hCE-2	Liver carboxylesterase-2
LMWP	Low molecular weight protamine
MALDI-TOF MS	Matrix-Assisted Laser Desorption/Ionization-Time-Of-Flight Mass Spectra
MEM-α	Minimum essential medium α
MRT	Mean residence time
PEG	Polyethylene glycol

PCR	Polymerase chain reaction
P2T	Pyridine-2-thione
RBC	Red blood cells
SCID	Severe combined immunodeficiency
SDS-PAGE	Sodium dodecyl sulfate-polyacrylamide gel electrophoresis
SPDP	N-succinimidyl 3-(2-pyridyldithio)-propionate
$t_{1/2}$	Half-life

Abstract

Cocaine esterase (CocE) is the most efficient cocaine-metabolizing enzyme tested *in vivo* to date, displaying a rapid clearance of cocaine and a robust protection against cocaine's toxicity. A major obstacle to the clinical application of CocE, however, lies in its short *in vivo* half-life, proteolytic degradation, and induced immune response. To overcome these issues, PEGylation and cell encapsulation are employed in this dissertation study to modify CocE. These two strategies are designed to protect CocE from deactivation by circulating proteases and the host immune system, and therefore prolonging its *in vivo* half-life and reducing its immunogenicity.

PEGylation of CocE was successfully carried out and characterized. The PEG-CocE conjugates prepared in this study showed a purity of greater than 93.5%. As demonstrated by the enzyme-linked immunosorbent assay (ELISA), attachment of PEG to CocE apparently inhibited the binding of anti-CocE antibodies to the PEG-CocE conjugate. In addition, PEGylation yielded protection to CocE against thermal degradation and protease digestion. Preliminary *in vivo* results suggested that, similarly to native CocE, the PEG-CocE conjugates were also able to protect animals from cocaine-induced lethality.

Cell encapsulation of CocE was accomplished by creating a cell permeable form of CocE. Two cell penetrating peptides (CPPs), Tat and LMWP, were covalently linked to CocE, generating two chemical conjugates and four recombinant fusion proteins. The six CPP-CocE variants possessed a varied extent of cocaine hydrolyzing activity and cell permeability. The cellular uptake of CPP-CocE variants observed in HeLa cells, RBC, and nasal epithelial cells were found to be dependent upon incubation time and concentration. Moreover, the nasal epithelial cells transduced with CPP-DMCocEs

retained the ability to hydrolyze cocaine, indicating preservation of the enzymatic activity of the cell-encapsulated CPP-DMCocE variants.

In conclusion, the present studies suggest that PEGylation may prolong CocE's functionality in the circulation and reduce its potential immunogenicity. They also demonstrate that attachment of CPP groups enables CocE to become cell permeable and meanwhile maintains CocE's enzymatic activity. These strategies would not be valuable for potential clinical application of CocE, but also for other protein therapeutics with problems of *in vivo* stability and immunogenicity.

CHAPTER 1
Introduction and Specific Aims

1.1 Cocaine Intoxication

Cocaine is one of the most addictive and commonly abused illicit drugs in the United States. In 2009, estimated 5.3 million people in the United States had used cocaine in the past year, and 1.1 million of them were cocaine dependent (1, 2). In addition to its widespread prevalence and potential for addiction, cocaine is also a highly toxic substance that can be lethal. Cocaine may cause seizures, convulsions, aorta rupture, myocardial infarction, and sudden death (3-5). According to recent estimates, cocaine was involved in about 555,530 visits to hospital emergency departments in 2007; in half of these visits, patients needed immediate detoxification or treatment services (6). Given the extent of cocaine abuse and life-threating complications of cocaine toxicity, cocaine use has become a critical public health issue in the United States, pointing to the urgent need for effective treatments to combat cocaine abuse. Unfortunately, current treatments for cocaine toxicity still remain symptom-based; an effective pharmacotherapy to neutralize cocaine's toxic effects is still unavailable (7).

An alternative solution for treating cocaine toxicity is to accelerate cocaine metabolism, which can be accomplished by the administration of cocaine-hydrolyzing enzymes (8). These enzymes can break down cocaine in the circulation, so cocaine concentration at the sites of action, mainly in the central nervous system (CNS) and the cardiovascular system, will be insufficient to initiate pharmacological effects. Several cocaine-hydrolyzing enzymes, including a recently discovered bacterial cocaine esterase (CocE), have been shown successful in reducing cocaine concentration in circulation, as well as reversing cocaine's neurological and cardiovascular toxicity (9, 10).

1.2 Bacterial Cocaine Esterase (CocE)

CocE was found in 2000 from a bacterial strain *Rhidococcus* sp. MB1, which grows in the rhizosphere soil of the cocaine-producing plant *Erythroxylon coca* (11). The gene sequence and crystal structure of CocE have been well studied by several research groups (11-13). CocE is a globular 574 amino-acid monomeric esterase with molecular weight of ~ 65 kDa. It consists of three domains: DOM1, DOM2, and DOM3 (Figure 1). DOM1 contains the catalytic triad of Serine (S) 117, Aspartate (D) 257, and Histidine (H) 287 in the canonical α/β hydrolase fold. The catalytic triad composed of S-D-H residues is a hallmark shared by all esterases, and essential for the cocaine-hydrolyzing activity. DOM2 is an α-helical structure inserted into the two linear sequence segments of DOM1. DOM3 is a very large jelly-roll-like β structure that interacts intensively with the other two domains and appears to govern the arrangement of the overall tertiary structure. All three of these domains contribute to the active site pocket, which is located in a cleft formed at the interface of all three domains. N- and C- termini of CocE are exposed outside the enzyme surface, which is an advantage for enzyme modification by means of biological recombination.

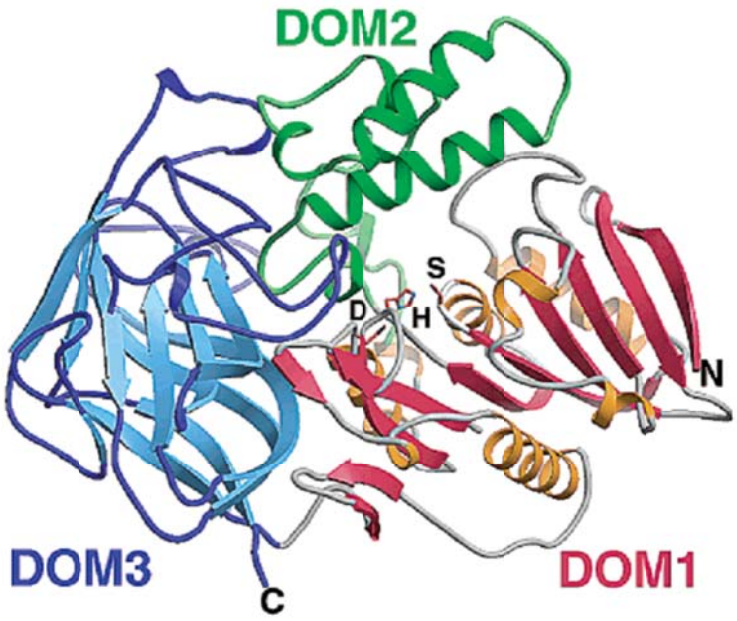

Figure 1 Ribbon diagram of CocE structure.

Compared to other naturally-occurring cocaine-hydrolyzing enzymes, *i.e.* serum butyryl-cholinesterase (BchE) and liver carboxylesterases (hCEs) (14) in mammals, CocE is more efficient and specific for cocaine metabolism. According to the specificity constant ($\frac{k_{cat}}{K_M}$), which represents the maximal possible rate of an enzyme converting a substrate (see Section 3.2.3 for detailed information), CocE hydrolyzes cocaine at least 800-fold faster than other native cocaine-hydrolyzing enzymes (Table 1). Moreover, unlike the other native cocaine-hydrolyzing enzymes, which accept a broad range of substrates besides cocaine (15, 16), CocE only hydrolyzes cocaine and cocaethylene, a toxic metabolite from cocaine and alcohol co-administration (13). Therefore, for cocaine overdose treatment, the administration of exogenous CocE would only metabolize cocaine, but not degrade any endogenous molecules in the circulation.

Table 1 Kinetics of natural-occurring enzymes involving cocaine hydrolysis.

Enzyme	k_{cat} (min^{-1})	K_M (μM)	k_{cat}/K_M ($sec^{-1}M^{-1}$)	Reference
BchE	4.1	4.5	1.5×10^4	(16)
hCE-1	0.06	120	8.3	(15)
hCE-2	7.2	390	3.1×10^2	(15)
CocE	468	0.64	1.2×10^7	(13)

In addition to its relative proficiency compared to other native cocaine-hydrolyzing enzymes, the kinetic profiles of CocE are also suitable for rapid cocaine elimination. According to the criteria suggested by Landry *et al.*, to prevent a significant amount of cocaine from entering the CNS, a cocaine-hydrolyzing enzyme for overdose treatment should have a $k_{cat} > 120$ min^{-1} and a $K_M < 30$ μM (17). Since the kinetic parameters of CocE ($k_{cat} = 468$ min^{-1}, $K_M = 0.64$ μM) meet these criteria, CocE should be sufficient for a rapid detoxification in cocaine overdose patients. In addition to its high efficiency for hydrolyzing cocaine, CocE does not generate any metabolites with side effects. CocE hydrolyzes cocaine to ecgonine methyl ester and benzoic acid (13); these two metabolites are physiologically inert and can be excreted directly in urine (14).

Because of its advantages over other native cocaine-hydrolyzing enzymes, CocE has been extensively investigated for its ability to counteract cocaine's toxic effects. Research on animal models has shown that CocE significantly reduced the plasma cocaine concentration, as well as the lethality, at high cocaine doses (10, 18-20). It also has showed a robust protection against cocaine toxicity to the CNS and cardiovascular system. However, in spite of encouraging results in animals, there are still two major obstacles to the clinical applications of CocE in humans, and only one of which has been successfully solved.

1.3 Major Obstacles to the Clinical Applications of CocE

The first drawback of CocE is thermal stability. Native CocE is extremely unstable and rapidly deactivated at physiological temperature; its *in vitro* half-life at 37 °C is only ~13.7 min (10). To improve its thermal stability, two mutants of CocE (CocE-T172R/G173Q and CocE-L169K) have been developed through a computational structure analysis, which was designed to stabilize CocE by increasing the buried enzyme surface area (21, 22). The mutations on T172R/G173Q and L169K extended the *in vitro* half-life to ~4.5 hours and ~2.9 days, respectively, representing a ~20-fold and ~300-fold improvement over native CocE.

The remaining challenge to using CocE as a treatment is its immunogenicity. All exogenous proteins (including CocE) are prone to be cleared by serum proteases in circulation. Moreover, since CocE is a bacterial protein, after entering the circulation, CocE can be highly immunogenic and initiate a large production of anti-CocE antibodies. This extensive immune response will not only deactivate CocE, but more importantly, be potentially deleterious to the host.

While the thermal stability of CocE has been successfully improved by computationally-designed mutation, its proteolytic degradation and induced immune response remain to be critical issues, which must be solved prior to any potential clinical application. Therefore, the major scope of this dissertation is to create a more

proteolysis-resistant, less immunogenic form of CocE. Two potential strategies, PEGylation and cell encapsulation, are employed in this dissertation to overcome the stability and immunogenicity issues, and the characteristics of these two strategies are now discussed in the following section.

1.4 Potential Strategies to Enhance Therapeutic Efficacy of CocE

1.4.1 PEGylation

PEGylation, in terms of its terminology, means the modification of protein or other macromolecules by attaching one or several polyethylene glycol (PEG) chains (23). Due to the dynamic mobility of their bulky chains, PEG groups can generate a steric hindrance on the protein surface, and therefore shield the protein from the binding of proteases and antibodies in circulation. Over their non-PEGylated counterparts, PEGylated proteins usually exhibit several advantages, including reduction or elimination of protein immunogenicity, protection against degradation by metabolic enzymes, and extension of the residence time in the circulation (23). Several PEGylated therapeutic proteins have been approved by the FDA for clinical use, such as PEG-adenosine deaminase (Adagen®) for the treatment of severe combined immunodeficiency (SCID), PEG-asparaginase (Oncaspar®) for the treatment of leukemia, and PEG-interferon α2b (PegIntron®) for the treatment of chronic hepatitis C virus infection (24).

1.4.2 Cell Encapsulation

Another potential approach to improve the stability and immunogenicity of CocE is encapsulating CocE in cells. As long as CocE is confined inside the cells, it can be protected from proteolytic degradation in circulation, as well as detection by the host immune system. However, the cell membrane is only permeable for small (< 400-500 Da) lipophilic molecules but not for macromolecules (25) including CocE. To solve this permeability issue for cell encapsulation, in this dissertation, a cell permeable form of CocE is developed by attaching CocE to cell penetrating peptides (CPPs).

Cell Penetrating Peptides (CPPs)

CPPs, also known as peptide transduction domains (PTDs) or membrane translocation sequences (MTSs), are a group of short peptides that are able to cross the cell membrane. Except for their short length (less than 30 amino acids) and positive charge, CPPs have few features in common (26). CPPs can consist of natural or unnatural/modified amino acids, which can be either polycationic (a cluster of arginine or lysine) or amphipathic (a combination of lipophilic and hydrophilic amino acids) that is net positively charged at a physiological pH.

In addition to their own cellular uptake, via covalent or electrostatic linkage, CPPs can deliver a wide range of cell-impermeable "cargos" into the cytosol. These "cargos" can be small molecules or macromolecules, including anti-cancer molecules (27, 28), proteins (29, 30), peptides (31, 32), oligonucleotides (33), siRNA (34), plasmids (35), nano-particles (36), and MRI-contrast agents (37). Since there is no limitation on the type of CPP-carried cargo, this CPP-mediated intracellular delivery generated considerable interest. In fact, over the last decade, the concept of CPP-mediated delivery was applied in more than 300 studies, and this number is still growing strongly (38-41).

Although the cellular uptake of CPP and CPP-cargo has been widely investigated for most cell types, the mechanism of CPP-mediated cellular uptake remains unclear. The first step in the CPP-mediated internalization, for which there is a consensus, is the electrostatic interaction between positively-charged CPPs and the negatively charged extracellular matrix proteins, mainly heparan sulfate proteoglycans (42). This electrostatic binding accumulates CPP (or CPP-cargo) at the cell surface, and initiates the pathways afterwards for the cellular uptake. Currents models for two proposed pathways for CPP-mediated cellular uptake are demonstrated in Figure 2 (43).

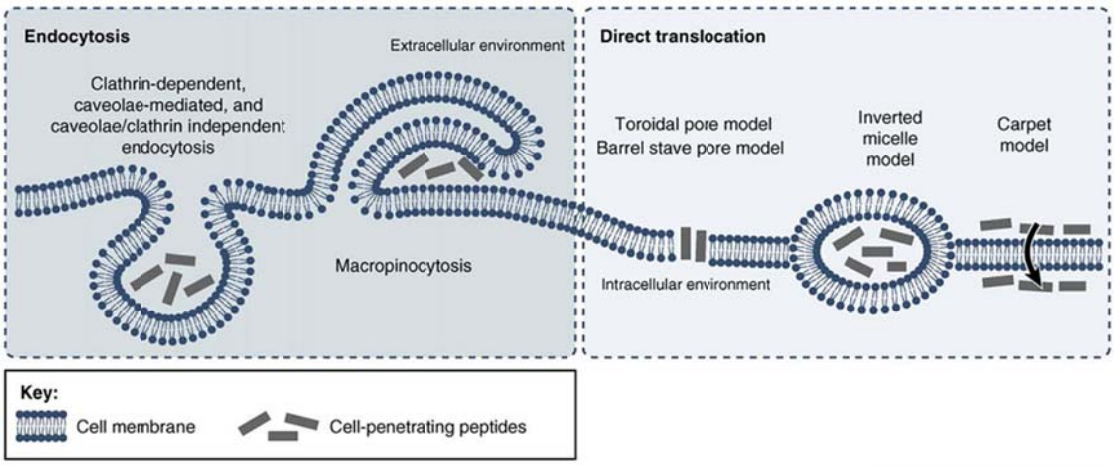

Figure 2 Currents models for the two pathways of CPP-mediated cellular uptake.

The first proposed pathway, endocytosis, is an energy- and receptor-dependent reaction. In this pathway, the clustering of CPP/CPP-cargo on the cell surface triggers the activation of a specific group of cell receptors, and forms the cell membrane around the CPP-clustering region into small vesicles. These vesicles containing CPP/CPP-cargo are destined to endosomes, where most CPP/CPP-cargo will be degraded rapidly by the acidic pH and various hydrolyzing enzymes. Therefore, the endosomal entrapment of CPP/CPP-cargo is the major limitation in the endocytosis pathway (44), which can also drastically reduce the bioavailability of the CPP-mediated cellular delivery.

Another proposed pathway is direct translocation into the cytoplasm. The cationic amino acids and lipophilic domains of the CPP have a high affinity to the cell membrane phospholipids, so CPP can insert into the cell membrane and temporarily destabilize it. This temporary destabilization can cause transient holes or inverted micelles in the cell membrane, and facilitate the internalization of CPP/CPP-cargo. Because this pathway only involves the interaction between the CPP/CPP-cargo and the cell membrane, it is independent from the cell receptors, and also insensitive to temperature or endocytosis inhibitors.

Due to the endosomal entrapment issue in the endocytosis pathway, direct translocation is a more favorable pathway for the CPP-mediated delivery of proteins. According to all of the current studies of CPP-mediated internalization, however, the two aforementioned pathways of cellular uptake usually occur simultaneously for most CPPs and CPP-cargo (41). Nevertheless, the preference for the two cellular uptake pathway of each CPP/CPP-cargo can be altered by a variety of parameters, including the nature and structures of the CPPs and cargo, the type of cells and membrane composition, and the detailed conditions when conducting the cellular uptake.

Red Blood Cells (RBC) Encapsulation for CocE

Among all cell types which can be employed as carriers for CocE encapsulation, the use of RBCs appears to be most appealing, because RBC offer several unique advantages as carriers for delivering a therapeutic enzyme like CocE. In terms of their physiological properties, RBC are biocompatible and biodegradable, especially when autologous cells are used. The biconcave shape of RBC also provides a large surface-to-volume ratio (1.9 x 10^4 cm/g) that is available for enzyme loading. From a pharmacodynamic perspective, owing to their enucleated and relatively inert intracellular environment, RBC would not only protect the loaded enzymes from proteases and immune responses in circulation, but also protect the host from any side effects such as immunogenicity. From a pharmacokinetic prospective, the normal life-spam of RBC is 120 ± 20 days (45), which is significantly longer than any known synthetic drug carrier.

On the other hand, as a small and lipophilic molecule, cocaine can readily cross the cell membrane and diffuse into the cell. This rapid cellular uptake also occurs in circulation. According to a study of intravenous cocaine injection in humans, cocaine in circulation can rapidly accumulate in the red blood cells (RBC) and reach the maximal concentration within five minutes (46). More interestingly, the cocaine concentrations in RBC remain two-fold higher than the concentrations in plasma (46). This strengthens the reason to develop an enzyme formulation to efficiently digest cocaine inside the RBC.

The first attempts to load a therapeutic enzyme into RBC were carried out in 1973 (47). To date, RBC encapsulation for enzymes has resolved many inherent drawbacks in enzyme replacement therapies, such as short half-lives, immune and allergic reactions, and host toxicity (48). Thus, this approach has been studied for treating enzymatic deficiencies or intoxications such as acute lymphoblastic leukemia (49), Gaucher's disease (50), alcoholism (51), and methanol intoxication (52).

When loading therapeutic enzymes into RBCs, the loading process should be taken to prevent damage to the RBC membrane. If the RBC membrane is compromised during the process, the hemoglobin and cytoskeletons inside RBC would leak out, which results in uniconcave or spherical, pink or pale-colored RBC known as "RBC-ghosts". RBC-ghosts with abnormal morphology will be recognized by the host immune system as foreign entities, leading to a rapid phagocytosis and clearance. However, current enzyme loading approaches, such as osmosis (exposing cells to a hypotonic solution), electroporation (inducing pores on the cell membrane by a strong external electrical field), and drug-induced endocytosis (using primaquine or hydrocortisone to trigger membrane internalization by stomatocyte formation) all require disruption of the cell membrane to increase permeability (53).

Unlike the aforementioned methods, CPP-mediated enzyme loading does not alter the physical properties and chemical compositions of RBC. According to the results from our group, CPP-mediated RBC encapsulation will not cause cell membrane perturbation, but rather produces a morphologically normal and enzyme-loaded RBC (54, 55). Moreover, the loading efficiency of this CPP-medicated method was shown to be comparable to all other current methods.

The scheme for loading CPP-CocE into RBC is shown in Figure 3. The CPP-mediated loading can be easily achieved by incubating CPP-CocE with RBC. Since CPP-CocE is cell permeable, it can pass through the RBC membrane and enter the cells. After the loading process, the CPP-CocE-loaded RBC can be injected into a cocaine overdosed patient. Any cocaine molecule diffusing into the enzyme-loaded RBC will be

rapidly converted into inactive metabolites, and the enzyme inside the RBC will be available again for next run of cocaine digestion.

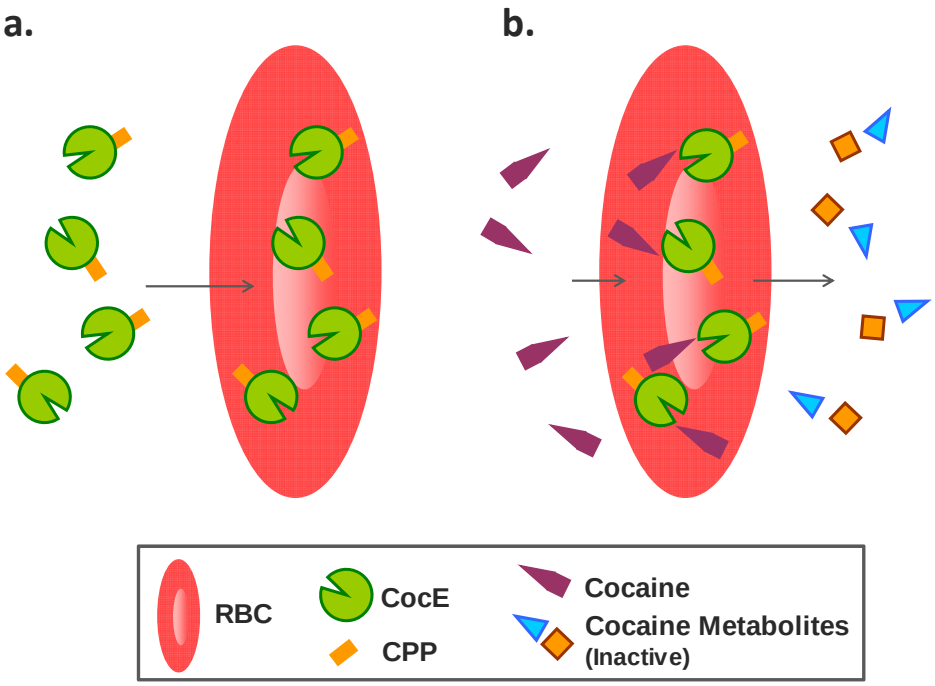

Figure 3 CocE-loaded RBC as a treatment to reduce cocaine concentration in circulation.

1.5 Specific Aims

The research objective of this dissertation is to improve the thermal stability and immunogenicity of CocE. On this basis, the following specific aims will be addressed:

1. To modify CocE by PEGylation.
2. To produce CPP-attached CocE variants and systemically compare their *in vitro* properties.
3. To encapsulate CPP-CocE variants into cells and evaluate the properties of the CPP-mediated cellular uptake.

CHAPTER 2
CocE PEGylation

Enhancing cocaine metabolism by administration of cocaine esterase (CocE) has been considered as a promising treatment strategy for cocaine overdose and addiction, as CocE is the most efficient native enzyme yet identified for metabolizing the naturally occurring cocaine. A major obstacle to the clinical application of CocE, however, lies in its thermo-instability, rapid degradation by circulating proteases, and potential immunogenicity. PEGylation, namely by modifying a protein or peptide compound via attachment of polyethylene glycol (PEG) chains, has been proven to overcome such problems and was therefore exploited in this CocE investigation.

The PEG-CocE conjugates prepared in this study showed a purity of greater than 93.5%. Attachment of PEG to CocE apparently inhibited the binding of anti-CocE antibodies to the conjugate, as demonstrated by the enzyme-linked immunosorbent assay (ELISA) assay. In addition, PEGylation yielded protection to CocE against thermal degradation and protease digestion. Furthermore, preliminary *in vivo* results suggested that, similarly to native CocE, the PEG-CocE conjugates were able to protect animals from cocaine-induced toxic effects. Overall, this study provides evidence that the PEGylation may serve as a tool to prolong CocE functionality in the circulation and reduce its potential immunogenicity.

2.1 Introduction

Cocaine is a well-known tropane alkaloid acting as a powerful central nervous stimulant and reinforcing drug (56). Therefore, the abuse of cocaine continues to be a

major societal and health problem (57). Recently, a bacterial cocaine esterase, namely CocE that is found in *Rhodococcus* sp. MB 1 and lives in soil surrounding the coca plant, has been reported to possess a high efficiency in degrading cocaine by hydrolyzing the benzoyl ester of cocaine to produce inactive metabolites, ecgonine methyl ester and benzoic acid (12). CocE is a globular, 574-amino acid bacterial enzyme with a molecular weight of ~63 kDa, and is among the most efficient protein catalysts characterized to-date for the hydrolysis of cocaine (12). The major obstacles to clinical application of CocE in treatment of cocaine overdose, however, lie in its temperature-dependent inactivation, with an *in vitro* plasma half-life of approximately 15 min at physiological temperature (37 °C) (18). In addition, CocE is prone to enzymatic degradation by circulating proteases. Moreover, since CocE is a bacterial protein that is foreign to the mammalian genome, immunogenicity remains to be a serious concern with regard to its real-time clinical use. While thermo-stable variants of CocE have been developed with a nearly 30-fold increase in plasma half-life observed in both *in vitro* and *in vivo* studies (21), rapid proteolytic degradation and its triggered response by the host immune system remain to be the most critical issues that must be addressed prior to any potential application in clinical practice (10). PEGylation, in terms of its terminology, means modification of a protein molecule or a carrier cargo (*e.g.* liposome) by attaching one or several polyethylene glycol (PEG) chains (23). The PEGylated conjugates normally exhibit several advantages including a reduction or elimination of protein immunogenicity, protection against degradation by metabolic enzymes, and prolongation of the residence time in the circulation (23, 58). Such benefits stem from the steric hindrance effect on the protein molecule by these surrounding bulky PEG chains possessing unparalleled special dynamic mobility; a hallmark protection mechanism by PEG. Several examples of success have already been reported. For instance, PEG-asparaginase (Oncaspar®, ENZON Phamaceuticals Inc., Bridgewater NJ) has been approved by the FDA for clinical use since 1994 in treating acute lymphoblastic leukemia (59). In addition, PEG-interferon α2a (Pegasys®, Roche, Nutley NJ) by utilizing branched PEG 40 kDa was introduced into the market in 2001 for treating hepatitis C (60, 61). Moreover, branched PEG-anti-VEGF aptamer (Pegaptanib®, Macugen™, OSI

Pharmaceuticals, Melville, NY) has been approved since 2004 for selective management of age-related macular degeneration (62, 63).

In this study, conjugation of CocE with both linear and branched PEG40K was investigated. The chemically synthesized PEG-CocE conjugates were purified by passing through an anion-exchange column. Sodium dodecyl sulfate-polyacrylamide gel electrophoresis (SDS-PAGE) was applied to assess the apparent molecular mass and purity of the PEG-CocE conjugates. *In vitro* assays were carried out to determine the effect of PEGylation on the functionality of CocE in hydrolyzing cocaine. The protective effect of PEG on the *in vitro* thermo-stability and against trypsin digestion of CocE was evaluated at 37 °C. ELISA was employed to evaluate the recognition ability of the PEG-CocE conjugates towards anti-CocE polyclonal antibodies. Lastly, the feasibility of *in vivo* application of PEGylated CocE was examined by using a rodent model.

2.2 Materials and Methods

2.2.1 Materials

Different types of PEG polymers were obtained from Nektar Therapeutics (San Carlos, CA). Unless otherwise stated, chemicals and reagents were from Fisher Scientific Co. (Pittsburg, PA) or Sigma (St. Louis, MO). Water was distilled and deionized (ddH_2O).

2.2.2 Methods

Preparation of wild type (WT) CocE and CocE mutant T172R/G173Q

The wild type CocE and CocE mutant T172R/G173Q were prepared according to procedures described previously (13, 21). Point mutations were generated using the Site-Directed Mutagensis Kit (QuickChange, Stratagene, La Jolla CA), and the double mutant was generated using single-point mutations as the templates. Wild type and mutant cDNAs were cloned by utilizing the bacterial expression vector, pET-22b (+). All enzymes were expressed as 6× His-tagged proteins in *E. coli* BL-21 (DE3) cells that were

grown at 37 °C. Protein expression was induced with 1 mM isopropyl-β-thiogalactopyranoside for 12 h at 18 °C.

Cells were pelleted, resuspended in 50 mM Tris–HCl buffer (pH 8.0) containing 150 mM NaCl, 1 mM dithiothreitol (DTT), and a protease inhibitor cocktail (34 μg/ml each of L-tosylamido-2-phenylethyl chloromethyl ketone, 1-chloro-3-tosylamido-7-amino-2-heptanone and phenylmethylsulfonyl fluoride, as well as 3 μg/ml each of leupeptin and lima bean trypsin inhibitor) and then lysed using a French press (Thermo Fisher Scientific Corp, Needham Heights MA). His-tagged enzymes were enriched 6-fold by using Talon metal affinity chromatography (Clontech Laboratories, Inc., Mountain View CA), and purified using the Q-Sepharose (GE Healthcare, Piscataway NJ) anion-exchange column. CocE was eluted from the Q-Sepharose column with 150–450 mM NaCl linear gradient buffer (pH 8.0) containing 20 mM HEPES, 2 mM $MgCl_2$, 1 mM EDTA, and 1 mM DTT. The peak fractions were pooled, concentrated by using a centrifugal filter device (Carrightwohill, Co. Cork, Ireland), snap frozen in liquid nitrogen, and then stored at −80 °C prior to use.

Preparation of PEG-CocE conjugate via amine group-directed PEGylation

CocE (3 mg/ml) in 50 mM HEPES buffer at pH 8.0 was mixed with mPEG-NHS ester (MW: 5500 Da) at differing [NH2]:[mPEG] molar ratios ranging from 1:2 to 1:10, based on the number of lysine residues on CocE (8 Lys). Conjugation reaction was performed for 30 min to 1 h at 4 °C in the presence of gentle shaking. The reaction mixture was concentrated and purified by centrifugal filtration (MWCO: 30,000 Da) at 4 °C by adding 10× volumes of cold PBS (50 mM, pH 7.4) four to five times. Prior to and immediately after the conjugation reaction, initial rates of cocaine hydrolysis by the enzyme were measured by monitoring decrease in UV absorbance at 240 nm at 37 °C for 60 s, following the addition of 50 μL 0.5 μg/ml CocE to 950 μL solutions containing a substrate concentration ranging from 7.8 to 125 μM. On an average, approximately 70% of initial enzyme activity was recovered immediately after the PEGylation reaction.

Preparation of PEG-CocE conjugates via sulfhydryl group-directed PEGylation

Prior to the conjugation reaction, CocE was treated with 50 mM DTT for 30 min to break down the disulfide bonds, and the excess DTT was removed by using a Sephadex G-25 desalting column. Solutions containing 4 mg/ml DTT-treated CocE in 50 mM phosphate buffer (pH 7.4) were mixed with the linear PEG5K- or branched PEG40K-maleimide (Jenkem Technology, Allen TX) at a molar ratio of 1:10. The conjugation reaction mixture was stirred for 12 h at 4 °C, and purified with a Q-Sepharose anion-exchange column eluted with 50 mM phosphate buffer (pH 7.4) containing 1 mM EDTA and a linear gradient of 0–500 mM NaCl. Fractions were collected and concentrated by using an ultra-filtration device (MWCO: 10,000 Da).

MALDI-TOF MS (Matrix-Assisted Laser Desorption/Ionization-Time-Of-Flight Mass Spectra) analysis

The samples were desalted with Pipette Tip (ZipTip, Millipore) by utilizing a saturated solution of sinapinic acid in water/acetonitrile (1:1, v/v) and 0.1% trifluoroacetic acid as the matrix solution. Aliquot containing 1 μL of the sample and matrix mixture was spotted onto a well of the sample plate and dried. Mass calibration was performed using bovine serum albumin and cytochrome c as the standards. Mass spectra were taken with linear mode Micromass TofSpec-2E (Waters, Milford MA) equipped with a high mass PAD detector. Data were processed with a MassLynx 3.5 software.

SDS-PAGE analysis

Fractions obtained under the NaCl gradient were analyzed by gradient (4–20% acrylamide; Invitrogen, Carlsbrad CA) type slab-SDS-PAGE. Gels were stained with coomassie blue, and then analyzed using a densitometer equipped with a digital camera (FE-280,Olympus, Tokyo, Japan) and Image Processing and Analyzing software (ImageJ, National Institutes of Health, Bethesda MD).

Thermal stability and resistance to trypsin digestion

Thermal inactivation was monitored by measuring the change in cocaine hydrolysis rate. Samples containing 1.6 μM of CocE or PEG-CocE were incubated at 37 °C, and aliquots were taken periodically and subject to enzyme activity assay at 37 °C. The rate of cocaine hydrolysis was determined by calculating the change of the absorbance over a 1-min period at 240 nm using a spectrophotometer (BioTek, Winooski VT). The value attained at each time point was divided by that at the initial time point to obtain the relative value.

The resistance to trypsin digestion was evaluated by mixing trypsin and CocE at a trypsin/CocE ratio of 1:10 (w/w) and incubating with agitation at 37 °C. The samples (CocE or PEG-CocE) were periodically removed to evaluate the cocaine hydrolyzing activity similar to the thermal stability test.

ELISA assay

The plates were coated with 100 μL of sheep anti-CocE polyclonal serum diluted to 1/2500 in coating buffer, and then the plates were incubated overnight at 4 °C. The liquid in the plate was removed and the plates were washed with PBS-Tween (1 ml Tween in 1 L phosphate buffered saline (PBS)) solution. The non-specific protein binding sites were blocked by adding the blocking TENTC buffer (pH 8.0) containing 50 mM Tris, 1 mM EDTA, 150 mM NaCl, 0.05% Tween 20, and 0.2% casein. The plates were incubated for 1 h at room temperature. PEG-CocE or CocE solutions (100 μL) were then loaded onto the wells and the plates were incubated for 4 h at room temperature. After washing the plates with the PBS-Tween buffer, an aliquot of 100 μL of rabbit anti-CocE polyclonal serum diluted 1/2500 in TENTC buffer was added into each well and the plates were incubated for 1 h at room temperature. The plates were thoroughly washed with PBS-Tween solution, followed by addition of 100 μL horseradish peroxidase-labeled goat anti-rabbit IgG (KPL, Gaithersburg MD) diluted 1/10,000 in TENTC buffer into each well. The plates were then washed with PBS-Tween solution, and 100 μL of Lumiglow substrate (KPL) were then loaded into each well.

Measurements were conducted by recording the absorbance at 430 nm, and data were fitted to a bar graph (Microsoft Excel, Seattle, WA).

In vivo experiments

Male NIH-Swiss mice (25–32 g) were purchased from Harlan Inc. (Indianapolis, IN). All mice were allowed *ad libitum* access to food and water, and were maintained on a 12-h light–dark cycle with lights on at 6:30 AM to keep at a temperature of 21–22 °C. Experiments were performed in accordance with the Guide for the Care and Use of Laboratory Animals as adopted and promulgated by the National Institutes of Health. The experimental protocols were approved by the University Committee on the Use and Care of Animals at the University of Michigan.

Cocaine-induced toxicity was evaluated by the occurrence of lethality, according to a previously established protocol (10, 18); where lethality was defined as cessation of observed movement and respiration. A preliminary study was performed to determine the ability of PEG5K-CocE to protect cocaine-induced toxicity. Following i.p. administration of several doses of cocaine (320, 560, and 1000 mg/kg; n=8 for each group), mice were immediately placed individually in Plexiglas containers for observation. After 1 min, CocE or PEG5K-CocE (0.3 mg) was administered through the tail vein to each of the animals. Dose–response curves of cocaine-induced lethality were used to compare the *in vivo* protective effect of native CocE versus the PEG-CocE conjugates.

Statistical analysis

Results are represented as means ± S.D., and data analysis and curve-fitting were conducted by using the Prism 5 (GraphPad Software, San Diego CA) and SPSS 16.0.2 (GraphPad, Chicago, IL). Two-way analysis of variance (ANOVA) was used to test for differences between groups and the level of significance value considered was 0.01.

2.3 Results

2.3.1 Characterization of PEGylated CocE

Initially, PEGylation reaction was performed using different types of PEG derivatives. According to information published in the literature, there were 9 primary amine groups in CocE including those in the 8 lysine residues as well as one at the terminal end of CocE (12). Monomethoxy-PEG succinimidyl ester (mPEG-NHS; MW5000 Da) was reacted with these primary amine groups on CocE. Results from MALDI-TOF showed that one to four PEG chains were conjugated to each CocE monomer (Figure 4). However, PEGylation of CocE via the amine groups was later found to lead a rapid destabilization and loss of the cocaine hydrolyzing activity of the enzyme (data not shown), and this conjugation strategy was therefore abandoned.

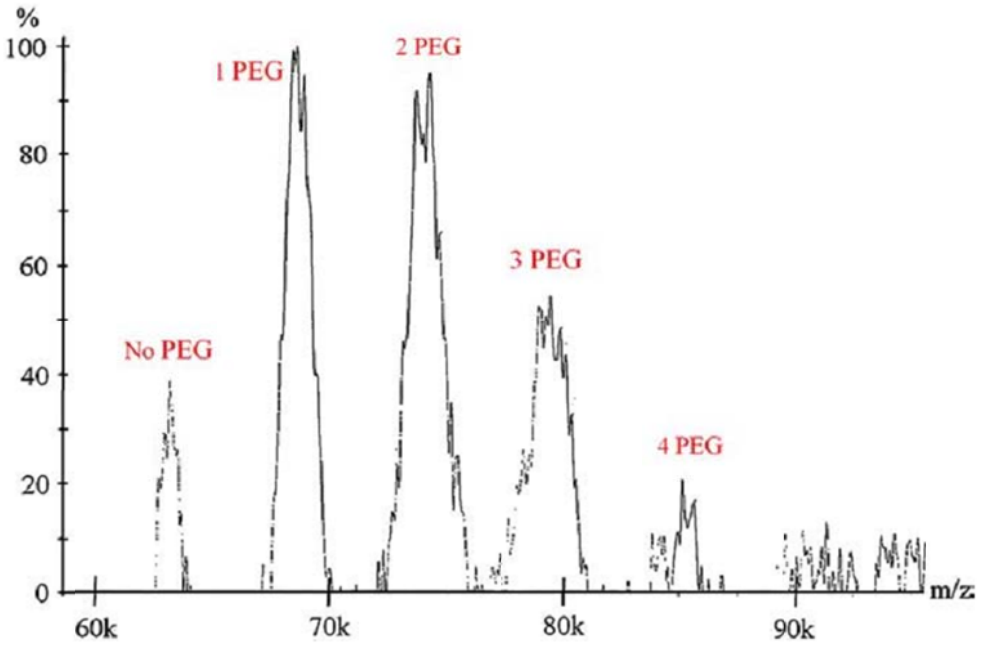

Figure 4 MALDI-TOF spectra of the PEG-CocE conjugates prepared by coupling PEG succinimidyl ester with the primary amine groups on CocE. Results showed that one to four PEG molecules were linked to each CocE monomer.

PEGylation via the thiol groups was conducted afterwards by utilizing monomethoxy-PEG maleimide (mPEG-MAL; MW 5000 Da). It should be noted

PEGylation at thiol groups of cysteine residues not involved in the disulfide bond formation is one of the most specific methods for conjugation (64). In DTT-treated CocE, there were four free cysteine residues available for conjugation, and two of them were more accessible to PEGylation, based on analysis of the three-dimensional structure of CocE (12). Hence, PEG-maleimide was used to take advantage of thiol addition to the activated double bond, known as the Michael addition, to yield stable thioether linkages (65). PEGylation process was performed at the pH 7.0–7.4 to minimize side reaction between the amine group and the maleimido terminal of PEG.

Results from MALDI-TOF showed that one to three PEG chains were conjugated to each CocE monomer (Figure 5); with two PEG per monomer CocE being the major species. However, further characterization of the properties of these PEG-CocE conjugates revealed the lack of necessary protection of the enzyme's stability, probably due to the fact that CocE was a relatively large molecule and therefore single and short-chain PEG failed to yield sufficient steric stabilization effect on CocE. To this regard, use of larger molecular weight, branched PEG was further explored. It should also be pointed out that using large, branched PEG would help offset the shortage of sites on CocE for PEGylation, as attachment of one branched PEG would be equivalent to the attachment of multiple linear PEG chains.

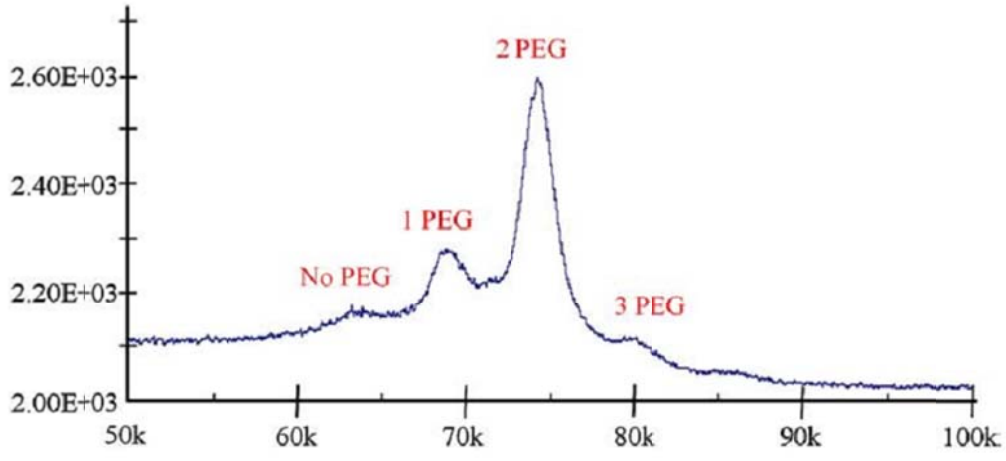

Figure 5 MALDI-TOF spectra of the PEG-CocE conjugates prepared by coupling PEG maleimide (linear chain, M: 5000 Da) to the thiol groups on the cysteine residues of CocE. One to three PEG molecules were found to be linked to each CocE monomer.

Following covalent attachment of PEG40K, ion-exchange chromatography using a Q-Sepharose anion-exchange column was applied to separate the PEG-CocE conjugates from unreacted CocE based on differences in charge screening ability between these two species. As shown in Figure 6, the PEGylation reaction mixture was separated by Q-Sepharose into five fractions. Fraction #5 was confirmed to contain primarily unreacted CocE, as native CocE conducted on a separate Q-Sepharose chromatography exhibited an almost identical elution retention time as Fraction #5. On the other hand, Fractions #3 and #4 appeared to be PEG-CocE conjugates at a different degree of PEGylation. It is noteworthy that native CocE exists as a dimeric structure (personal communication). Also, according to the MALDI data (Figure 8, as will be discussed next), no more than one branched PEG40K could be attached to one molecule of CocE. To this regard, Fraction #3 was speculated to be the dimeric CocE with two branched PEG chains (termed PEGylated "homodimer" since there was one PEG per monomeric CocE) since it occurred at a lower salt concentration due to a higher degree of PEGylation thereby yielding a higher degree of charge screening effect towards the Q-Sepharose resin, whereas Fraction #4 seemed to correspond to the dimeric CocE with branched PEG on one of the monomeric unit of CocE dimer (termed PEGylated "hetero-dimer" thereafter). Apparently, Fractions #1 and #2 corresponded to the excess level of PEG polymer and benzoic acid in the conjugation mixture, respectively.

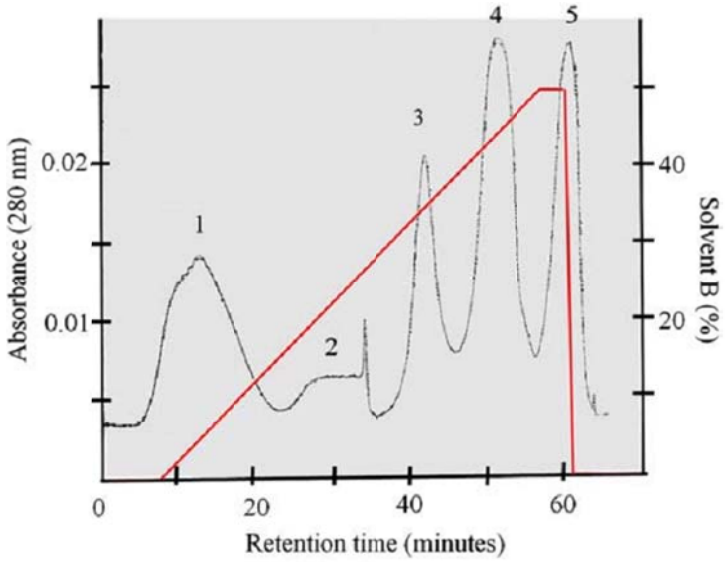

Figure 6 Ion-exchange chromatography of the reaction mixture of the PEGylation reaction.

SDS-PAGE analysis provided evidence to confirm this speculation. Unlike ion-exchange chromatography, SDS-PAGE would dissociate the dimeric CocE into monomeric units, thereby rendering it possible to characterize compositions of the PEG-CocE conjugates (*i.e.* homo- and hetero-dimers) obtained from different fractions in Figure 6. As displayed in Figure 7, Fraction #3 seen in the previous figure yielded a major upper band and a minor lower band on SDS-PAGE (*i.e.* Lane #2). While the upper band corresponded to PEGylated CocE based on the estimated molecular weight, the lower band represented the CocE molecule without PEGylation based on the migration distance observed for native CocE (Lane #4). Based on densiometric evaluation of the gel profile, the purity of the PEGylated CocE seen in the top band was approximately 93.5%; suggesting the presence of primarily PEG-CocE homo-dimers in this fraction. On the other hand, Fraction #4 displayed a mixture of an evenly distributed PEGylated and unreacted CocE monomers (Lane #3), where the bottom band was in almost identical intensity as the top band, implicating the presence of mainly PEG-CocE hetero-dimers in this fraction. MALDI-TOF mass spectroscopy, often employed to identify a purified PEGylated product (65), was used to determine the number of PEG molecules attached to each CocE monomer in Fraction #3 of Figure 6. As shown in Figure 8, mass spectra of Fraction #3 yielded a major peak with a m/z ratio of 10,6223 Da, suggesting the presence of one PEG molecule on a CocE; based on its precise correlation to the mass of PEG (40 kDa) and a monomeric CocE (note: a separate MALDI-TOF spectra of native CocE showed a major peak at a m/z ration of 63,338 Da; data not shown). It should be pointed out that, unlike results seen in Figure 5, in which more than two short 5 kDa PEG chains could be attached to each CocE monomer, only one of the large and branched PEG molecules could be successfully conjugated to each CocE monomer; obviously due to the large hydrodynamic size of the branched PEG. Nevertheless, later studies (see below) of this PEG-CocE conjugate showed that attaching one branched PEG was already effective in yielding steric repulsion against proteolytic degradation and recognition by opsonizing antibodies.

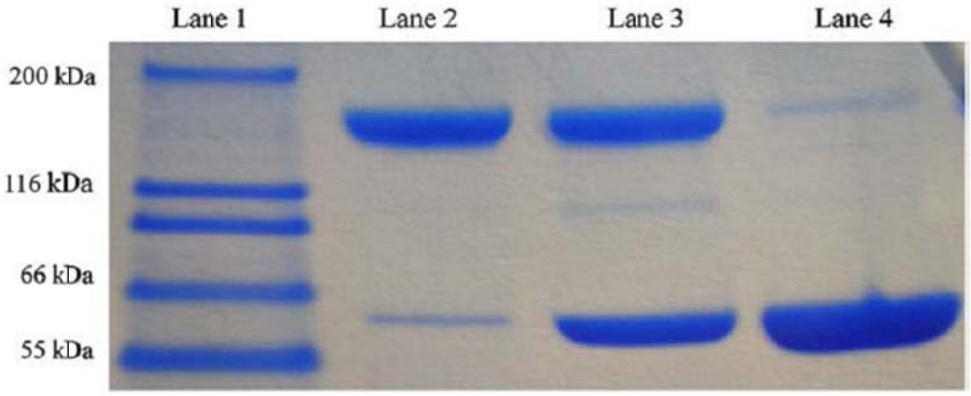

Figure 7 SDS-PAGE analysis of Fractions #3 and #4 obtained from the elution profile of Figure 6. Lane 1 showed the molecular weight markers. The top band in Lanes #2 and #3 represented the PEG-CocE monomeric subunit, whereas the bottom band in Lanes #2, #3, and #4 represented CocE monomeric subunit.

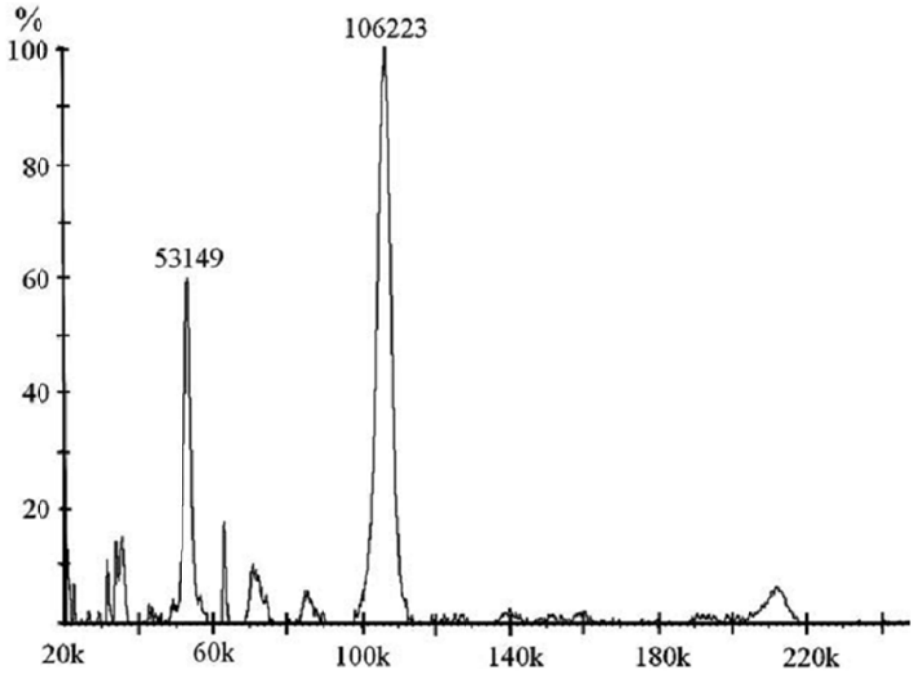

Figure 8 MALDI-TOF spectra of Fraction #3 obtained from the elution profile of Figure 6.

A large discrepancy between the calculated molecular weight by the MAlDI-TOF (~105 kDa) method and the SDS-PAGE assay (116-200 kDa) by using the gradient gel was observed. The discrepancy, however, could be accounted for in terms of the difference in the hydrodynamic radii between the compact globular CocE protein and linear PEG polymer (66) and, as a consequence, movement of PEGylated CocE in the SDS-PAGE gel matrix was reduced thereby yielding an apparently larger molecular weight on the calculation (66, 67).

2.3.2 Stability against thermal denaturation and trypsin digestion

After PEGylation, CocE retained approximately 56-75% of its original activity. While the chemical conjugation process undoubtedly would result in a certain degree of irreversible damage on the enzyme, this reduction in biological activity of PEG-CocE could also be attributed to some topological changes occurring in the structure of the enzyme, or to PEG-related steric impediment that could have disturbed protein-receptor interactions and diminished the accessibility of CocE to its substrates or receptor binding sites (68). When compared with native CocE without PEG protection, Figure 9 showed that the PEG-CocE conjugates were obviously more stable against thermal denaturation. This could be related to a mechanism reported by other investigators, which suggested that PEGylation could induce a blocking of the intermolecular interactions that were involved in thermal instabilities (69, 70). More importantly, PEG-CocE conjugates exhibited a much stronger resistance to protease digestion than native CocE, as statistically significant difference was observed in the trypsin digestion kinetic profiles Figure 10. This finding was somewhat anticipated, as it was demonstrated previously that branched PEG could provide an "umbrella-like" structure, yielding a protection against the approaching and attack by circulating proteases or cells (71, 72). Ample examples of PEG-mediated protection against protease digestion have been reported in the literature, including PEGylated interferon-α, tumor necrosis factor, epidermal growth factor, etc (67, 68, 73).

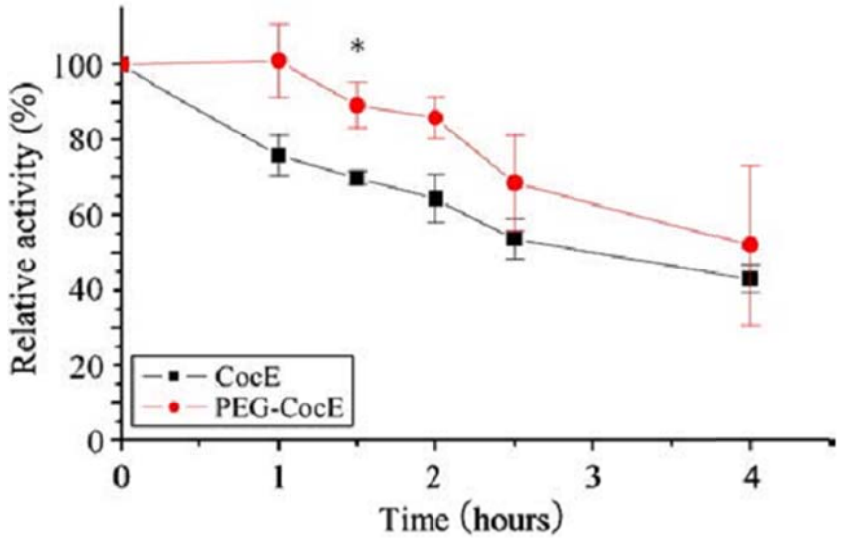

Figure 9 Time course of thermal inactivation of CocE and PEG-CocE at 37 °C. The y-axis represented the ratio of cocaine hydrolyzing activity at a certain time point over the initial activity. *Represented that the difference was statistically significant ($p<0.01$).

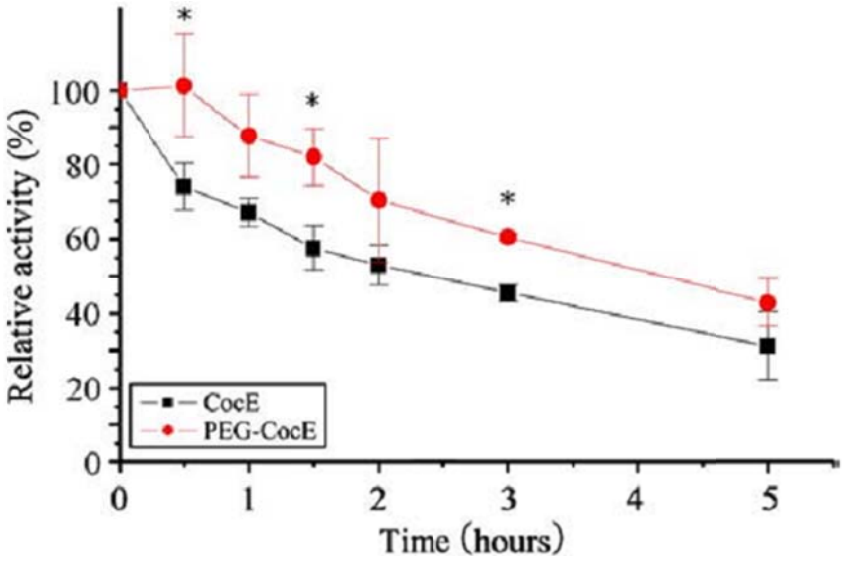

Figure 10 Resistance to trypsin digestion of CocE and PEG-CocE. PEGylated or unmodified CocE were incubated with trypsin at a trypsin:CocE ratio of 1:10. Reactions were carried out at 37 °C. The PEG-CocE conjugates displayed stronger resistance to trypsin digestion than native CocE. *Represented that the statistically significant difference was seen ($p<0.01$).

2.3.3 Reduction of immunogenicity by PEGylated CocE

ELISA was conducted to evaluate whether PEGylation could shield the recognition of CocE by specific anti-CocE antibodies. Figure 11 showed that statistically significant differences in fluorescence intensity between unprotected CocE and PEGylated CocE were observed (2-Way ANOVA, $p<0.01$) over the entire concentration range tested, indicated a decrease in antibody recognition of the PEG-protected CocE. The reduction of 70.4% in antibody recognition is seen with PEG-CocE from the highest concentration when compared with the same concentration of native CocE. Apparently, this reduction in immunoreactivity was attributed to the steric hindrance yielded by the long and branched PEG chains that blocked the interaction between CocE and its specific antibodies; consistent with findings by other investigators on other PEGylated proteins (68). Also in agreement with literature reports, both the chain length and molecular size of PEG would yield different effects on the protection (23, 74). While the branched, 40-kDa PEG was able to reduce the immunogenicity of CocE, early attempt on the use of the 5-kDa straight chain PEG failed to yield a shielding effect on CocE against anti-CocE recognition (data were not shown); similar to the findings by Caliceti and Veronese (23) on PEGylated urinase, in which branched 10-kDa PEG was found to be far more effective than linear 5-kDa PEG in dodging antibody detection. It should be noted that because of the presence of a certain degree (~6%) of unreacted CocE impurity in the obtained PEG-CocE preparation (see above), the observed ELISA results actually represented the minimal degree of PEG-induced protective effects.

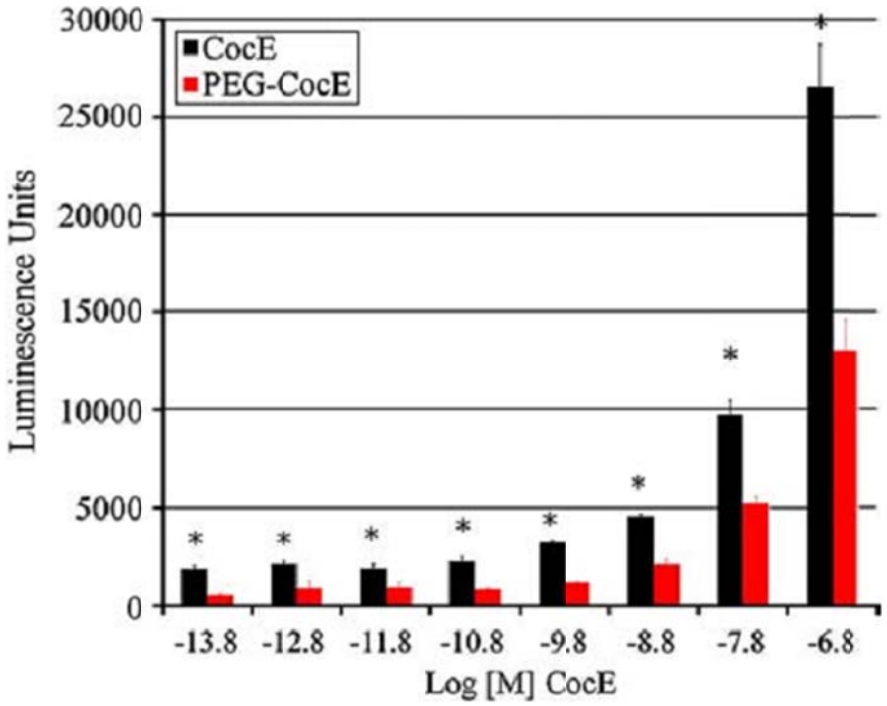

Figure 11 ELISA assay to assess antibody recognition towards CocE and PEG-CocE. Statistical analysis was performed by utilizing 2-Way ANOVA, and * represented that the difference was statistically significant ($p<0.01$).

Indeed, *in vitro* results correlated very well with *in vivo* findings. It was routinely observed that the effectiveness of CocE therapy gradually declined after repeated administration of CocE to cocaine-challenged mice, with speculation that the development of increased anti-CocE antibody titers had offset the efficacy of CocE during the rescue experiments of cocaine overdose (75). To this regard, PEGylation could play a crucial role on the success of utilizing CocE in clinical practice in treatment of cocaine abuse or overdose.

2.3.4 *In vivo* protection against lethal dose cocaine injection in mice

The previously established rodent model of acute toxicity (10, 18) was used to evaluate the effect of PEGylated CocE against cocaine-induced dose-dependent lethality in mice. When PBS solution was intravenously administered into control mice 1 min

before intraperitoneal injection of 100 mg/kg lethal dose of cocaine, all (100%) animals died within a short period of less than 15 min. In sharp contrast, when mice were given 0.3 mg of either CocE or PEG-CocE 1 min before i.p. injection of cocaine at a dose 3 times higher than the lethal dose (*i.e.* 320 mg/kg), all animals were rescued from cocaine-induced lethality. As displayed in Figure 12, a dose of merely 0.3 mg of CocE or PEG-CocE before cocaine insult already produced a 10-fold shift in the cocaine dose-dependent toxicity profiles. Further increase of the lethal cocaine dose reversed the protective effect by CocE or PEG-CocE in a dose-dependent manner. Indeed, a dose of 1000 mg/kg i.p. cocaine was needed to surmount the protective effect of CocE. It should be pointed out that at an identical dose of 0.3 mg, PEG-CocE exhibited the same potency as native CocE in hydrolyzing cocaine, despite it only consisted of 50% of CocE base on calculation of the protein mass in the PEG-CocE conjugates. This was speculated to attribute to the improved circulating half-life of PEG-CocE due to the steric protection by PEG against proteolytic degradation, although further pharmacokinetic investigation deemed necessary to validate this hypothesis. Nonetheless, this finding corroborated well with several published reports on PEGylated proteins (61, 76-80). For instance, PEGylated α-interferon Pegasys®, which retained only 7% of the antiviral activity of the original protein, still displayed a greatly improved *in vivo* efficacy compared with the unmodified enzyme, primarily due to a markedly improved pharmacokinetic behavior (61). In addition, the *in vitro* ribosome-inactivating activity of PEGylated trichosanthin mutants (PEG20K-Q219C) was found to decrease more than 10-fold yet the *in vivo* activity was increased by 3-fold over the unprotected protein (76). Furthermore, *in vitro* biological activity of PEGylated growth hormone decreased with increasing the number of attached PEG chains, yet the half-life and *in vivo* potency was reported to increase accordingly (77). Extensive investigations of the optimal conditions for CocE PEGylation, *in vivo* efficacy against cocaine toxicity, as well as pharmacokinetics, biodistribution, and clearance of the PEG-CocE conjugates are currently in progress in our laboratory.

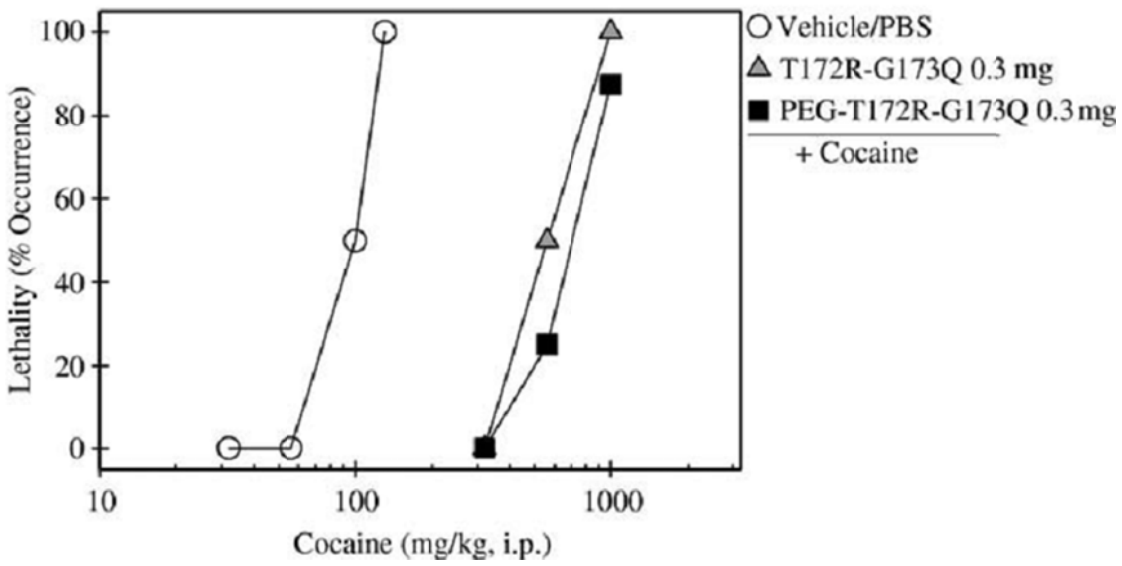

Figure 12 Protective effects of PEG-CocE against cocaine-induced toxicity. Each data point represents the percentage of mice (n=8 for each dosing condition) suffering cocaine-induced lethality.

2.4 Conclusions

In summary, PEGylation of CocE was successfully carried out and characterized. Both *in vitro* and animal studies provide the proof-of-concept evidence of the feasibility and utility of utilizing PEG protection against thermal denaturation, protease degradation, and clearance by specific opsonizing antibodies. Importantly, our results also showed the practicality of utilizing PEGylated CocE in protecting animals from lethal cocaine toxicity. Further investigations of the efficacy and safety of this novel treatment modality of cocaine overdose and abuse are currently under way in our laboratory, with the ultimate goal of bringing this project to a successful clinical translation.

CHAPTER 3
Development of Cell Permeable CocE

A cell permeable form of CocE was proposed by attaching CPP to CocE in Chapter 1. Therefore, the aim for this chapter is to develop CPP-attached CocE (CPP-CocE) variants and systemically compare their *in vitro* properties. CPP and CocE are designed to be linked via covalent bonding, which can be created by either chemical conjugation or biological recombination approach. In chemical conjugation approach, CPP is linked to CocE via a disulfide bond. In biological recombination approach, CPP and CocE are expressed as "CPP-CocE fusion proteins", in which CPP groups are expressed in tandem at the beginning or the end of CocE sequence. A systemic comparison of these CPP-CocE variants is also performed, including the examination of their absolute yield per batch, recovery percentage, enzyme specific activities, and *in vitro* stability at 37 °C.

Six CPP-CocE variants were successfully created by employing two model CPPs, Tat and Low Molecular Weight Protamine (LMWP). Two types of disulfide-bridged chemical conjugates, Tat-S-S-CocE and LMWP-S-S-CocE, were purified by heparin affinity chromatography. Four recombinant CPP-CocE fusion proteins, Tat-N-CocE, LMWP-N-CocE, CocE-C-Tat, and CocE-C-LMWP, were expressed and purified in *E. coli* as soluble proteins. These six CPP-CocE variants contain one CPP group on the surface on each CocE molecule. Among all of the CPP-CocE constructs, LMWP-S-S-CocE showed the highest cocaine-hydrolyzing activity, and CocE-C-Tat had the largest production yield. Interestingly, Tat-N-CocE possessed the longest *in vitro* half-life compared with any CocE variants reported previously. Based on the overall results, either Tat-N-CocE or CocE-C-Tat seemed to be the most preferable CPP-CocE variants,

but a cellular uptake study is needed to ensure the cell penetrating activity of all six CPP-DMCocE variants. This uptake study will be discussed in Chapter 4.

3.1 Introduction

In this dissertation, two model CPPs are employed for the development of CPP-attached CocE variants (CPP-CocEs), which can cross the cell membrane and be encapsulated inside the cells. One model CPP utilized in this dissertation is Tat, the first discovered (81) and most widely studied CPP (82). It was derived from the cell-permeable HIV transcriptional transactivator, and has the sequence YGRKKRRQRRR (81, 83). Tat-mediated intracellular delivery, which has been proved in many cell types, is more efficient than other non-CPP-mediated intracellular delivery (84) and does not cause cell membrane damage (85). Moreover, after the first proof of concept provided by Dowdy's group in 1999 (86), this Tat-mediated delivery has been applied *in vivo* to the treatment of various diseases. Currently, several clinical trials are underway to assess the potential of the Tat-mediated delivery for systemic administration of several therapeutic macromolecules, including a protein kinase C inhibitor (87) and siRNA (41).

Another CPP applied in this dissertation is low molecular weight protamine (LWMP). LMWP is a CPP discovered in our laboratory from enzymatic digestion of protamine (88), and has sequence VSRRRRRRGGRRRR. Because of the structural similarity to Tat (cationic, arginine-rich, and in the length of 10-15 amino acids), it is rational to assume that LMWP also possesses similar cellular uptake behavior. In 2003, Park *et al.* showed that LMWP had cellular penetrating activity and kinetics comparable to those of Tat (89). *In vitro* studies later demonstrated that LMWP was also able to transfer its attached proteins, genes, or other cargo molecules into various types of cells (30, 89, 90). Similar to Tat, this LMWP-mediated cellular uptake did not cause any perturbation or damage to the cell membrane (91). In the animal models, LMWP-mediated delivery has also been applied successfully in the treatment of solid tumors, acute lymphoblastic leukemia, and hypoxic-angiogenesis (33, 55, 92).

In addition to its cell penetrating ability, LMWP offers several exclusive advantages over Tat and other CPPs. Tat and other CPPs can only be chemically synthesized, which can be inefficient and expensive especially for a large-scale production. However, enzymatic digestion of protamine allows LMWP to be directly manufactured in mass quantities, in limited time, and at low cost. The process of LMWP preparation and purification has been fully characterized (93). A further advantage is that LMWP is derived from protamine, which is a FDA-approved clinical drug. Thus, LMWP is also supposed to be safe for humans. This proposition has been supported by the *in vivo* toxicity profile of LMWP, which demonstrated no acute toxicity and immunogenicity (94).

In this dissertation, CPP and CocE are linked via covalent bonding, which can be created by either chemical conjugation or biological recombination approach. In chemical conjugation approach, CPP and CocE are linked via a disulfide bond, which is mediated by a bifunctional cross-linker *N*-succinimidyl 3-(2-pyridyldithio)-propionate (SPDP). In biological recombination approach, the genes of the CPP and CocE are cloned and expressed in tandem. The product is a "CPP-CocE fusion protein", a single protein with the CPP sequence fused at the beginning or the end of CocE sequence. CPP-CocE fusion proteins are expressed as histidine-tagged proteins in *E. coli*, and purified by Talon™ metal affinity chromatography and Q-Sepharose anion-exchange chromatography. A systemic comparison of the CPP-CocE variants is also performed, including the examination of their absolute yield per batch, recovery percentage, and enzyme specific activities. Due to its importance for the following *in vivo* application, the *in vitro* stability of CPP-CocE at 37 °C is also tested, and their half-lives at 37 °C will be used as an indicator for accessing thermal stability.

3.2 Materials and Methods

3.2.1 Materials

pET22b(+)-CocE-T172R/G173Q plasmid was kindly provided by Dr. Roger Sunahara (Department of Pharmacology, University of Michigan). This plasmid is a

bacterial expression vector derived from Novagen® pET-22b(+) (Merck KGaA, Darmstadt, Germany), and leads to an over expression of the CocE double mutant CocE-T172R/G173Q (DMCocE) with an additional exogenous 6-histidine tag (LEHHHHHH) at its C-terminus. Tat peptide (H_2N-YGRKKRRQRRR-COOH) was synthesized with approximately 98% purity by GenWay Biotech Inc. (San Diego, CA). LMWP was produced based on previously described procedures (93). SPDP and *E. coli* BL21 Star™ (DE3) competent cells were purchased from Invitrogen (Carlsbad, CA). Carbenicillin, isopropyl-β-thiogalactopyranoside (IPTG), dithiothreitol (DTT), leupeptin, and soybean trypsin inhibitor were purchased from Sigma-Aldrich (St. Louis, MO). DNA primers (purified by standard desalting or HPLC) used for sequencing and site-directed mutagenesis were synthesized by Integrated DNA Technologies Inc. (Coralville, IA). Phusion® site-directed mutagenesis kit and DNA restriction endonucleases (NdeI, NcoI, KpnI, BamHI, and DpnI) were purchase from New England Biolabs (Ipswich, MA). *E. coli* DH5α competent cells and pEXP-5-NT/TOPO® TA Expression Kit were purchased from Invitrogen (Carlsbad, CA). Cocaine hydrochloride was obtained from the National Institutes on Drug Abuse (Bethesda, MA). A Bradford protein assay kit was purchased from Bio-Rad Laboratories (Hercules, CA). Water was distilled and deionized (ddH_2O). All other reagents were of analytical grade.

3.2.2 Construction of CPP-Attached CocE Variants (CPP-CocEs)

Chemical Conjugation

Schematic procedures for conjugating CPP and CocE are shown in Figure 13. First, CPP (Tat or LMWP) must be activated by SPDP (Figure 13, scheme a). In this reaction, the disulfide spacer and 2-pyridyldithio group was introduced into CPP on the basis of the reaction between CPP's primary amine and SPDP's NHS ester. The degree of completeness of CPP activation was measured by the addition of DTT or other reducing agent. Reducing agents can release pyridine-2-thione (P2T) from the activated CPP (CPP-PDP) (Figure 13, scheme b), and the P2T concentration can be determined by measuring the absorbance at 343 nm. After activation, the CPP-PDP was mixed with CocE. The 2-pyridyldithio group of CPP-PDP reacted with the sulfhydryl group of CocE,

resulting in the conjugation of CPP and CocE by the disulfide spacer of SPDP (Figure 13, scheme c).

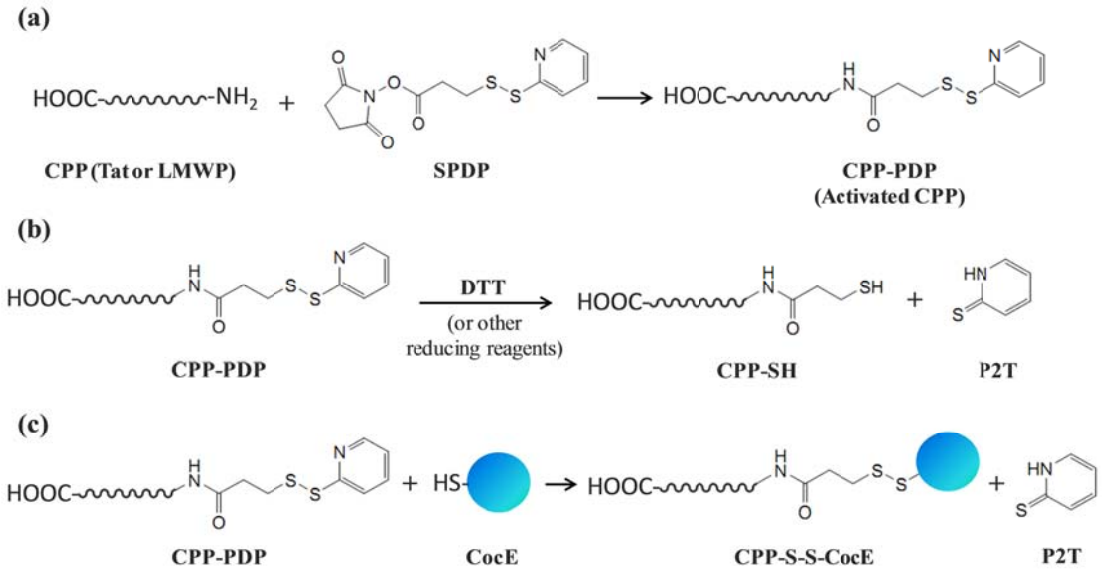

Figure 13 Chemical schemes to conjugate CPP and CocE by utilizing SPDP.

Expression and Purification of DMCocE

DMCocE was produced according to procedures described previously (21, 95) but with modifications. *E. coli* BL-21 (DE3) cells were transformed with pET22b(+)-CocE-T172R/G173Q plasmid, and then grown in 4-liter LB medium with 50 µg/ml of carbenicillin at 37°C. The expression of DMCocE was induced by the addition of 1 mM IPTG. After incubating for 12 h at 18 °C, the BL21 Star™ (DE3) cells were harvested by centrifugation at 4000 x *g* and 37°C for 30 min, and the cell pellets containing DMCocE were frozen at -80 °C overnight.

The harvested cell pellets containing DMCocE were resuspended in a purification buffer containing 50 mM Tris-HCl and 150 mM NaCl at pH 8.0, and then lysed with lysozyme (0.5 mg/ml) and Dnase (8 µg/ml) in the presence of 1mM $MgCl_2$. The histidine-tagged DMCocE was first enriched by Co^{2+} metal affinity chromatography using a Talon™ resin column (Clontech Laboratories Inc., Mountain View CA). After

being washed with 5 mM imidazole DMCocE was eluted with 100 mM imidazole in the aforementioned purification buffer (pH 8.0). The buffer fractions containing DMCocE were collected and then purified by Q-Sepharose anion-exchange chromatography using a Q-sepharose High Performance columm (GE Healthcare, Piscataway, NJ). DMCocE was eluted from the Q-Sepharose column with an NaCl linear gradient (Buffer A: 20 mM HEPES, 2 mM $_{MgCl2}$, 1 mM EDTA, 1 mM DTT, pH 7.4; Buffer B: 20 mM HEPES, 2 mM $_{MgCl2}$, 1 mM EDTA, 1 mM DTT, 1 M NaCl, pH 7.4). The peak fraction contained DMCocE with the purity of ~ 99%, which was determined by the SDS-PAGE analysis (described later). The fraction was then pooled and concentrated by using Amicon Ultra-15 centrifugal filter devices (molecular weight cut-off: 30,000 Da) (Millpore, Billerica, MA), snap frozen in liquid nitrogen, and then stored at −80 °C prior to use. All aforementioned procedures were carried out at 4 °C in presence of protease inhibitors (1 μM leupeptin and 5 μg/ml soybean trypsin inhibitor).

Activation of Tat and LMWP

To activate Tat and LMWP, a five molar excess of SPDP was dissolved in dimethyl sulfoxide (DMSO), and was then added drop-wise to a Tat or LMWP solution (5 mg/ml) prepared in a 0.1 M phosphate buffer, pH 8.0. The mixtures were reacted at room temperature for 2 hours with gently shaking. SPDP-activated Tat and LWMP, namely Tat-PDP and LMWP-PDP, were purified by FPLC on a heparin affinity column (GE Healthcare, Piscataway NJ), and eluted with a NaCl linear gradient (Buffer A: 50 mM Tri-HCl, pH 7.4; Buffer B: 50 mM Tri-HCl, 2 M NaCl, pH 7.4). Tat-PDP and LMWP-PDP were collected and then concentrated by ultrafiltration (molecular weight cut-off: 500 Da) (Spectrum Laboratories Inc., Rancho Dominguez, CA). The concentrations of purified Tat-PDP and LMWP-PDP were determined by monitoring P2T generation upon addition of DTT, and then the purified products were stored at −20 °C prior to use.

Preparation of LWMP-S-S-DMCocE and TAT-S-S-DMCocE chemical conjugates

To fully restore its surface sulfhydryl groups, before undergoing chemical conjugation, DMCocE was treated with DTT (10 mM) at 4 °C for 2 hours. The DTT in DMCocE solution was then removed by using Amicon Ultra-15 centrifugal filter devices

(molecular weight cut-off: 30,000 Da). For chemical conjugation, a three molar excess of Tat-PDP or LMWP-PDP was added into the DMCocE solutions, incubated at 4 °C for 12 hours, and then unreacted Tat-PDP/LMWP-PDP were removed by using Amicon Ultra-15 centrifugal filter devices (molecular weight cut-off: 30,000 Da). Tat-S-S-DMCocE and LMWP-S-S-DMCocE were then purified by heparin affinity chromatography; they were eluted from the heparin column with an NaCl linear gradient (Buffer A: 20 mM HEPES, 2 mM $MgCl_2$, 1 mM EDTA, 1 mM DTT, pH 7.4; Buffer B: 20 mM HEPES, 2 mM $MgCl_2$, 1 mM EDTA, 1 mM DTT, 2 M NaCl, pH 7.4). SDS-PAGE analysis was performed to determine the purity of Tat-S-S-DMCocE or LMWP-S-S-DMCocE in buffer fractions eluted from heparin columns. The two isolated CPP-CocE chemical conjugates were concentrated by using Amicon Ultra-15 centrifugal filter devices, snap frozen in liquid nitrogen, and then stored at −80 °C prior to use.

Biological Recombination

The schematic structures of four recombinant CPP-CocE fusion proteins produced in this dissertation are shown in Figure 14.

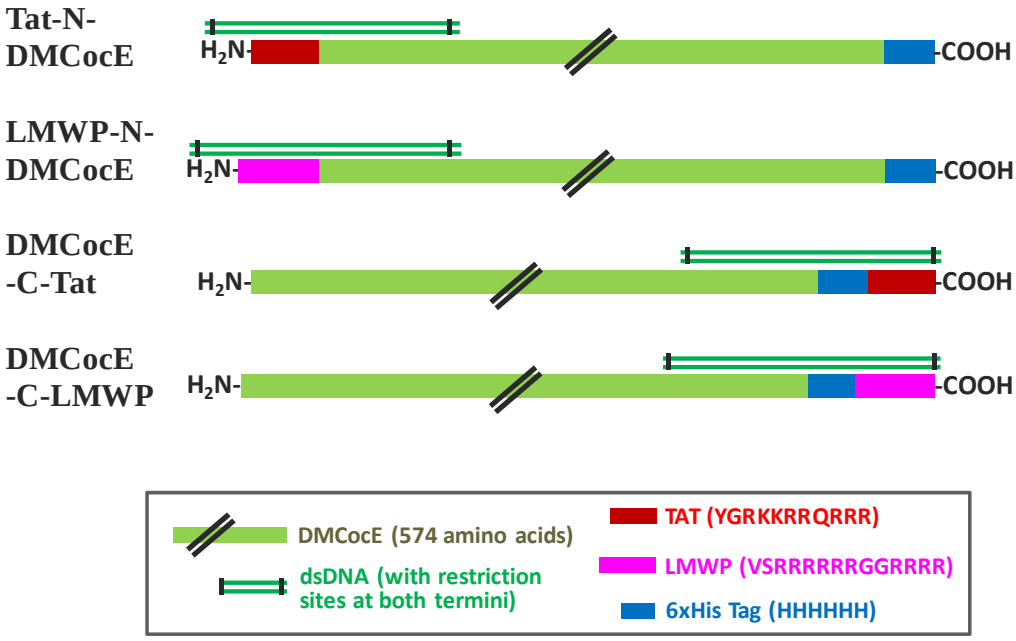

Figure 14 Schematic designs for four recombinant CPP-CocE fusion proteins. Double-stranded (ds) DNA fragments with restriction sites at both termini are generated by a polymerase chain reaction (PCR) to facilitate the insertion of CPP sequences; see the following paragraph for detailed explanation.

To construct the recombinant vectors expressing these four CPP-CocE fusion proteins, the DNA sequence encoding either Tat or LMWP needs to be inserted into either the N- or C-terminus of DMCocE. However, compared with the size of the bacterial vector expressing CocE (~7.1 kbp), the size of Tat and LMWP DNA sequences are much smaller (~50 bp). This significant difference in sizes between the CocE vector and the CPP sequences poses a challenge for DNA insertion. Therefore, in this dissertation, a two-step "indirect" insertion is applied to construct the recombinant vectors expressing CPP-CocE fusion proteins. The first step is to generate a double-stranded DNA with 400-600 base pairs, which encode CPP and part of the N- or C-terminal sequence of CocE (see Figure 14). This can be achieved by a PCR using an appropriate primer pair and the CocE vector as the template. Two restriction sites are also incorporated into the PCR product to facilitate the following DNA insertion. After confirming the PCR is successful, the second step is to amplify the CPP-encoding PCR product in a TOPO® vector. TOPO® vector is a linearized bacterial vector with

topoisomerase I covalently bound to each 3′ end, causing it readily to ligate theoretically any double-stranded DNA sequences ending with adenine (A) and form a recombinant circular plasmid. Therefore, the CPP-encoding PCR product can easily be cloned into a TOPO™ vector and amplified in a large amount. Finally, the third step is to treat the CocE vector, as well as the recombinant TOPO® vector bearing the CPP insert, with selected restriction enzymes. Restriction enzymes recognize a specific DNA sequence and cut the double-stranded DNA, generating an overhang "sticky" with complementary sequences. After being treated with restriction enzymes, the digested CocE vector and CPP insert (cut from the recombinant TOPO™ vector) can be annealed and ligated together, and form a complete recombinant vector ready to express a CPP-CocE fusion protein in *E. coli*.

Site-directed Mutagenesis

Since there is no appropriate restriction site in the C-terminal region of DMCocE, a BamHI restriction site was introduced at the end of DMCocE's C-terminal 6-histidine tag by Phusion® site-directed mutagenesis kit. One DNA primer was used to introduce mutation (with mutated codon in lowercase and BamHI site underlined): 5'-CCACCAC CACCACTagGATCCGGCTGCTAACAAAGC-3'. After the mutagenic PCR, the original pET22b(+)-CocE-T172R/G173Q plasmid was digested with the DNA restriction enzyme DpnI, which cuts only the DNA generated by bacteria (*i.e.* original plasmid), leaving the DNA generated from PCR (*i.e.* mutated plasmid) intact. Incorporation of mutations was confirmed by BamHI digestion and DNA sequencing (the DNA sequencing Core, University of Michigan). The mutated pET22b(+)-CocE-T172R/G173Q plasmid with one BamHI restriction site was then transformed into DH5α competent cells and amplified for the following DNA recombination.

Construction of vectors for recombinant CPP-DMCocE expression

The double-stranded DNA fragments encoding Tat or LMWP attached on either N-terminus or C-terminus of DMCocE were generated by PCR using the mutated pET22b(+)-CocE-T172R/G173Q vector (see *Site-directed Mutagenesis* in this section) as

a template. The DNA primers used for CPP-DMCocE constructions are listed below (with mutated codon in lowercase):

Table 2 Primers used for the construction of recombinant CPP-DMCocE vectors.

CPP-DMCocE Fusion Proteins	**Forward Primer**	**Backward Primer**
Tat-N-DMCocE	GAGATATACATATGtacggaagaaagaa gagaaggcaaagaaggagaggaGTGGACGG GAATTACAGTGTTGCC	GAGAATTGCTGCGAGTTG
LMWP-N-DMCocE	ATACATATGgtatcaagaaggagaaggagaa ggggaggtagaaggagaaggggaGTGGACG GGAATTACAGTGTTGCC	
DMCocE-C-Tat	AAGTAACCGGCACCGTCTCCGCC CGGCTGTTCGTGTC	AGCCGGATCCTAtctccttctttgccttctctt ctttcttccgtatccGTGGTGGTGGTGGTG GTGC
DMCocE-C-LMWP		AGCCGGATCCTAccttctccttctacctcccc ttctccttctccttcttgatactccGTGGTGGTG GTGGTGGTGC

After being cloned into TOPO™ vectors by using the pEXP-5-NT/TOPO® TA Expression Kit, the four recombinant TOPO™ vectors containing the CPP-encoding PCR product were transformed into DH5α competent cells and were amplified. Next, these four recombinant TOPO™ vectors, as well as the mutated pET22b(+)-CocE-T172R/G173Q vector (with a BamHI restriction site), were digested with two DNA restriction enzyme pairs: NdeI/NcoI (for generating Tat-N-DMCocE and LMWP-N-DMCocE) and KpnI/BamHI (for generating DMCocE-C-Tat and LMWP-C-DMCocE). The digested PCR products were then ligated into the mutated pET22b(+)-CocE-T172R/G173Q vector. All four resulting recombinant vectors were sequenced in both directions over the entire coding region. After their sequences were confirmed, these four recombinant vectors were transformed into *E. coli* BL-21 (DE3) cells for the expression of CPP-DMCocE fusion proteins.

Expression and purification of TAT-DMCocEs and LMWP-DMCocEs

The expression and purification scheme used for preparing DMCocE were also utilized to produce CPP-DMCocE fusion proteins (Tat-N-DMCocE, LMWP-N-DMCocE,

DMCocE-C-Tat, and DMCocE-C-LMWP). Detailed procedures have been described previously in this section and therefore will not be repeated here.

3.2.3 *In vitro* Characterization

SDS-PAGE Analysis

Buffer fractions eluted from a heparin affinity column (in chemical conjugates purification) and from Talon™ and Q-sepharose columns (in fusion proteins purification) were analyzed by SDS-PAGE to determine the product purity. Gels were stained with coomassie blue, and the images were processed with ImageJ (National Institutes of Health, Bethesda, MD).

Protein Assay

For all chemical/biological CPP-CocE variants, the protein concentration was determined by a Bradford protein assay after each purification step and immediately before the cocaine hydrolyzing activity study. Bovine serum albumin (BSA) was used as a standard because its molecular weight is similar to that of CocE (~65 kDa). Each protein sample was done in triplicate with at least three independent dilutions ($n \geq 3$).

Cocaine Hydrolyzing Activity Assay

Cocaine hydrolysis was measured by a modification of the real-time spectrophotometric assay originally developed by Larsen *et al*. (12). Cocaine hydrolyzing reaction was performed in a UV-transparent 96-well microplate, and initiated by adding 100 µl of CPP-CocE solutions to 100 µl cocaine solutions. The final concentration of CPP-CocE solutions was 50 ng/ml. Final cocaine concentrations were 1, 2.5, 5, 10, 25, 50, 100, and 250 µM. CPP-CocE and cocaine solutions were prepared in phosphate-buffered saline (PBS) at pH 7.4 (137 mM NaCl, 2.7 mM KCl, 10 mM sodium phosphate dibasic, and 2 mM potassium phosphate monobasic, pH of 7.4). The initial rate of cocaine hydrolysis was determined by monitoring the change in absorbance at 240 nm, where the difference in molar absorptivity between cocaine and its metabolites (ecgonine methyl ester and benzoic acid) was 6,700 M^{-1} cm^{-1} (96). Absorbance at 240

nm was modified at 15-second time points over 30 min by using a PowerWave XS microplate spectrophotometer (Biotek Instruments, Inc., Winooski, VT). All experiments were done in triplicate.

In vitro Stability at 37 °C

The *in vitro* thermal stability of different CPP-CocE fusion proteins was monitored by measuring the change in the cocaine hydrolysis rate. CPP-CocE fusion proteins (100 ng/ml) in PBS (pH 7.4) were incubated at 37 °C, and aliquots were taken at different time points (0.5, 1, 2, 3, 4, 6, 8, 10, and 12 hours). The remaining cocaine-hydrolyzing activity of the aliquots was assayed as described previously. All experiments were done in triplicate with at least three independent measurements ($n \geq 3$).

Data Analysis

Data analysis and curve-fitting were conducted by using Prism 5 (GraphPad Software, San Diego CA). For the cocaine hydrolyzing activity assay, the Michaelis-Menten equation was used in curve fitting:

$$y = \frac{E_t \cdot k_{cat} \cdot x}{K_M + x} \quad (1)$$

Cocaine concentration (x) and the initial cocaine-hydrolysis rate (y) was fitted to this equation with k_{cat} and K_M as adjustable parameters. k_{cat} refers to the turnover rate, which is the number of times each enzyme site converts the substrate to product per unit time. K_M is the Michaelis-Menten constant, representing the substrate concentration needed to achieve a half-maximum enzyme velocity. E_t is the concentration of enzymatic catalytic sites. For enzymes with one catalytic site per molecule (*e.g.* CocE, all chemical/biological variants of CPP-CocE), E_t equals the enzyme concentration.

In the results of the cocaine hydrolyzing activity assay, the values of k_{cat} and K_M were represented as means ± S.D. Enzyme specific activity and maximal velocity (V_{max}), another two major parameters for evaluating enzyme activity, were converted from k_{cat}:

Specific activity (the activity of an enzyme per milligram of total protein, usually expressed in μmol·min^{-1}·mg^{-1}, *i.e.* U/mg)

$$= k_{cat}(min^{-1}\ or\ sec^{-1}) \times \left(\frac{10^6(\mu mol)}{enzyme\ molecular\ weight \times 10^3(mg)}\right) \quad (2)$$

$$V_{max} = k_{cat} \times E_t \quad (3)$$

The ratio of $\frac{k_{cat}}{K_M}$ was also calculated as an index of cocaine-hydrolyzing efficiency. In the comparison of enzymes sharing the same substrate and catalytic mechanism (*e.g.* CocE, and all chemical/genetic variants of CPP-CocE), a higher $\frac{k_{cat}}{K_M}$ represents an increasing k_{cat} (a higher catalytic power) or a decreasing K_M (a higher affinity of the enzyme towards the substrate). These two criteria lead to a better enzyme efficiency (97).

For the analysis of *in vitro* stability at 37 °C, the apparent k_{cat} ($k_{cat,\ app}$) and K_M ($K_{M,\ app}$) of each incubated aliquot was determined by the Michaelis-Menten equations described in the previous paragraph. The ratio of $\frac{k_{cat,app}}{K_{M,app}}$, which reflects the apparent cocaine-hydrolyzing "effectiveness" of each incubated aliquot, was evaluated as a percentage of the $\frac{k_{cat}}{K_M}$ value of the non-incubated CPP-CocE fusion proteins. Many chemical and biological reactions follow a single-phase exponential decay in which reaction properties (*e.g.* amount, concentration) decrease at a rate proportional to its value. Therefore, the single-phase exponential decay was selected for fitting the *in vitro* enzyme efficiency decay with incubation time:

$$y = (y_0 - plateau) \cdot e^{-kx} + plateau \quad (4)$$

Incubation time (x) and the remaining cocaine-hydrolyzing efficiency (y) were fitted to this equation with k and plateau as adjustable parameters. In this equation, k is the rate constant, and the plateau is the y value at infinite time. y_0 is the y value when x is zero, and set to 100 in this *in vitro* stability study. Another two kinetic parameters derived from the rate constant, half-life ($t_{1/2}$) and mean residence time (MRT), can be utilized to assess the rates of activity decay more intuitively. Specifically, $t_{1/2}$ is the time

it needs for an activity to decrease by half, and it is computed as $\frac{ln2}{k}$. MRT is the average duration that a CPP-CocE variant molecule remains active, and is computed as $\frac{1}{k}$.

3.3 Results and Discussion

3.3.1 Construction of CPP-Attached CocE Variants (CPP-CocEs)

Production and Purification of CPP-CocE Chemical Conjugates

Theoretically, two types of functional groups in CocE can be used in the chemical conjugation for attaching CPP: (1) primary amines at the N-terminus and lysine residues, and (2) sulfhydryl groups at cysteine residues. According to information published in the literature, CocE (and DMCocE) has nine primary amine groups and four sulfhydryl groups (12, 98). Since modification on the primary amine groups of DMCocE would lead a loss of its enzymatic activity (98), the chemical conjugation scheme utilizing the sulfhydryl groups of DMCocE was selected in this dissertation.

Two disulfide-bridged chemical conjugates, Tat-S-S-DMCocE and LMWP-S-S-DMCocE, were synthesized by using a heterobifunctional cross-linker SPDP. The elution profile (Figure 15) indicated that both of these two chemical CPP-CocE conjugates could be purified by heparin affinity chromatography. In absence of the CPP group, the unreacted DMCocE displayed no binding affinity to the heparin column, and eluted before the salt gradient started. In contrast, Tat-S-S-DMCocE and LWMP-S-S-DMCocE bound to the heparin column and eluted at ~0.8 M or higher concentrations of NaCl, suggesting that these two CPP-CocE chemical conjugates bind strongly to the heparin column.

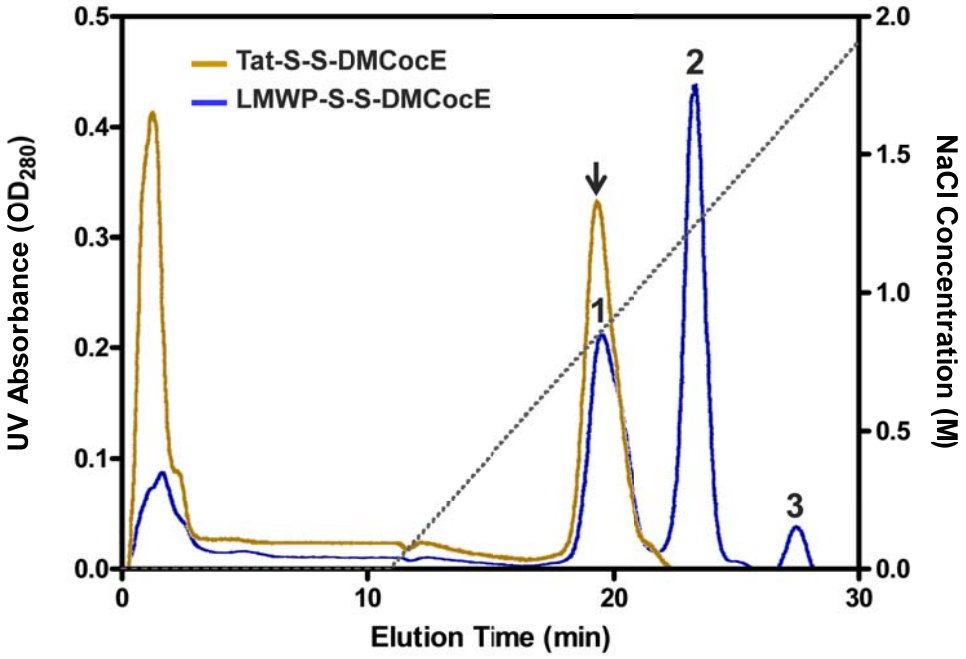

Figure 15 Chromatograms of Tat-S-S-DMCocE (yellow line) and LMWP-S-S-DMCocE (blue line) in a heparin column. NaCl concentration applied in elution is shown in dashed line. Tat-S-S-DMCocE (indicated in arrow) eluted at 0.75 M NaCl, whereas LMWP-S-S-DMCocE eluted in three peaks at 0.8 (peak #1), 1.2 (peak #2), and 1.6 M (peak #3) of NaCl. Unreacted DMCocE eluted at the beginning without NaCl.

Another interesting observation from the heparin chromatogram is that, during the chemical conjugation reaction between LMWP-PDP and DMCocE, at least three variants of LWMP-S-S-DMCocE with different numbers and/or locations of LMWP were generated. Based on its backbone and three-dimensional structure (12), each CocE (and DMCocE) molecule has four sulfhydryl groups, and three of them are on the surface and more accessible to chemical conjugation. Moreover, LMWP is known to have a strong binding affinity to a heparin column (93). Thus, it is rational to anticipate that these three LMWP-S-S-DMCocE variants eluting at 0.8, 1.2, and 1.6 M NaCl have one, two, and three LMWP groups conjugated on each DMCocE molecule. However, this expectation needs to be proved by an assay which can accurately identify the exact molecular weight for fragile macromolecules, such as Matrix-Assisted Laser Desorption/Ionization-Time-Of-Flight mass spectra (MALDI-TOF MS). On the other hand, only one variant of Tat-

S-S-DMCocE was formed during the chemical conjugation reaction between Tat-PDP and DMCocE, and the ratio of unreacted DMCocE in this conjugation reaction was shown to be higher than that in the LMWP-S-S-DMCocE conjugation reaction. One possible explanation would be that, according to their amino acid composition, Tat has a lower isoelectric point (pI) value (12.7) than LMWP (13.5). At pH 7.4, Tat is presumably less positively-charged comparing to LMWP, and therefore would present a weaker electrostatic attraction with the negatively-charged CocE (pI ~4.7). Since the electrostatic attraction between CPP and CocE could facilitate the chemical conjugation afterwards, the weaker interaction between Tat and CocE might explain the lower efficiency of the TAT-S-S-DMCocE conjugation, which generated fewer variant and a higher ratio of unreacted DMCocE, compared to that of the LMWP-S-S-DMCocE conjugation.

Table 3 shows the production and purification of CPP-DMCocE chemical conjugates. The amount of chemical conjugate produced from 16 mg DMCocE is 3.9 mg in LMWP-S-S-DMCocE, and 1.05 mg in Tat-S-S-DMCocE. For LMWP-S-S-DMCocE, that amount equals 18.5% of yield in activity. The yield in activity of Tat-S-S-DMCocE was not determined as the amount was insufficient for cocaine-hydrolyzing activity assay.

Table 3 Purification of CPP-DMCocE chemical conjugates. For LMWP-S-S-DMCocE, #1-#3 refers to the three forms isolated by a heparin affinity column (see Figure 15).

		Total Protein (mg)	**Specific Activity** (U/mg)	**Total Activity** (U)	**Yield** (%)
DMCocE (Reactant)		15.83	41.40	655.36	100
Tat-S-S-DMCocE		1.05	Not Determined		
LMWP-S-S-DMCocE	**#1**	1.13	36.74	41.44	18.5
	#2	2.10	28.05	58.78	
	#3	0.67	30.95	20.74	

These two CPP-DMCocE chemical conjugates created in this dissertation have a major advantage owing to their disulfide linkage. Since disulfide bond is cleavable under a mild reductive condition, once the disulfide-bridged CPP-DMCocE conjugates enter the reductive intracellular environment, the linkage between the CPP and its coupled DMCocE molecule will be rapidly cleaved, resulting in the release of DMCocE. This "detachable" behavior of CPP can minimize any potential interference from CPP, and therefore maintain the enzymatic activity of DMCocE. More importantly, without the coupled CPP group, CocE itself is not cell permeable and will be permanently entrapped inside the cells. Thus, the CPP detachment can prevent the backward translocation of DMCocE from the cytoplasm to the extracellular environment, and guarantee the effectiveness of cell encapsulation.

Despite the advantage of detachable CPPs, however, this disulfide-bridged CPP-DMCocE conjugates have two major limitations. First, since activated CPP can randomly attach any one of the three surface sulfhydryl groups, this causes differences in the CPP locations and numbers on each CPP-DMCocE conjugates. Apparently, according to the elution profile from a heparin affinity column (Figure 15), three forms of LWMP-S-S-DMCocE with different numbers and/or locations of LMWP were generated in this chemical conjugation. Second, because not all of the reactants (CPP and DMCocE) could be converted to the desired products (CPP-DMCocE conjugates), an additional purification process afterwards was required to separate CPP-CocE conjugates from unreacted CPP/CocE. These aforementioned limitations would not apply only to the disulfide-bridged CPP-CocE conjugates in this dissertation, but also potentially to all CPP-DMCocE products derived from chemical conjugation strategy. In contrast, CPP-DMCocE products created in a genetic recombination strategy, which are discussed in next section, did not have these limitations.

Production and Purification of CPP-CocE Fusion Proteins

Four recombinant vectors derived from pET22b(+)-CocE-T172R/G173Q were developed for expression and purification of four CPP-CocE fusion proteins in *E. coli*. pTat-N-DMCocE (Figure 13, a) and pLMWP-N-DMCocE (Figure 13, b) contained the Tat or LMWP sequence on the N-terminus of DMCocE. In contrast, pDMCocE-C-Tat (Figure 13, c) and pDMCocE-C-LMWP (Figure 13, d) included the Tat or LMWP sequence on the C-terminus (after the exogenous 6-histidine tag) of DMCocE. An additional glycine (Gly) residue was inserted between CPP and DMCocE (for pTat-N-DMCocE and pLWMP-N-DMCocE) or the C-terminal 6-histidine tag (for pDMCocE-C-Tat and pDMCocE-C-LMWP) as a spacer facilitating a free bond rotation of CPP groups.

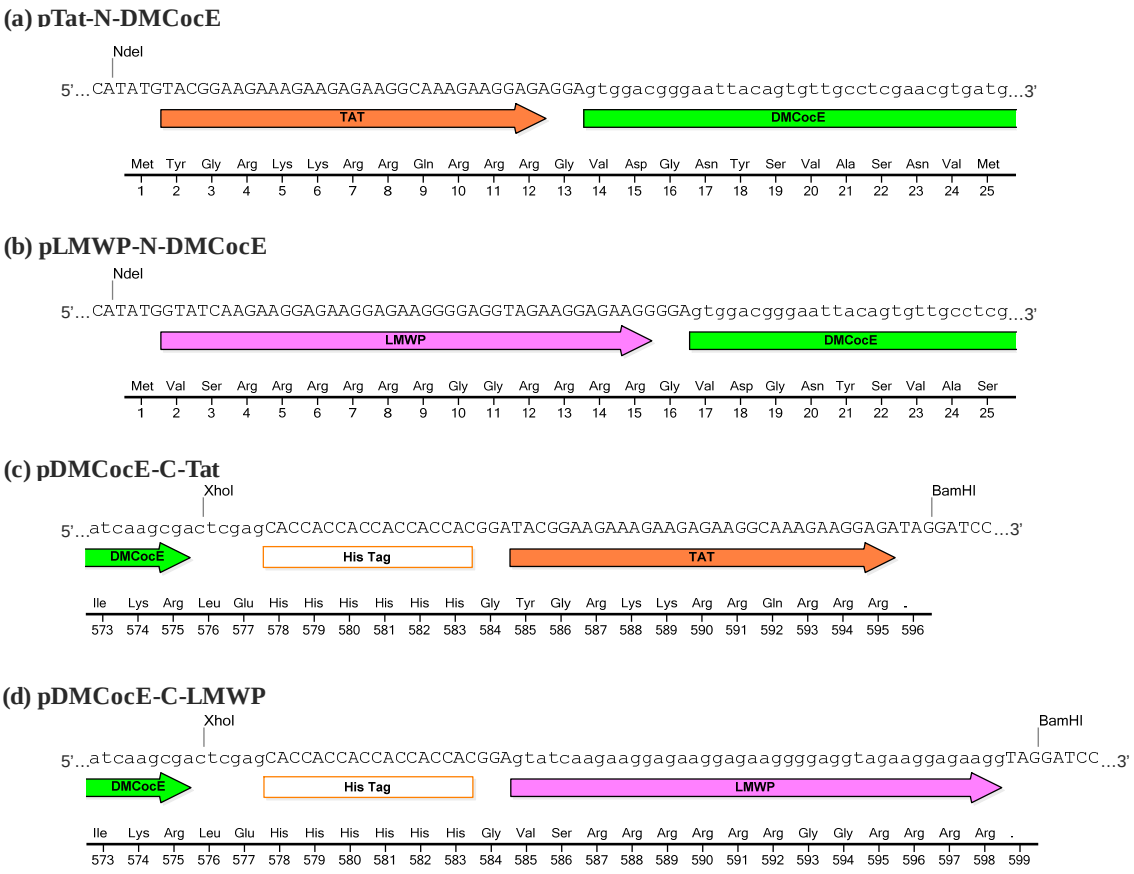

Figure 16 Schematic maps of DNA sequences in the N-terminal (a, b) or C-terminal (c, d) expression regions of recombinant vectors of four CPP-CocE fusion proteins. Except BamHI sites, all other restriction sites (NdeI, XhoI) are from the parental plasmid pET22b(+)-CocE-T172R/G173Q.

These four CPP-CocE fusion proteins were able to be expressed as soluble and histidine-tagged proteins in *E. coli*; only a small amount was insoluble and found in the pellet of cell lysate (Figure 17). Most CPP-CocE fusion protein did not appear in the flow-through or in the wash buffer containing 5 μM imidazole, indicating that the binding affinity between the 6-histidine tag and the Co^{2+} metal ion in the Talon™ column was not damaged by the addition of CPP groups. However, there was still a small fraction in the wash fractions of Tat-CocE fusion proteins (Tat-N-DMCocE and DMCocE-C-Tat). This may due to the interference of the Tat group on the 6-histidine tag, or the high protein expression level exceeding the total column binding capacity.

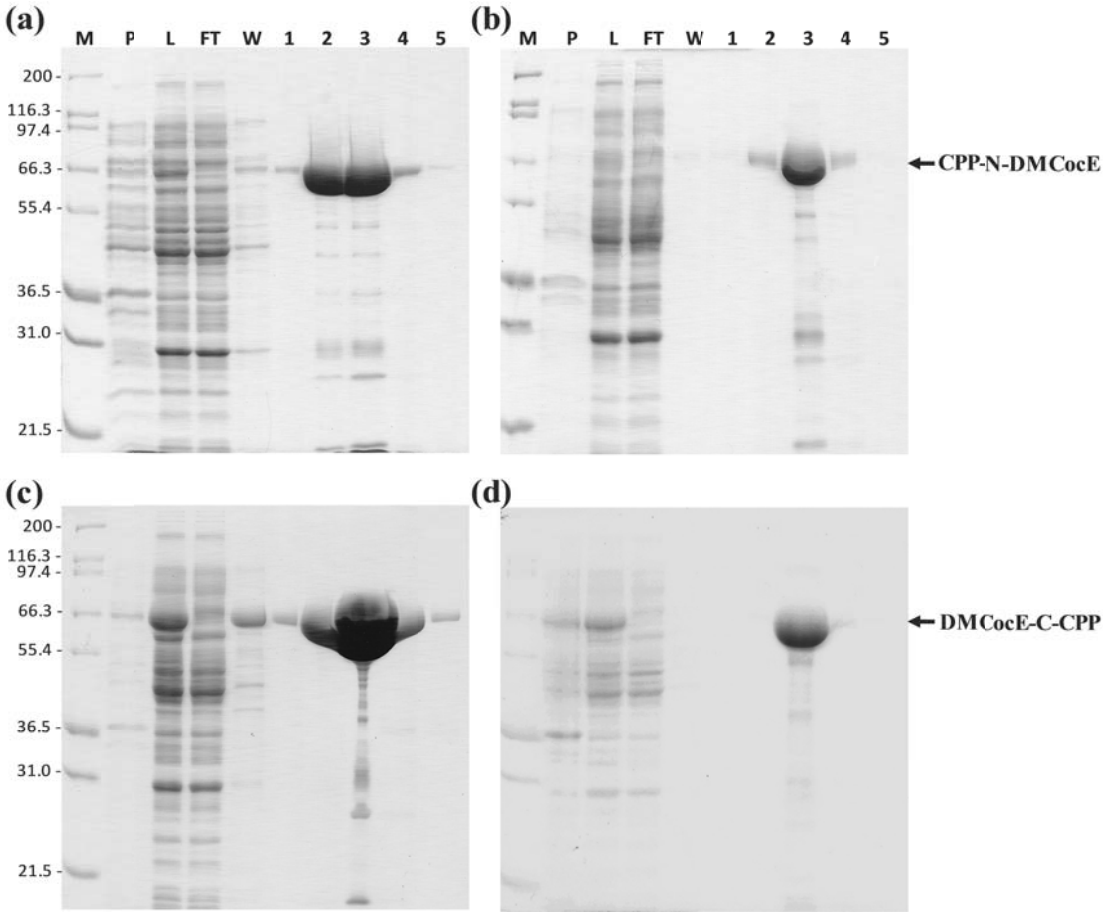

Figure 17 SDS-PAGE analysis of expression and purification of four CPP-DMCocE fusion proteins. Lane M: Mark12™ protein molecular weight standard; lane P: the pellet fraction of cell lysate; lane L: the supernatant fraction of cell lysate; lane FT: flow-through fraction; lane W: wash fraction; lane 1-5: elution fraction containing DMCocE. Lane FT to 5 were obtained after passing through from the Talon™ column.

Contaminants in the crude extract of the four CPP-CocE fusion proteins from a Talon™ column could be further separated by Q-Sepharose anion-exchange chromatography. After Q-sepharose purification, the purity of CocE was at least 99%, which was determined by the image analysis of SDS-PAGE results.

The recovery of four CPP-DMCocE fusion proteins in each purification step is shown in Table 4. Similar to the expression of DMCocE in *E. coli* (data not shown), approximately 700 mg of total soluble protein was produced from the cultures expressing CPP-CocE fusion proteins. Since it is known that DMCocE is non-toxic to *E. coli*, this result suggests that CPP-CocE fusion proteins are also not toxic or harmful to *E. coli*, because the expression of these fusion proteins did not decrease the production of the total soluble bacterial proteins. The CPP-CocE fusion protein produced in the highest mass quantity (mg) is DMCocE-C-Tat (73 mg), followed by Tat-N-DMCocE (33 mg), DMCocE-C-LMWP (10 mg), then LMWP-N-DMCocE (7 mg). The amount of CPP-CocE fusion proteins accounts for 1-10% of the total soluble proteins in *E. coli*.

Table 4 Purification of recombinant CPP-CocE fusion proteins from the culture supernatant of *E. coli*.

CPP-CocE Fusion Proteins	Fraction	Total Protein (mg)	Total Activity (U)	Specific Activity (U/mg)	Yield %
Tat-N-DMCocE	Cell Lysate Supernatant	720.6	1421.3	2.0	100
	Co-Sepharose CL (Talon)	34.8	1006.1	28.9	70.8
	Q-Sepharose HP	32.7	985.9	30.1	69.4
LMWP-N-DMcocE	Cell Lysate Supernatant	758.7	286.3	0.4	100
	Co-Sepharose CL (Talon)	8.0	239.4	29.9	83.6
	Q-Sepharose HP	7.3	231.9	31.8	81.0
DMCocE-C-Tat	Cell Lysate Supernatant	727.9	3494.5	4.8	100
	Co-Sepharose CL (Talon)	75.8	2398.9	31.6	68.6
	Q-Sepharose HP	73.3	2379.4	32.5	68.1
DMCocE-C-LMWP	Cell Lysate Supernatant	704.1	371.5	0.5	100
	Co-Sepharose CL (Talon)	10.6	300.4	28.3	80.9
	Q-Sepharose HP	10.3	299.3	29.0	80.6

The first purification step, Co^{2+} metal affinity chromatography, successfully enriched the CPP-CocE fusion proteins in the cell lysate supernatant. From the initial cell lysate supernatant to the Talon™ column eluate, the specific activity of cocaine hydrolysis increased from < 5 to approximately 30 U/mg, indicating an at least six-fold increase. However, a major protein loss also happened in the Co^{2+} metal affinity chromatography. For LMWP-N-DMCocE and DMCocE-C-LMWP, the yields from the cell lysate supernatant were 83.6 % and 80.9 %, representing approximately a 20 % loss of the initial activity of LMWP-CocE fusion proteins. Since no LMWP-CocE fusion proteins eluted in the wash buffers from the Talon™ column (see Figure 17), the protein lost at the Co^{2+} metal affinity chromatography was assumed to elute in the beginning flow-through buffer. For Tat-N-DMCocE and DMCocE-C-Tat, the yields from the cell lysate supernatant were 70.8 % and 68.6 %. These were lower than the yield of LMWP-N-DMCocE and DMCocE-C-LMWP, indicating approximately 30% loss of the initial activity of Tat-CocE fusion proteins in this purification step. For these two Tat-CocE fusion proteins, in addition to the eluted fraction in flow-through buffers, the protein loss could be also attributed to the wash-out from the wash buffer, based on the observation in the SDS-PAGE analysis (see Figure 17).

The second purification step carried out by Q-Sepharose anion-exchange chromatography was applied to separate the impurities co-eluting with the CPP-CocE fusion proteins. According to Table 4, the recovery from the Talon™ column eluate to the Q-sepharose chromatography was at least 97%, and the specific enzyme activity was further increased 2-5%. After the Q-sepharose purification step, CPP-CocEs was at least 99% (determined by SDS-PAGE analysis). More importantly, after the Q-Sepharose anion-exchange purification step, all of the four CPP-DMCocE fusion proteins showed a specific activity around 30 U/mg. This consistent specific activity among the four fusion proteins implicated that the purification scheme works consistently. Moreover, the percentage yield after purification was supposed to higher because of the higher initial mass quantity, which is independent with purification process.

Lastly, according to the yields in mass quantity of all four CPP-CocE fusion proteins, these proteins showed a significantly lower production yield (7-73 mg) compared with native DMCocE (~350 mg, data not shown). More interestingly, the C-terminal, Tat-attached CPP-DMCocE variants showed higher production yield compared with the N-terminal, LMWP-attached variants. As discussed in last paragraph, the amount of total soluble protein remained constant from the cultures expressing either DMCocE or CPP-DMCocE fusion proteins. Thus, it is unlikely that the CPP-DMCocE fusion proteins are toxic or harmful to *E. coli* and decrease the overall protein expression. The most possible explanation for the different expression levels among DMCocE and CPP-DMCocEs could be the codon usage bias in *E. coli*. Both Tat and LMWP are composed of a cluster of arginine and lysine, which are encoded in the rare codons in *E. coli* and translated much slower than other amino acids (99-101). Thus, incorporation of Tat or LMWP could hamper the overall expression of CPP-CocE fusion proteins, leading to a lower production yield of the CPP-DMCocE fusion proteins (99). The CPP interference could be even more pronounced when these arginine/lysine-rich sequences are inserted at the N-terminus (102), where the protein translation starts.

Generally speaking, the biological recombination strategy provides a better control of the CPP numbers and locations on a CPP-DMCocE fusion protein, as its primary structure is exactly encoded in its DNA sequence. Despite this advantage, however, a major limitation of CPP-DMCocE fusion proteins must be addressed. CPP sequence can only be expressed in tandem, *i.e.*, at the beginning (N-terminus) and the end (C-terminus) of the DMCocE sequence. According to its three-dimensional structure (see Figure 1), the two termini of DMCocE are exposed outside the surface and away from the enzyme catalytic center. Therefore, for all CPP-DMCocE fusion proteins created in this dissertation, the incorporated CPP groups are supposed to neither be buried inside, which could lead to reduced or no cellular uptake, nor to destroy CocE's enzymatic activity. This proposition has been supported by the elution profile from a heparin affinity column (Figure 18) and the enzyme kinetics (Table 5), which will be discussed in detail later. On the other hand, the best cell host and conditions for expressing most CPP fusion proteins can only be determined empirically. If a CPP fusion protein is expressed with a low yield

or in an inactive/insoluble form, it is necessary to modify the expression conditions or transfer the CPP fusion gene to another expression cell host. Fortunately, *E. coli* expression system established for CocE and its thermally stable variants (12, 21) is also applicable to generate CPP-CocE fusion proteins in a soluble form.

3.3.2 *In vitro* Characterization of CPP-CocEs

Binding Affinity to a Heparin Column

Tat-S-S-DMCocE and LMWP-S-S-DMCocE, two chemical CPP-CocE conjugates, have shown a strong binding affinity to a heparin column previously (see Figure 15), and thus the results are not repeated here. As for Tat-N-DMCocE and DMCocE-C-Tat, the elution chromatogram (Figure 18) indicated that these two Tat-CocE fusion proteins were also able to bind a heparin affinity column, and did not elute until at approximately 1 M NaCl. These results suggest that the Tat attaching to either N- or C- terminus of DMCocE is not buried inside the enzyme, and therefore it can bind strongly to the heparin column. Unlike Tat-DMCocE fusion proteins, native DMCocE showed no binding affinity to the heparin column and eluted before the salt gradient. In summary, the binding affinity of CPP-DMCocE fusion proteins to a heparin column indicates that the CPP groups are exposed on the enzyme surface, which is favorable for the interaction with the negatively charged extracellular proteins and facilitates cellular uptake.

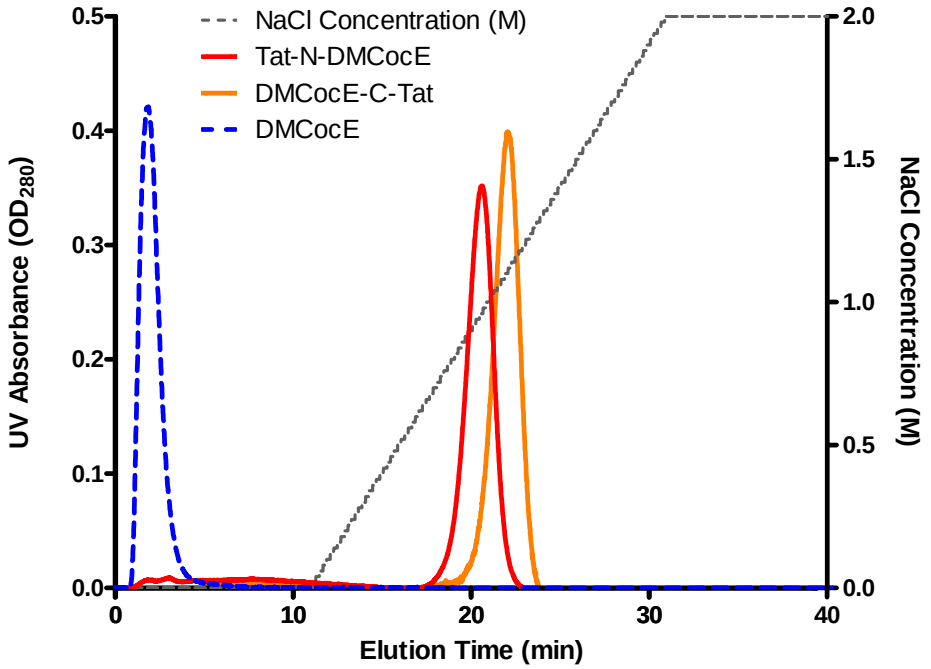

Figure 18 Chromatograms of Tat-N-DMCocE (red line) and DMCocE-C-Tat (orange line) in a heparin column. NaCl concentration applied in elution is shown in dashed line. Tat-N-DMCocE eluted at 0.9 M NaCl, whereas DMCocE-C-Tat eluted at 1.2 M NaCl. As a reference, DMCocE (dashed blue line) eluted at the beginning without NaCl.

Cocaine Hydrolyzing Activity

The specific cocaine hydrolyzing activity of the disulfide-bridged LMWP-S-S-DMCocE chemical conjugate, as well as the four CPP-DMCocE fusion proteins, is shown in Table 5. The three types of LMWP-S-S-DMCocE chemical conjugates have cocaine-hydrolyzing efficiency slightly lower to that of native DMCocE. In contrast, compared with native DMCocE, the four fusion proteins show a ~50% reduction of cocaine-hydrolyzing efficiency. The reduction of cocaine-hydrolyzing activity in the CPP-DMCocE fusion proteins results from their slightly lower k_{cat}, and significantly higher K_M (ranging from 30% to 70% of increase) compared with native DMCocE. Among these fusion proteins, Tat-N-DMCocE has the lowest K_M, and therefore possesses the highest affinity towards cocaine as well as the highest cocaine-hydrolyzing efficiency ($\frac{k_{cat}}{K_M}$).

To sum up, although attaching Tat or LMWP on DMCocE does not abolish the enzyme activity, this attachment still reduce the binding affinity (*i.e.* increase the K_M value) of CocE to its substrate cocaine. The reduction in substrate binding affinity of CPP-attached DMCocE variants could be attributed to the electrostatic interaction between cocaine and Tat/LMWP at a physiological pH. At pH 7.4, both cocaine and Tat/LMWP are positively charged, thus the presence of Tat or LMWP could have a repulsive interaction with cocaine and interfere the initial collision between cocaine molecule and the CocE catalytic center. Moreover, compared with native DMCocE, all LMWP-S-S-DMCocE chemical conjugates displayed less reduction in the enzymatic activity than that of CPP-DMCocE fusion proteins, including the two LMWP-DMCocE variants. Since the sulfhydryl groups potential for LMWP conjugation are known to be away from CocE's catalytic center (13, 98), it suggests that the location might be more influential than the number or type of the attached CPP groups on CocE functionality.

Table 5 Kinetic parameters of CPP-CocE variants for cocaine hydrolysis.

CocE Variants		k_{cat} (min^{-1})	K_M (μM)	k_{cat}/K_M ($min^{-1}\mu M^{-1}$)	37 °C, 12 hour $k_{cat,app}$ (min^{-1})	37 °C, 12 hour $K_{M,app}$ (μM)	37 °C, 12 hour $k_{cat,app}/K_{M,app}$ ($min^{-1}\mu M^{-1}$)
DMCocE		2691 ± 77	28.76 ± 2.6	93.6			
LMWP-S-S-DMCocE	**#1**	2388 ± 216	32.84 ± 8.9	72.7	Not Determined		
	#2	1823 ± 56	23.44 ± 2.4	77.8			
	#3	2012 ± 79	25.42 ± 3.2	79.2			
CPP-CocE Fusion Proteins	Tat-N-DMCocE	1957 ± 38	39.59 ± 2.2	49.4	1972 ± 71	69.84 ± 6.2	28.2
	LMWP-N-DMCocE	2065 ± 32	49.04 ± 2.0	42.1	651 ± 59	159.20 ± 27.5	4.1
	DMCocE-C-Tat	2110 ± 45	44.79 ± 2.5	47.1	707 ± 81	114.20 ± 27.8	6.2
	DMCocE-C-LMWP	1887 ± 41	41.47 ± 2.1	45.5	1043 ± 273	518 ± 186.5	2.0

In vitro Stability at 37 °C

The *in vitro* stabilities at 37 °C of the four CPP-DMCocE fusion proteins were assessed by monitoring their apparent cocaine-hydrolyzing "effectiveness" $\frac{k_{cat,app}}{K_{M,app}}$ over time (Figure 19, Table 6). The attachment of CPP groups had different impacts on the stability of each CPP-CocE fusion protein. Compared with native DMCocE, the two C-terminal CPP-CocEs (Tat-C-DMCocE and LMWP-C-DMCocE) were less stable, whereas LMWP-N-DMCocE possessed a half-life and MRT similar to those of DMCocE. Interestingly, Tat-N-DMCocE showed a prolonged half-life and MRT; which was 1.3-fold higher compared to those of DMCocE, and comparable to the most stable CocE variant known to date (22). Based on an additional *in vitro* stability study with prolonged time points, Tat-N-DMCocE still possessed 52% of cocaine-hydrolyzing efficiency after incubation at 37 °C for 24 hours (data not shown).

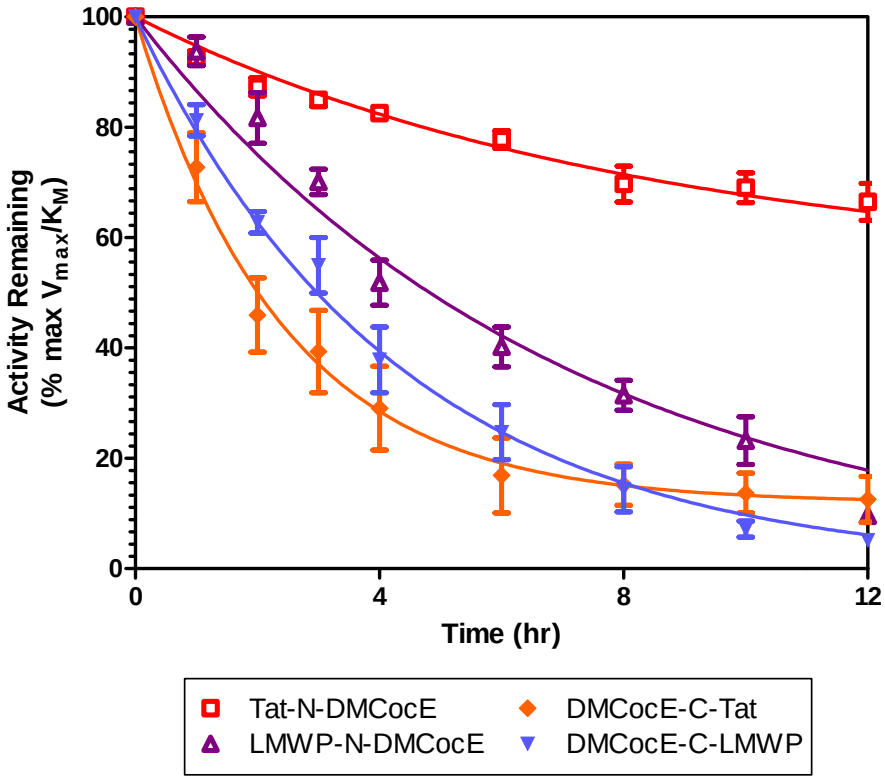

Figure 19 *In vitro* thermal stability of four CPP-CocE fusion proteins at 37 C°.

Table 6 *In vitro* stability kinetics of DMCocE and CPP-DMCocE fusion proteins.

CocE Variants	$t_{1/2}$ (hr)	MRT^{+} (hr)
DMCocE	4.28*	6.17*
Tat-N-DMCocE	5.76 ± 1.45	8.31 ± 2.09
LMWP-N-DMcocE	4.83 ± 1.78	6.96 ± 2.57
DMCocE-C-Tat	1.66 ± 0.39	2.39 ± 0.56
DMCocE-C-LMWP	2.98 ± 0.57	4.29 ± 0.83

*Data cited from Narasimhan *et al.* (95); no standard deviation available.

According to the literature published recently (95), in the *in vitro* and non-reductive environment, CocE (and DMCocE) molecules undergo dimerization, which involves many residues in the N- and C-terminus of CocE. This dimerization would not impact the enzymatic activity of CocE variants, but play an essential role for their *in vitro* stabilization. Moreover, all mutations stabilizing the CocE dimerization have shown to significantly improve the CocE thermal stability (21, 22, 95). Given that the CocE dimerization greatly involves the N- and C-terminal regions of CocE molecule, and it has a major influence on CocE's stability, it is rational to assume that attaching CPP on the N-terminus of DMCocE could somehow enhance the dimerization, and therefore elongate the *in vitro* stability a 37 °C. On the other hand, attaching CPP on the C-terminus of DMCocE generates a large, positively charged region composed of Tat/LMWP group and the C-terminal 6-histidine tag. This large and positively charged region could have a strong electrostatic attraction to the counter part of C-terminal CPP-DMCocEs, which are negatively charged proteins at pH 7.4, and then lead to an accelerated aggregation. Aggregation was known to be the major deactivation mechanism of CocE (95), and a common issue in many CPP fused, negatively charged proteins (103).

Another interesting observation is that the efficiency decay curve of DMCocE-C-Tat did not completely follow the one-phase exponential decay during the 12-hour incubation

(data not shown); it showed a slower decrease after incubating for six hours. This did not appear in the other three CPP-DMCocE fusion proteins, native CocE, or any known CocE variants published previously (13, 21, 22, 95). Thus, it will be interesting to understand the detailed mechanism resulting in the prolonged residual activity of this DMCocE-C-Tat fusion protein.

3.4 Conclusions

Two types of disulfide-bridged chemical conjugates, Tat-S-S-DMCocE and LMWP-S-S-DMCocE, were successfully generated and purified by heparin affinity chromatography. Four recombinant CPP-DMCocE fusion proteins, Tat-N-DMCocE, LMWP-N-DMCocE, DMCocE-C-Tat, and DMCocE-C-LMWP, were also successfully constructed and expressed in *E. coli* as soluble proteins. These six CPP-CocE variants contain one CPP group on the surface on each CocE molecule, and two sub-types of LWMP-DMCocE chemical conjugates would process two or even three LMWP groups per DMCocE molecules. All six CPP-DMCocE constructs were able to be purified by Q-sepharose anion exchange chromatography, and their purity was at least of ~98%, based on the analysis of SDS-PAGE.

The *in vitro* characteristics of two chemical CPP-DMCocE conjugates (Tat-S-S-DMCocE, LMWP-S-S-DMCocE) and four recombinant CPP-DMCocE fusion proteins (Tat-N-DMCocE, LMWP-N-DMCocE, DMCocE-C-Tat, and DMCocE-C-LMWP) were compared and summarized in Table 7. LMWP-S-S-DMCocEs showed the highest cocaine-hydrolyzing activity among all of the CPP-DMCocE constructs, probably because the LMWP conjugation sites are away from CocE's catalytic center and therefore have the least interference on CocE's functionality. The low production yield (3.9 mg per batch) of LMWP-S-S-DMCocE, however, would be an obstacle to any further application and needed to be optimized. In contrast, the fusion protein DMCocE-C-Tat had the largest production yield, which is approximately 20-fold compared with LMWP-S-S-DMCocE. Another fusion protein, Tat-N-DMCocE, possessed the highest cocaine-hydrolyzing activity among four CPP-DMCocE fusion proteins, and the longest *in vitro*

half-life compared with any known CocE variants. Given the difference in expression level and *in vitro* half-life among four CPP-DMCocE fusion proteins, attaching Tat or LMWP on the C-terminus of CocE could reduce the potential interference on overall expression, but also accelerate the aggregation, of CPP-DMCocE fusion proteins. In conclusion, compared with the number and type, the location of the attached CPP groups seemed be more influential on the functionality, stability, and expression level of CPP-CocE variants.

Table 7 *In vitro* characteristics of CPP-DMCocE variants.

	Yield in Mass Quantity Per Batch* (mg)	**% Efficiency Compared with DMCocE**	***In Vitro* $t_{1/2}$ at 37 ^{o}C (hr)**
Chemical Protein Conjugates			
Tat-S-S-DMCocE	1.1	n/a	n/a
LMWP-S-S-DMCocE	3.9	77-85	n/a
Recombinant Fusion Proteins			
Tat-N-DMCocE	32.7	53	5.76
LMWP-N-DMCocE	10.3	45	4.83
DMCocE-C-Tat	73.3	50	1.66
DMCocE-C-LMWP	7.3	49	2.98

* Based on current facility in our lab.

To facilitate the following cellular uptake study, the production yield, cocaine-hydrolyzing activity, and *in vitro* thermal stability were the major parameters in this part of the dissertation. Based on the overall results, either Tat-N-DMCocE or DMCocE-C-Tat seemed to be the most preferable CPP-CocE variants. A cellular uptake study to ensure the cell penetrating activity of all six CPP-DMCocE variants will be continued in Chapter 4.

CHAPTER 4
Cell Encapsulation of CPP-CocEs

By linking CPP and CocE via chemical conjugation or biological recombination, six CPP-CocE variants were successfully produced and systemically compared in Chapter 3. On this basis, the aim for this chapter is to evaluate the cell encapsulation feasibility of six CPP-CocE variants by assessing their cellular uptake ability, and elucidate the potential correlation between cell uptake extent and incubation time/concentration. A fluorophore FITC was applied as a probe to visualize and quantify the cellular uptake of CPP-CocEs in living HeLa cells and rabbit RBC, which were are selected as the model to assess the cellular uptake behavior. To perform cellular uptake study, cells were incubated with varied concentrations (in the range of 2-20 μM) of FITC-labeled CPP-CocEs at 37 °C. At the specified time points, the treated cells were extensively washed, and the intracellular fluorescence from internalized FITC-labeled CPP-CocEs was then analyzed.

All six FITC-labeled CPP-CocEs showed cellular uptake ability in HeLa cells, but their intracellular distribution phenotypes were different. Compared with other CPP-CocE variants, C-terminal CPP-CocE fusion proteins exhibited nuclear enrichment, homogenous cytoplasmic distribution, and a greater extent of overall cellular uptake. Therefore, C-terminal CPP-CocE fusion proteins would be preferable for conducting cell encapsulation. Moreover, in HeLa cells and RBC, the CPP-mediated internalization was positively correlated, but not increasing linearly, with incubation time and concentration.

4.1 Introduction

Last chapter provides data for a systemic comparison of the six CPP-CocE variants produced by either chemical conjugation or biological recombination. Their absolute yield per batch, recovery percentage, enzyme specific activities, and *in vitro* stability at 37 °C were assessed and summarized in Table 7. In this chapter, the comparison of the six CPP-CocEs is completed by evaluating their cellular uptake ability, which represents their feasibility for cell encapsulation. The cell-encapsulated CocE can be protected from proteolytic degradation in circulation, as well as detection by the host immune system (see Chapter 1).

Among all potential cell types which can be employed to encapsulate CPP-CocE, RBC and HeLa cells, a human cervical carcinoma cell line utilized in a number of literature regarding CPP-mediated cellular delivery (92, 104-106), are selected as the model to assess the cellular uptake behavior of CPP-CocE variants. In cellular uptake study, fluorescein isothiocyanate (FITC) is attached to all six CPP-CocEs, and applied as a probe to visualize and quantify the cellular uptake of CPP-CocEs in living cells. Under excitation by a laser with a wavelength of 494 nm, the FITC-labeled CPP-CocEs emit yellowish green fluorescence with a maximum at 520 nm. Therefore, the intracellular fluorescence signal can accurately reflect the amount and distribution of the FITC-labeled CPP-CocEs inside the cells.

Specifically, to perform the cellular uptake study, cells are incubated with varied concentrations (in the range of 2-20 μM) of FITC-labeled CPP-CocEs at 37 °C. At the specified time points, the treated cells are extensively washed to remove the FITC-labeled enzymes that merely attach on the outer cell membrane. In this post-incubation wash, heparin is added in the wash buffer to facilitate the removal of the non-internalized CPP-CocEs (107), which is achieved by competing for binding of the heparan sulfate proteoglycans to the CPP moieties of CPP-CocEs (see Section 1.4.2). The intracellular fluorescence can then be analyzed by the visualization using fluorescence microscopy, or the quantification using a microplate reader equipped with a proper fluorescence channel. This cellular uptake information combined with the *in vitro* activity and stability profile,

which was assessed in Chapter 3, can indicate which CPP-CocE variants would be more preferable for the further development.

4.2 Materials and Methods

4.2.1 Cells and Reagents

Human cervical carcinoma cell line HeLa was obtained from the American Type Culture Collection (Manassas, VA). Pooled rabbit RBC (in 10% suspension) was purchased from Lampire Biological Laboratories, Inc. (Pipersville, PA).

Minimum Essential Medium α (MEM-α), fetal bovine serum (FBS), 1X PBS (pH 7.4), Hoechst 33258, and Hank's balanced salt solution (HBSS) without calcium or magnesium were from Invitrogen (Carlsbad, CA). FITC, heparin sulfate (in sodium salt form), and radio immunoprecipitation assay (RIPA) buffer were purchased from Sigma-Aldrich (St. Louis, MO). Water was distilled and deionized (ddH_2O). All other reagents were of analytical grade.

4.2.2 Fluorescence Labeling

Six CPP-CocE constructs prepared in Chapter 3, including two chemical conjugates (Tat-S-S-LMWP and LMWP-S-S-DMCocE) and four fusion proteins (Tat-N-DMCocE, LMWP-N-DMCocE, DMCocE-C-Tat, DMCocE-C-LMWP), as well as DMCocE, were labeled with FITC at their primary amino groups. CPP-CocE solutions (10 mg/ml in 0.1 M carbonate buffer, pH 9.2) were reacted in a 1:20 molar ratio with a FITC solution in dimethylformamide (DMF) at 4 °C overnight with gentle shaking. The final DMF concentration in the reaction mixture was less than 5%. After reaction, the excess FITC was removed using a Sephadex G-25 desalting column (GE Healthcare, Piscataway NJ). The concentration and degree of labeling of the FITC-labeled DMCocE and CPP-CocE constructs was determined by measuring the absorbance at 280 nm and 494 nm. After concentration using Amicon Ultra-15 centrifugal filter devices (molecular weight cut-off: 30,000 Da), all the FITC-labeled enzymes were snap frozen in liquid nitrogen, and then stored at −80 °C prior to use.

4.2.3 HeLa Cell uptake of FITC-labeled CPP-CocE Variants

HeLa cells were seeded at a density of 3 x 10^4 cells/cm^2 in the BD PureCoat™ amine-surface 24-well plate (Bedford, MA), and grown in MEM-α medium supplemented with 10 % (v/v) FBS. After they reached a confluence at ~50 % (approximately 24 hours after seeding), cells were incubated with FITC-labeled DMCocE or CPP-CocEs in a FBS-free MEM-α medium for the indicated time at 37 °C. The concentrations of FITC-labeled enzymes were in the range of 2-10 μM. After incubation, the treated HeLa cells were washed three times with 10 mg/ml of heparin sulfate in PBS (pH 7.4), and the cell nuclei were counter-stained with 5 μg/ml of Hoechst 33258 in PBS for 20 min at 37 °C. To visually detect the cellular uptake, cell fluorescence was examined by a Nikon Eclipse TE2000S inverted fluorescence microscope using a 20X objective and three channels (DIC (differential interference contrast), DAPI, and FITC). Cell images were acquired and analyzed by Metamorph® software (Molecular Devices Corporation, Sunnyvale, CA). To quantitatively evaluate the cellular uptake, cells in each well were lysed with 500 μl of RIPA buffer (containing 1 μM leupeptin, 5 μg/ml soybean trypsin inhibitor, 150 mM NaCl, 1.0% IGEPAL® CA-630, 0.5% sodium deoxycholate, 0.1% SDS, and 50 mM Tris, pH 8.0), incubated for 30 min at 4 °C, and 100 μl per well of total cell lysate was transferred into a white opaque 96-well microplate. Fluorescence in the 96-well microplate was read in a Synergy 2 Multi-Mode Microplate Reader (Biotek Instruments, Inc., Winooski, VT). Two excitation wavelengths, 360 nm and 485 nm, were used to detect the cellular DNA (counterstained with Hoechst 33258) and the intracellular CPP-CocEs (labeled with FITC), respectively. For each well, the intensity of the fluorescence excited at 485 nm was normalized by the intensity at 360 nm to correct for the differences in cell number between wells. The average fluorescence reading from a group of three wells, which was incubated in a FBS-free MEM-α medium without the FITC-labeled enzymes but subjected to the same wash/lysis process, was applied as a blank for the microplate reader data. Fluorescence measurement was done in triplicate, and all experiments were independently conducted twice (n = 2).

4.2.4 RBC Encapsulation of FITC-labeled Enzymes

Rabbit RBC were washed three times with ten-fold volume of HBSS, and then incubated with varied concentrations of FITC-labeled DMCocE or CPP-CocEs in HBSS for the specified time at 37 °C. The density of rabbit RBC at incubation was 10^8 cells/ml. After incubation, the treated RBC were washed three times with HBSS containing 10 mg/ml heparin sulfate, and diluted to a density of 2 x 10^6 cells/ml for the following examination.

To visually detect the encapsulation, the fluorescence from the FITC-labeled enzymes was examined by a Nikon Eclipse TE2000S inverted fluorescence microscope using a 20X objective and two channels (DIC, and FITC). RBC (2 x 10^6 cells/ml) were mixed with trypan blue (final concentration 0.1%), incubated at room temperature for 20 min, and the RBC images were acquired and analyzed by Metamorph® software (Molecular Devices Corporation, Sunnyvale, CA). To quantitatively evaluate the cellular uptake, the fluorescence 100 µl of the trypan-blue treated RBC was read in a Synergy 2 Multi-Mode Microplate Reader (Biotek Instruments, Inc., Winooski, VT) at 485 nm.

4.3 Results and Discussion

4.3.1 HeLa Cell Encapsulation

Cellular Uptake Phenotypes of Six CPP-CocE Variants

After incubating with HeLa cells for two hours at 37 °C, at the concentration of 5 µM, all six FITC-labeled CPP-CocEs penetrated and accumulated into the living HeLa cells, generating a significant intracellular fluorescence (Figure 20). At the same concentration of 5 µM, FITC-labeled DMCocE showed no cell penetrating activity and left almost undetectable fluorescence signals after wash. Thus, the cell penetrating ability of the CPP-CocEs can be attributed to the attached CPP groups, namely Tat or LMWP. On the other hand, the morphology of the cells treated with CPP-CocEs appeared normal and similar to that of PBS-treated cells. The normal cell morphology of the CPP-CocE treated cells excludes the possibility that the uptake is due to the cell membrane disruption. This suggestion was further supported by the result of a trypan blue staining,

in which damages cells with compromised cell membrane integrity were stained in blue (data not shown).

Although all six CPP-CocEs possess cell penetrating activity, their distribution after getting into cells showed different phenotypes. First, compared with CPP-CocE chemical conjugates, CPP-CocE fusion proteins exhibited a clear enrichment in the nucleus (Figure 20, e-h). It is known that Tat and LMWP are highly positively charged and have a high binding affinity to the negatively-charged DNA (108, 109). Since the Tat and LMWP groups are permanently attached to the CPP-CocE fusion proteins, based on their membrane penetrating and DNA-binding activity, these two CPPs could carry their "CocE cargo" across the nuclear membrane and enter the nucleus. In contrast, for the CPP-CocE chemical conjugates generated in this dissertation, the disulfide bond between CPP and CocE will be rapidly cleaved in the reductive intracellular environment. While the free CPP group proceeds into the nucleus, the released CocE cannot cross the nuclear membrane and therefore remains in the cytoplasm. Moreover, this nuclear accumulation of CPP-CocE fusion proteins appeared more obvious for DMCocE-C-Tat and DMCocE-C-LMWP (Figure 20, g and h). It is known that a poly-histidine sequence (n>5) also possesses a DNA binding affinity (110). Thus, for DMCocE-C-Tat and DMCocE-C-LMWP, in which their CPP groups are attached to the C-termini and right after and the 6-histidine tags, the DNA binding affinity of the CPP group would be enhanced by the adjacent 6-histidine tag, leading to a more distinct nuclear localization.

Second, some CPP-CocE constructs showed a homogenous distribution in the cytoplasm. When utilizing CPP to deliver a protein into cells, at least some degree of CPP-protein would be internalized via endocytosis and therefore localize within endosomes (see Section 1.4.2), forming condensed "bright spots" or vesicular structures in the cytoplasm under microscope (92, 105). However, one chemical conjugate LMWP-S-S-DMCocE (Figure 20, d), as well as two fusion proteins DMCocE-C-Tat (Figure 20, g) and DMCocE-C-LMWP (Figure 20, h), dispersed evenly and without any condensation in the cytoplasm. This homogenous distribution suggests that, after getting internalized, these three CPP-CocE constructs were not confined inside the cytoplasmic sub-

compartments such as endosomes. In comparison, other chemical conjugate (Tat-S-S-DMCocE, Figure 20, c) and fusion proteins (N-Tat-DMCocE and N-LMWP-DMCocE, Figure 20, e, f) still showed a "spotty" distribution in the cytoplasm (Figure 20, c, e, f). To sum up, among all six CPP-CocE constructs, the chemical conjugate with more CPP groups (LWMP-S-S-DMCocE), as well as the fusion proteins with the C-terminal CPP group (DMCocE-C-Tat and DMCocE-C-LMWP), appeared to be distributed homogenously in the cytoplasm and not confined inside the endosomes. For these three CPP-CocE constructs, it would be rational to assume that this homogenous cytoplasmic distribution is due to neither the CPP type nor the linkage between CPP and CocE, but due to the location and numbers of the CPP groups. Further investigation for cytoplasmic distribution among different CPP-CocEs, however, is still needed to support this assumption and elucidate the detailed mechanism.

Regardless of its exact mechanism, the non-endosomal-confined cytoplasmic distribution is favorable for the CPP-mediated cell encapsulation for CocE. Because of the acidic pH and various proteolytic enzymes inside the endosomes, most CPP-CocE reaching the endosomes will be degraded rapidly. Clearly, a CPP-CocE construct will be more preferable for cell encapsulation if it has a greater extent of non-endosomal-confined distribution and cellular uptake. The assessment of the cellular uptake extent, as well as factors impacting the cellular uptake, will be continued in the following experiments.

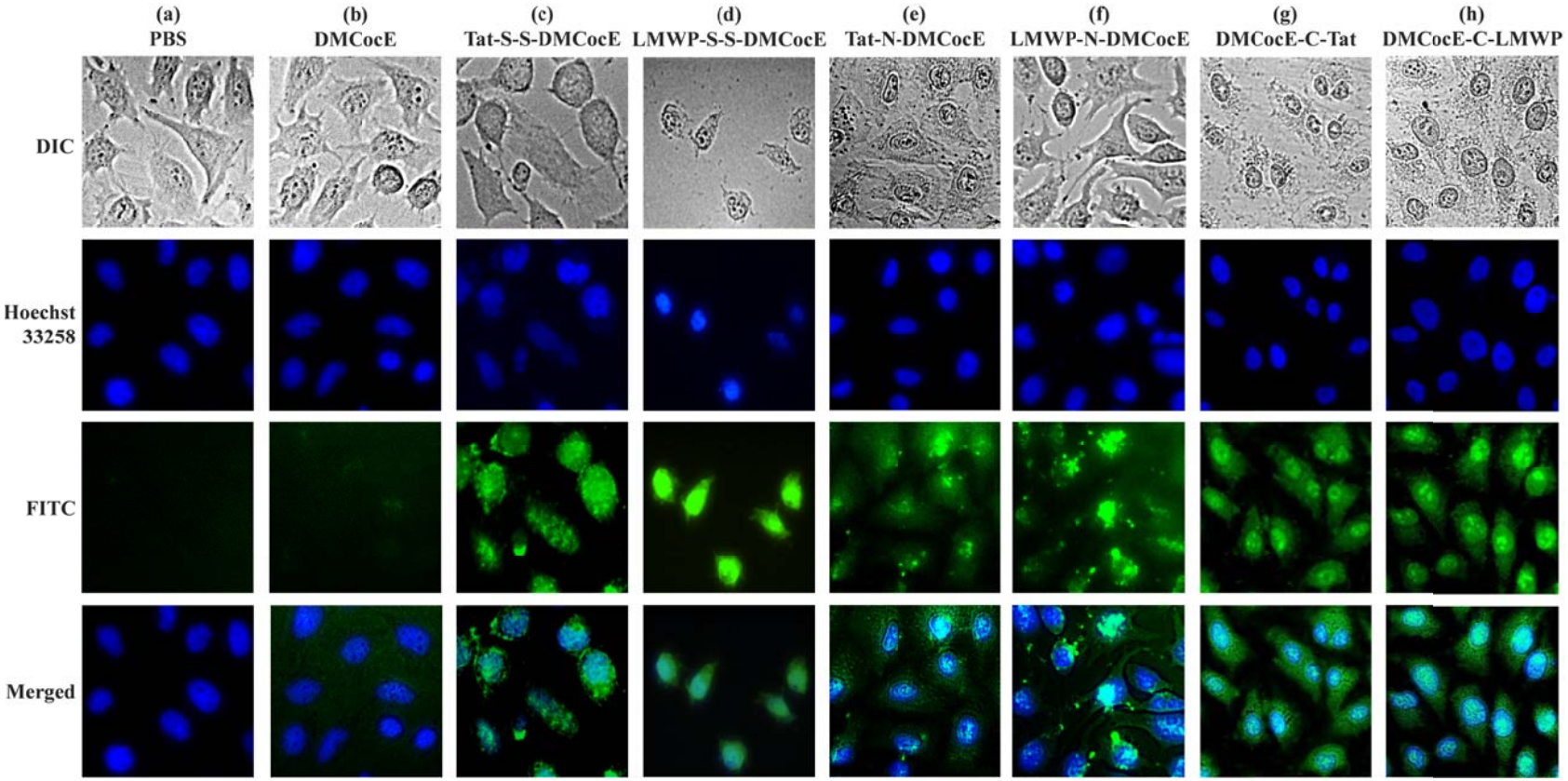

Figure 20 Internalization of six CPP-CocE constructs in HeLa cells. HeLa cells were incubated with 5 μM of DMCocE (b) or CPP-CocEs (c-h) for 2 hours at 37 °C. After incubation, the cells were washed extensively with 10 mg/ml heparin in PBS, counterstained the nuclei with Hoechst 33258, and their images were acquired by fluorescence microscopy. Nucleus was detected in the DAPI channel (blue), and DMCocE and CPP-CocEs were detected in the FITC channel (green). Cell morphology was acquired from the DIC microscopy in gray scale.

Cellular Uptake Level is Dependent upon CPP-CocE Type and Incubation Time

Figure 21 shows the time course of the cellular uptake of four CPP-CocE fusion proteins. The two chemical conjugates, Tat-S-S-DMCocE and LMWP-S-S-DMCocE, were excluded from this study due to their insufficient yield in production (see Table 7). As cells cannot maintain longer than four hours in absence of FBS supplement, the cellular uptake was monitored up to four hours. During the entire four-hour incubation, the cellular uptake levels of C-terminal CPP-CocE fusion proteins (DMCocE-C-Tat and DMCocE-C-LMWP) were approximately two-fold higher than the N-terminal constructs (Tat-N-DMCocE and LMWP-N-DMCocE). The difference in cellular uptake among N-terminal and C-terminal CPP-CocE fusion proteins is probably due to the augmented cell-penetrating activity by the presence of the histidine tag along with the fused CPP at the C-terminus. This difference in cellular uptake levels was also observed in the previous study (Figure 20, e-h), in which both DMCocE-C-Tat and DMCocE-C-LMWP also showed higher extent of cell internalization compared with Tat-N-DMCocE and LMWP-N-DMCocE. Meanwhile, according to Figure 21, the difference in cellular uptake level within the two types of N- or C-terminal CPP-CocE fusion proteins was not as obvious as that between the two types of fusion proteins. To sum up, combined with the fluorescence microscopy results from Figure 20, the C-terminal CPP-CocE fusion proteins showed a more homogenous cytoplasmic distribution, as well as a greater extent of overall cellular uptake, and therefore would be more preferable for cell encapsulation.

As for the correlation between the cellular uptake level and the incubation time, the internalization was increasing within the first two hours of incubation. After two hours, the cellular uptake level showed no significant increase. The only exception is DMCocE-C-Tat, which continuously decreases the uptake level after two hours.

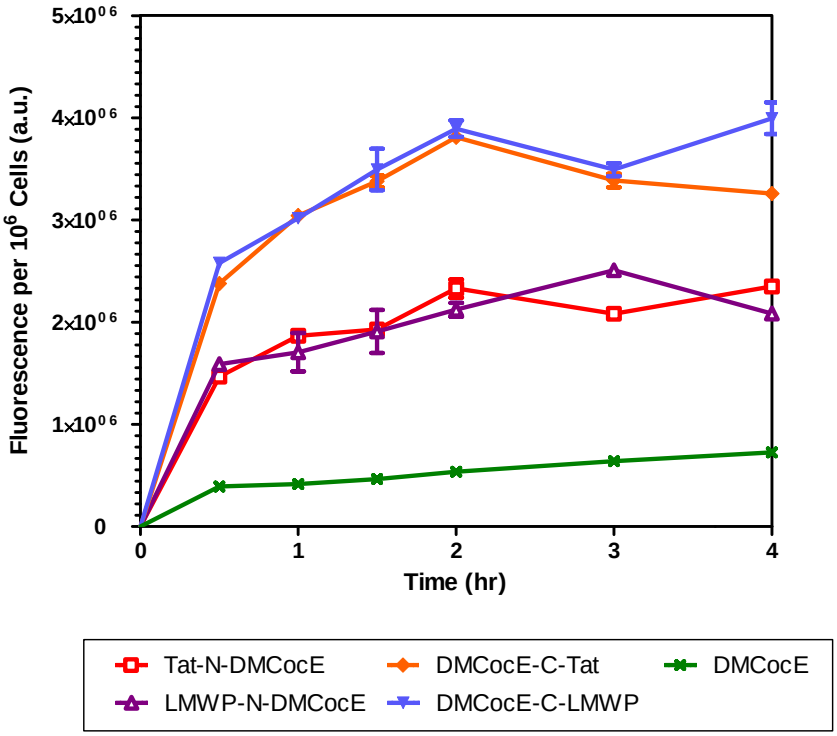

Figure 21 Kinetics of cell internalization of four CPP-CocE fusion proteins. HeLa cells were incubated with 5 μM of FITC-labeled DMcocE or CPP-CocE fusion proteins for a pre-determined time points at 37 °C. The cellular uptake of each CPP-CocE fusion protein (labeled with FITC) was estimated from the mean fluorescent signal of 10^6 cells.

Cellular Uptake Behavior is Dependent upon Incubation Concentration

In order to find out the optimal concentration for loading CPP-CocEs into cells, the incubation time in this concentration-dependent experiment is set at two hours, based on the time when cellular uptake level reaches to (see Figure 21). Due to the lower yield of production (see Table 7), and to avoid inconsistency of mixing two batches, the two LMWP-CocE fusion proteins (LMWP-N-DMCocE and DMCocE-C-LMWP) are not included in this concentration-dependency study.

Figure 22 and Figure 23 show the concentration-dependent internalization and distribution in HeLa Cell of Tat-N-DMCocE and DMCocE-C-Tat, respectively. The selected concentration range (2-10 μM) for the HeLa cellular uptake covered proteins

concentrations used in most studies of CPP-mediated cellular delivery . Both figures demonstrate that the levels of cellular internalization are positively correlated with the concentration of these two CPP-CocEs. Moreover, compared with cells treated with lower concentrations, the morphology was not altered in presence of 10 μM of Tat-CocEs.

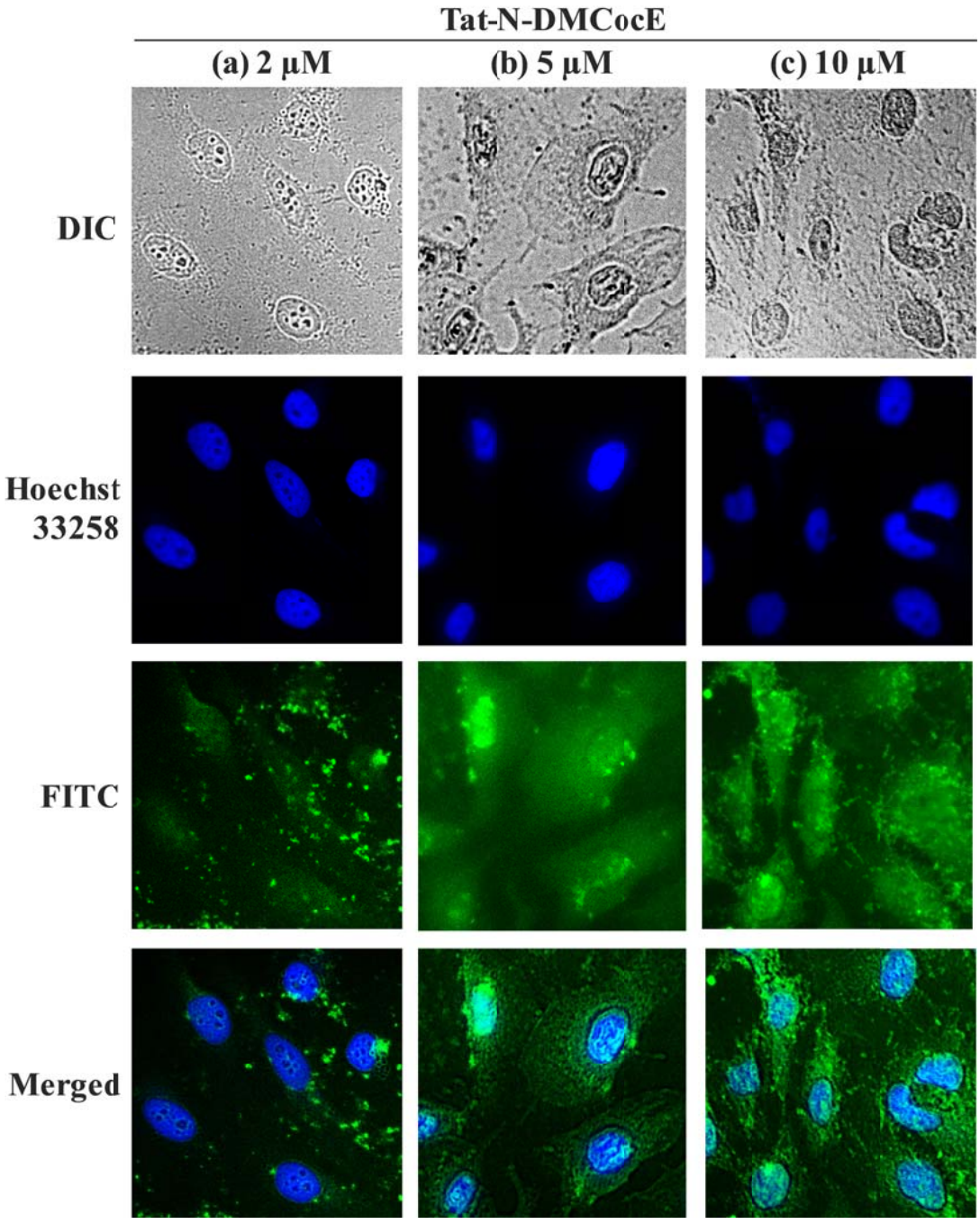

Figure 22 Concentration-dependent internalization of Tat-N-DMCocE in HeLa cells. HeLa cells were incubated with (a) 2, (b) 5, and (c) 10 μM of FITC-labeled Tat-N-DMCocE at 37 °C for two hours. After incubation, the cells were washed extensively with 10 mg/ml heparin in PBS, counterstained the nuclei with Hoechst 33258, and their images were acquired by fluorescence microscopy. Nucleus was detected in the DAPI channel (blue), and DMCocE and CPP-CocEs were detected in the FITC channel (green). Cell morphology was acquired from the DIC microscopy in gray scale.

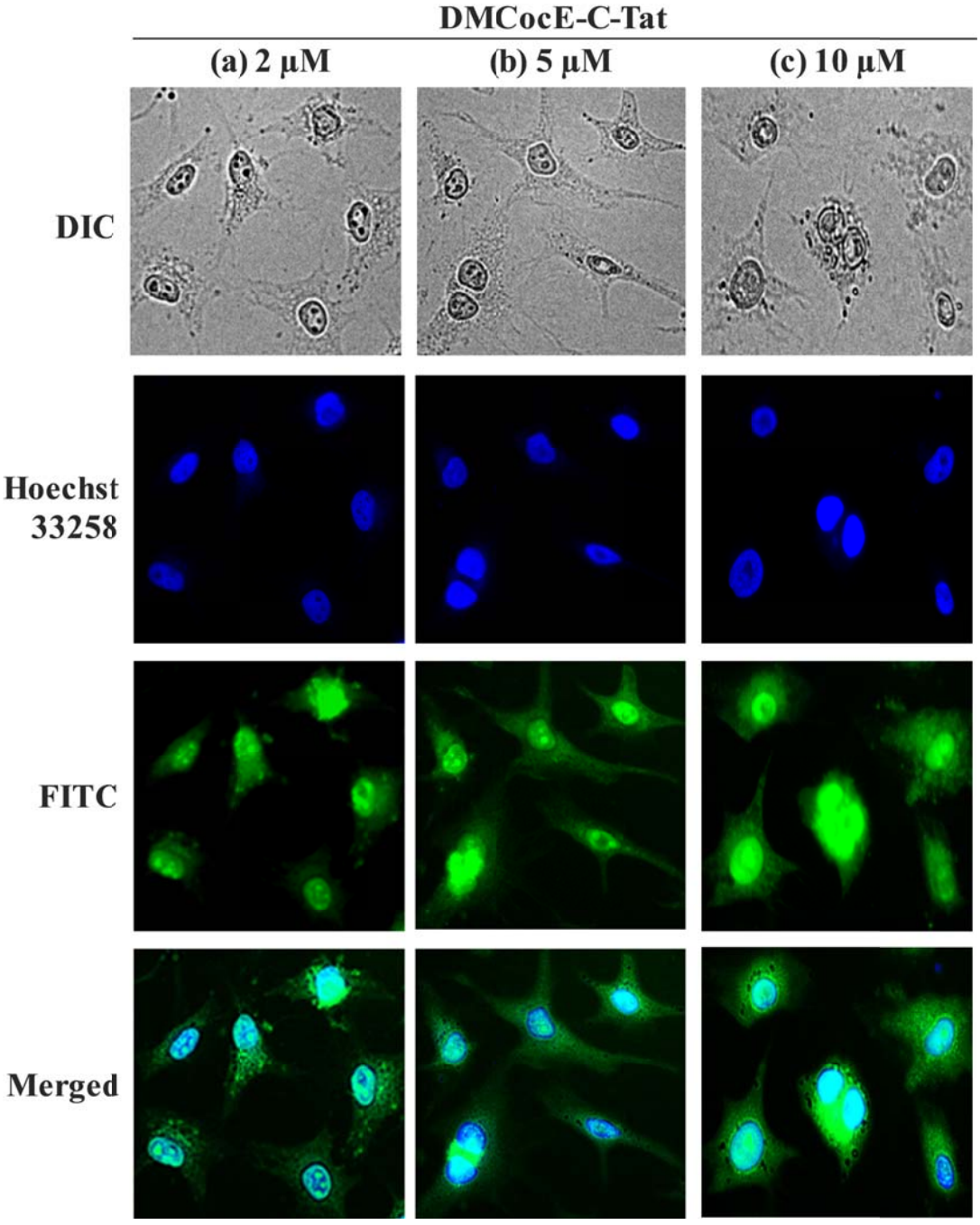

Figure 23 Concentration-dependent internalization of DMCocE-C-Tat in HeLa cells. HeLa cells were incubated with (a) 2, (b) 5, and (b) 10 μM of FITC-labeled DMCocE-C-Tat at 37 °C for two hours. After incubation, the cells were washed extensively with 10 mg/ml heparin in PBS, counterstained the nuclei with Hoechst 33258, and their images were acquired by fluorescence microscopy. Nucleus was detected in the DAPI channel (blue), and DMCocE and CPP-CocEs were detected in the FITC channel (green). Cell morphology was acquired from the DIC microscopy in gray scale.

In order to obtain a more accurate assessment, the treated HeLa cells were measured by the fluorescence microplate reader. Figure 24 shows that the cellular uptake of DMCocE-C-Tat is proportional with the increasing concentration. After incubation time of 4 hours, the mean fluorescence intensity of 10^6 cells is 2.2 x10^6, 3 x10^6 and 7.4x10^6 at concentrations of 2 µM, 5 µM and 10 µM, respectively. This suggests that the cell internalization does not increase linearly with higher concentration. In addition to the non-linear enhancement, the fluorescence value for 10 µM kept increasing with incubation time, whereas the fluorescence value for lower concentrations (2 and 5 µM) reach a maximum after two hours.

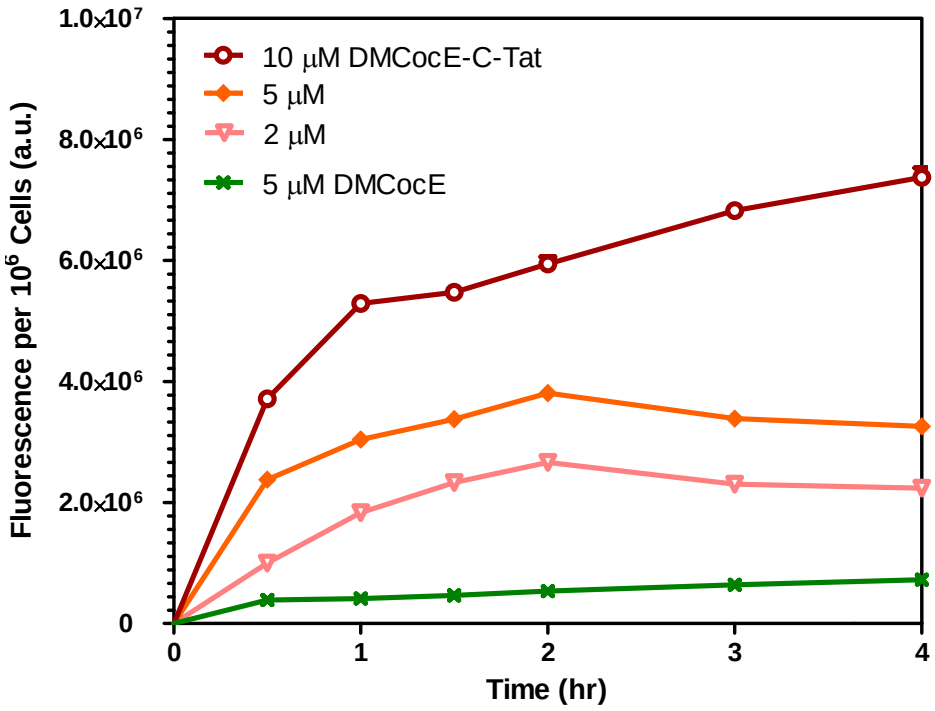

Figure 24 Kinetics of cell internalization of DMCocE-C-Tat in different concentrations. HeLa cells were incubated with 5 µM of FITC-labeled DMcocE or 2, 5, and 10 µM of FITC-labeled DMCocE-C-Tat at a pre-determined time points at 37 °C. The cellular uptake of each FITC-labeled enzymes was estimated from the mean fluorescent signal of 10^6 cells.

4.3.2 RBC Encapsulation

For the convenience of future animal experiments regarding cocaine toxicity, the RBC used in the encapsulation study should come from the same species as in animal experiments. Rodents (mice and rats) are most commonly used as the animal model for cocaine intoxication. Compared with humans, rodents metabolize cocaine by the same mechanism and experience similar types of cocaine-induced toxicity (111-113). However, there is no commercialized mouse RBC product available on the market, and rat RBC is too fragile for the loading process (personal communication). Therefore, rabbit RBC, which have a similar morphology as rodent RBC and are available for purchase in sufficient quantities, are used in this RBC encapsulation experiment.

According to the results from the HeLa cell study in Section 4.3.1, when the incubation concentration reached at 10 μM, the CPP-CocE internalization becomes proportional to incubation time during the entire four-hour incubation. Therefore, the incubation concentrations in the RBC encapsulation study is set at 10 and 20 μM, which equal one- and two-fold of the upper limit in the HeLa cell study. As higher concentrations are used in the RBC study, fluorescence from non-internalized FITC-labeled enzymes could become more obvious and not be completely removed by heparin wash. To eliminate this interference, trypan blue was applied after incubation to quench the FITC fluorescence from the enzyme attached to the outer cell membrane. Since trypan blue can only quench the fluorescence from nearby FITC molecules, and it cannot cross the cell membrane, only the extracellular fluorescence is quenched by trypan blue; the intracellular fluorescence from internalized CPP-CocE will remained undisturbed (114).

The RBC incubated with the FITC-labeled DMCocE (10 μM and 20 μM) showed a weak fluorescence on the cell surface, with no observable uptake of the labeled-enzyme within the interior of the RBC (Figure 25). The similar weak fluorescence on the cell surface was also observed in the RBC treated with 10 μM of FITC-labeled DMCocE-C-Tat. When RBC incubated with 20 μM of FITC-labeled DMCocE-C-Tat, however, significant intracellular fluorescence was detected within the RBC. The fluorescence

intensity reading (Figure 26) also supported the observation from fluorescence microscopy. For the three groups of RBC treated with cells treated with FITC-labeled DMCocE (10 and 20 μM) and 10 μM FITC-labeled DMCocE-C-TAT, the fluorescence intensity slowly increased with the increasing incubation time. However, for the RBC incubated with 20 μM of FITC-labeled DMCocE-C-Tat, the fluorescence intensity dramatically increased at one hour of incubation. Compared with all the other three groups, its fluorescence intensity showed at least two-order of magnitude greater increase.

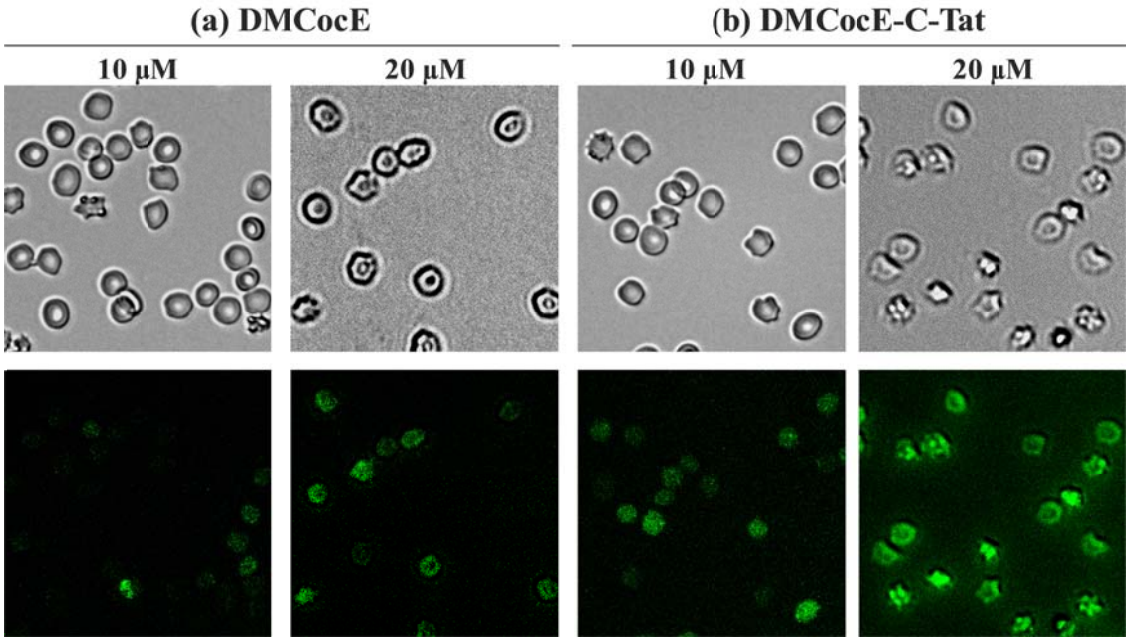

Figure 25 Concentration-dependent encapulation of DMCocE-C-Tat in RBC. Rabbit RBC (10^8 cells/ml) were incubated with FITC-labeled DMCocE (a) or DMCocE-C-Tat (b) in HBSS for two hours at 37 °C. After incubation, the treated RBC were washed three times with HBSS containing 10 mg/ml heparin sulfate, and diluted to a density of 2 x 10^6 cells/ml for fluorescence microscopy.

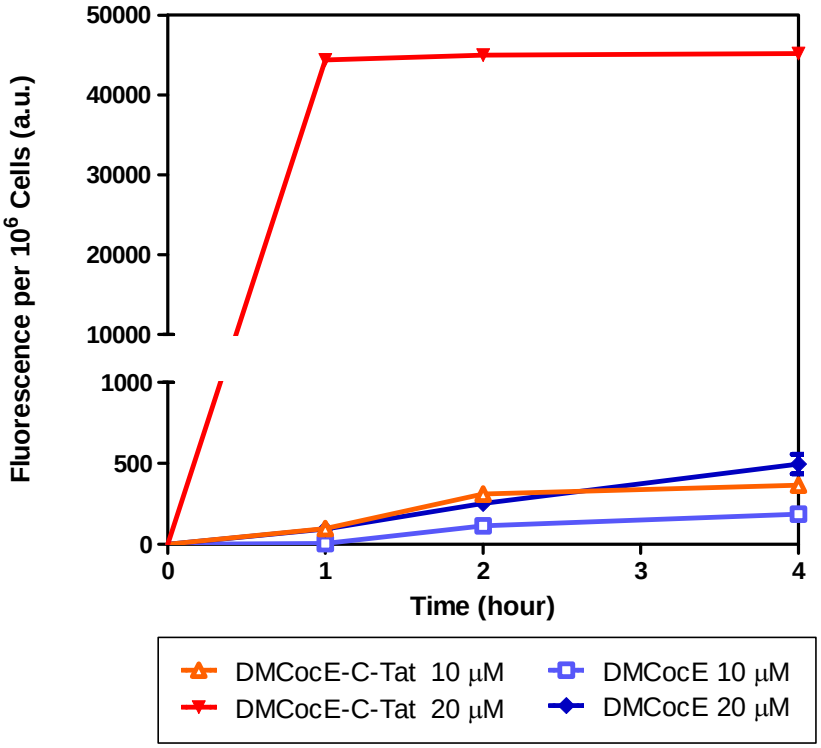

Figure 26 Kinetics of RBC uptake of DMCocE and DMCocE-C-Tat.

The morphology of the RBC treated with 20 μM of FITC-labeled enzymes was different than the cells treated with lower concentrations of enzyme. As the enzyme concentration increased, the RBC shape shifted from spherical biconcave to crenate, and the size also became smaller. Since the RBC treated with 20 μM of DMCocE-C-Tat were excluded from trypan blue staining (Figure 25, b), the possibility that the uptake was due to the cell membrane disruption can be ruled out. The possible explanation of the change in RBC morphology would be the hypertonic environment in presence of high enzyme concentration, which is a well-known physiological response of RBC (115).

4.4 Conclusions

In this chapter, the comparison of the six CPP-CocEs is completed by evaluating their cellular uptake ability, which represents their feasibility for cell encapsulation. A

fluorophore FITC is applied as a probe to visualize and quantify the cellular uptake of CPP-CocEs in living cells. RBC and HeLa cells are selected as the model to assess the cellular uptake behavior of CPP-CocE variants.

In HeLa cells, all six FITC-labeled CPP-CocEs penetrated and accumulated inside the cells, but their intracellular distribution were different. CPP-CocE fusion proteins exhibited a nuclear enrichment, and this nuclear accumulation was more obvious in DMCocE-C-Tat and DMCocE-C-LMWP. Moreover, LMWP-S-S-DMCocE, DMCocE-C-Tat, and DMCocE-C-LMWP were not confined inside the endosomes after getting into the cells. Since DMCocE-C-Tat and DMCocE-C-LMWP showed a more homogenous cytoplasmic distribution and a greater extent of overall cellular uptake, they appeared to be more preferable for cell encapsulation. By using DMCocE-C-Tat and Tat-N-DMCocE as models, CPP-mediated internalization was found to be dependent upon incubation time and concentration. At 2 μM and 5 μM, the CPP-mediated cellular uptake reached a maximum after two hours. However, at 10 μM, the CPP-mediated uptake kept increasing with incubation time during the entire incubation.

In RBC, only incubation with 20 μM of DMCocE-C-Tat generated a significant cellular uptake. For the three groups of RBC treated with cells treated with FITC-labeled DMCocE (10 and 20 μM) and 10 μM FITC-labeled DMCocE-C-TAT, the fluorescence intensity slowly increased with the increasing incubation time. However, for the RBC incubated with 20 μM of FITC-labeled DMCocE-C-Tat, the fluorescence intensity dramatically increased at one hour of incubation. Compared with all the other three groups, its fluorescence intensity showed at least two-order of magnitude greater increase.

CHAPTER 5
Nasal Delivery of CPP-CocEs

5.1 Introductions

In addition to cell encapsulation, CPP-mediated cell uptake could also be utilized to directly deliver CocE into the CNS. The major obstacle to deliver macromolecules (including CocE) into the brain is the blood-brain barrier (BBB), which allows only small (< 400-500 Da) lipophilic molecules to cross (116). As a small and highly lipophilic molecule, cocaine can freely pass the BBB and reach the brain parenchyma, where cocaine has its psychological effects. In contrast, CocE is impermeable to the BBB and therefore can be directly introduced into the CNS only by invasive administrations, *e.g.* surgery and intracranial injection. The ability of CPP to cross the BBB and carry its macromolecular "cargo" into the CNS has been shown to improve the medication outcomes of some CNS diseases, such as brain tumors, cerebral ischemia, and neurodegeneration (32, 117-119). Therefore, it will be interesting to see if the cell-membrane permeable CPP-CocE variants also have the potential to cross the BBB and reach the brain parenchyma.

One possible administration route for CPP-CocEs to the CNS is nasal delivery. After nasal administration, the CPP-CocE molecules escaping proteases and capillary clearance on the nasal mucous membrane would gain an opportunity to enter the CNS via the olfactory region (120). There are two proposed mechanisms for the olfactory pathway from nose to the CNS. The first mechanism involves the olfactory epithelial cells, from which the cell-permeable CPP-CocEs can passively diffuse though the vasculature underneath and then to the CNS (121-124). The second mechanism involves the olfactory neurons, which are able to actively transport the internalized CPP-CocEs on the olfactory bulbs in the CNS (124, 125). Compared with the first (epithelium-involved)

mechanism, the second mechanism (neuron-involved) will be more favored in CocE delivery from nose to the CNS, as for macromolecules active transport is usually more efficient than passive diffusion.

Because of their cell penetrating activity, the CPP-CocEs applied on the nasal mucous membrane should be able to utilize both mechanisms aforementioned to enter the CNS. Even though they cannot reach the CNS, the CPP-CocEs internalized in the nasal epithelial cells can escape proteases and capillary clearance on the nasal mucous membrane, and therefore can remain active. As long as the intracellular CPP-CocEs maintain cocaine hydrolyzing activity, they would continue digesting the cocaine in the nasal cavity, and preventing cocaine from entering the circulation.

5.2 Materials and Methods

5.2.1 Cells and Reagents

Human nasal septum carcinoma cell line RPMI-2650 was purchased from the American Type Culture Collection (Manassas, VA). Cocaine hydrochloride was from the National Institutes on Drug Abuse (Bethesda, MA). All reagents required for cell culture fluorescence microscopy were the same with Section 5.1.1 and therefore not described here.

5.2.2 RPMI-2650 Cell uptake of FITC-labeled CPP-CocE Variants

To determine the best condition for the maximal loading, the fluorescence microscopy was conducted by measuring the cellular uptake of FITC-labeled CPP-CocE variants in RPMI-2650 cells. Cells were seeded at the density of 1.5 x 10^5 cells/cm^2 in the BD PureCoat™ amine-surface 24-well plate, and used when they completely attached to the plate and reached a confluence at ~50% (approximately 3 x 10^5 cells/$cm^{2)}$. The process of maintaining RPMI-2650 cells, incubating the cells with FITC-labeled enzymes, and conducting fluorescence microscopy, was identical with Section 5.1.1 and therefore not described here.

5.2.3 Cocaine-Hydrolyzing Activity of RPMI-2650 Cells Loaded with CPP-CocEs

RPMI-2650 cells were seeded at the density of 3 x 10^4 cells/cm^2 in the BD PureCoat™ amine-surface 24-well plate, grown in the same conditions used in Section 5.1.1 and 5.3.1, and used when they completely attached to the plate and reached a confluence at ~50% (~ 2.5 x 10^5 cells/cm^2). To load enzymes, cells were incubated with varied concentrations (2 – 10 μM) of DMCocE or CPP-CocEs in a FBS-free MEM-α medium for three hours at 37 °C. After incubation, the treated RPMI-2650 cells were washed three times with PBS (pH 7.4) containing 10 mg/ml heparin sulfate. To assess the cocaine-hydrolyzing activity, 500 μM cocaine solution in 1X PBS (pH 7.4) was added into the treated cells (500 μl per well), and incubated at 37 °C with gentle shaking. A 100 μl aliquot of cocaine solution was taken out at 0.5, 1, and 1.5 hr, and the remaining cocaine level was determined by the spectrophotometric assay described in Section 4.1.3.

5.3 Results

This preliminary study is to see if the RPMI-2650 cells transduced with DMCocE-C-Tat will become capable of cocaine digestion. Before the transduction, the internalization efficiency of DMCocE-C-Tat (labeled with FITC) in RPMI-2650 cells was evaluated by measuring the intracellular fluorescence intensity. Similar with the results in HeLa cells (see Section 5.1.2), the uptake of DMCocE-C-Tat in RPMI-2650 are dependent upon with incubation time and enzyme concentration. According to the uptake kinetics (Figure 27), the uptake of DMCocE-C-Tat was positively correlated with the incubation time up to 3 hours, but dropped at the fourth hour. As for the correlation between the uptake and incubation concentrations, the cellular uptake of DMCocE-C-Tat is also positively correlated with increasing concentration. Like the nonlinear increase of uptake in HeLa cells, this concentration-dependent uptake in RPMI-2650 cell does not increase linearly either. After incubation time of 3 hours (when the maximal internalization occurs), the mean florescence intensity per 10^6 cells is 6 x10^4 at 2 μM, and 2.6 x10^5 at 10 μM of DMCocE-C-Tat, respectively. Note that the fluorescence readings in RPMI-2650 cells are significantly lower than those in HeLa cells. Besides the intrinsic difference of the uptake capacity among cell types, this lower fluorescence intensity of RPMI-2650

compared with HeLa cells may mainly result from the difference of cell size and morphology. The entire cell size and cytoplasmic portion of RPMI-2650 are smaller than HeLa cells. The result from fluorescence microscopy confirms this morphology difference (Figure 28), and also shows a less intensive FITC-labeled enzyme staining in the cytoplasm.

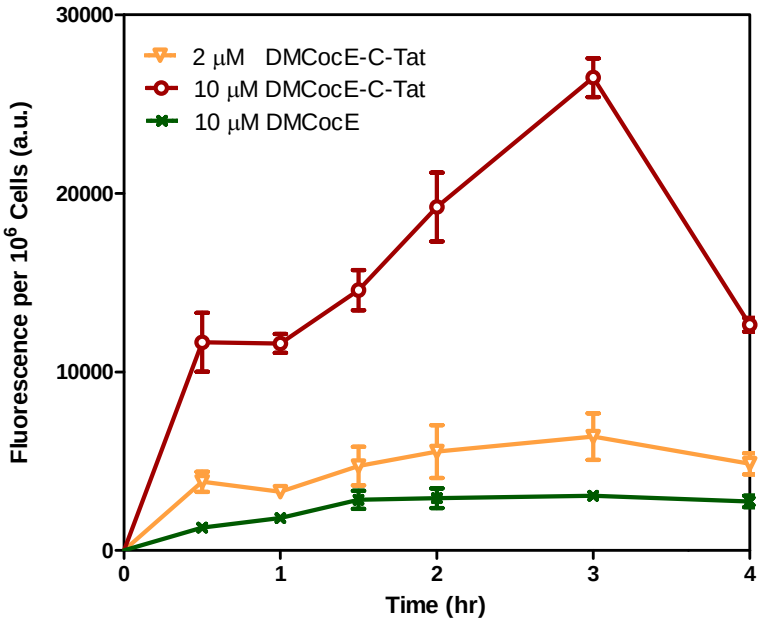

Figure 27 Kinetics of RPMI-2650 uptake of DMCocE-C-Tat with two different concentrations. RPMI-2650 cells were incubated with 5 μM of FITC-labeled DMcocE or 2 and 10 μM of FITC-labeled DMCocE-C-Tat at a pre-determined time points at 37 °C. The cellular uptake of each FITC-labeled enzymes was estimated from the mean fluorescent signal of 10^6 cells.

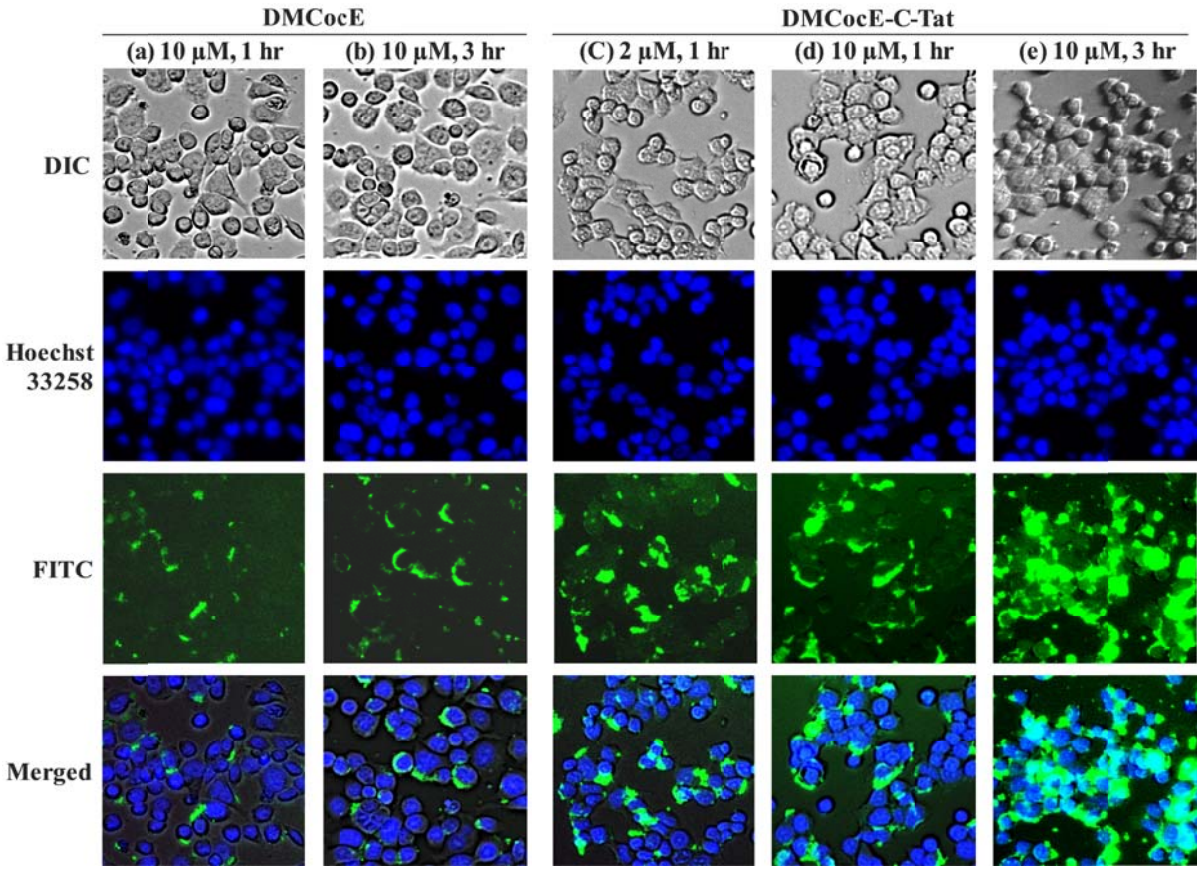

Figure 28 Time- and concentration-dependent internalization of DMCocE-C-Tat in RPMI-2650 cells. RPMI-2650 cells were incubated with 10 µM of DMCocE for 1 hour (a) or 3 hours (b) at 37 °C. After incubation, the cells were washed extensively, counterstained the nuclei with Hoechst 33258, and their images were acquired by fluorescence microscopy. Nucleus was detected in the DAPI channel (blue), and DMCocE and CPP-CocEs were detected in the FITC channel (green). Cell morphology was acquired from the DIC microscopy in gray scale.

Based on the results described in last paragraph, the incubation time in the following cell transduction experiment was set to three hours, which gives the maximal internalization of DMCocE-C-Tat in RPMI-2650 cells. Both Tat-N-DMCocE and DMCocE-C-Tat are used in this experiment in order to determine the effect of enzyme activity and stability on the cocaine-hydrolyzing efficiency of the transduced cells. For the RPMI-2650 cells treated with DMCocE, the cocaine degradation rate is similar to the cells treated with merely enzyme vehicle (PBS), indicating no DMCocE entering the cells or attaching to the cellular surface after post-incubation wash. For the RPMI-2650 cells transduced with Tat-CocEs, however, they become capable of hydrolyzing cocaine, and their cocaine-hydrolyzing activity is proportional to the enzyme incubation concentration. Moreover, compared with the cells transduced with Tat-C-DMCocE, the cells transduced with DMCocE-C-Tat degrade cocaine faster in the first 0.5 hour but slower afterwards. After reacting for 1.5 hours, regardless of the enzyme concentration, the remaining cocaine levels in the groups treated with DMCocE-C-Tat are all higher relative to the groups treated with Tat-N-DMCocE. Since Tat-N-DMCocE is more stable than C-Tat-DMCocE (the $t_{1/2}$ at 37 °C is 5.76 hr and 1.66 hr, respectively; see Table 6), it can be concluded that a CPP-CocE with better stability is favorable for cocaine detoxification, and this better stability can compensate for lower enzyme efficiency.

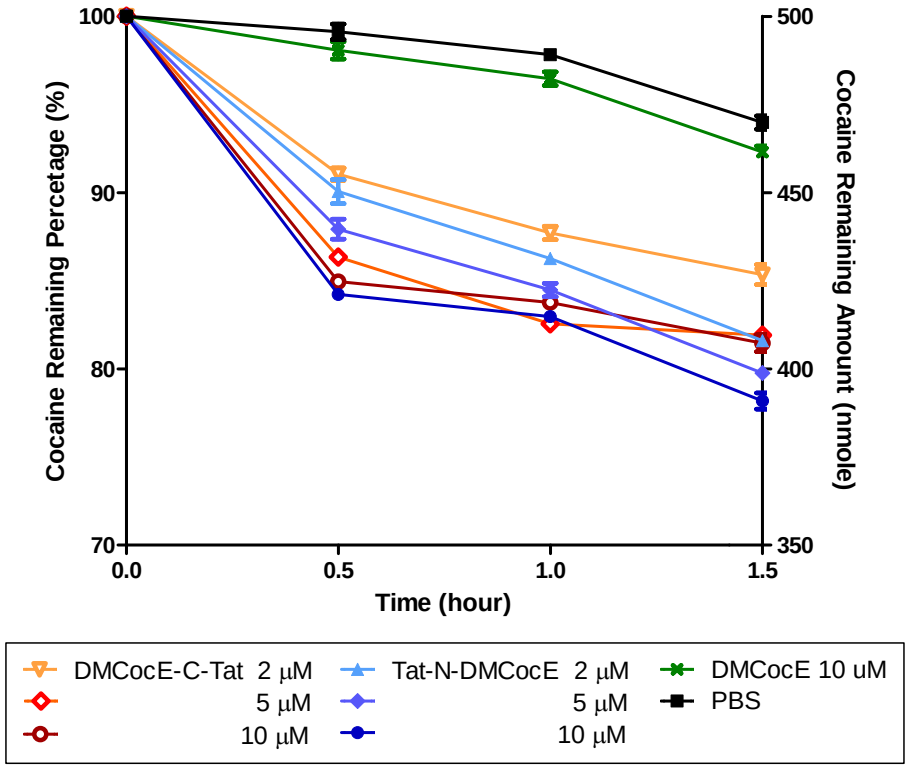

Figure 29 Degradation of cocaine in the CocE-transduced RPMI-2650 cells. When reach the density of 2.5 x 10^6 cells/cm^2, RPMI-2650 (seeded in 24-well plate) were incubated with vaired concentrations of Tat-N-DMCocE (solid blue points), DMCocE-C-Tat (hollow orange points), or 10 μM of DMCocE (green crossed points). After incubation for 2 hours at 37 C°, cells were extensively washed with 10 mg/ml heparin, and then reacted with 500 μM of cocaine in PBS (500 μl per well) at 37 C°. 100 μl aliquot per well was taken out at 0.5, 1, and 1.5 hr, and the remaining cocaine amount was determined by the absorbance at 240 nm (see Section 4.1.3). Cocaine level is presented in the percentage compared to the original concentration, as well as the calculated amount in the 500 μl solution in each well. Each point represents the mean of measurement in triplicates.

5.4 Conclusions

Similar with the results in HeLa cells and RBC (see Chapter 4), CPP-CocE were able to penetrate and accumulate in RPMI-2650 cells, and cellular uptake was also positively correlated upon incubation time and enzyme concentration. More importantly, the RPMI-2650 cells transduced with CPP-CocE became capable of hydrolyzing cocaine. In contrast, the cocaine degradation rates in the RPMI-2650 cells treated with DMCocE

was similar to the cells treated with merely enzyme vehicle (PBS). Moreover, compared with the cells transduced with Tat-C-DMCocE, the cells transduced with DMCocE-C-Tat degrade cocaine faster in the first 0.5 hour but slower afterwards. After reacting for 1.5 hours, regardless of the enzyme concentration, the remaining cocaine levels in the groups treated with DMCocE-C-Tat are all higher relative to the groups treated with Tat-N-DMCocE. Given that Tat-N-DMCocE is more stable than C-Tat-DMCocE at 37 °C (the $t_{1/2}$ at 37 °C is 5.76 hr and 1.66 hr, respectively), it can be concluded that the enzyme stability at 37 °C is also essential factor for cell transduction and encapsulation. Even with a lower enzyme efficiency, a CPP-CocE construct is still feasible for cell transduction and encapsulation, as long as it has a good *in vitro* stability at 37 °C .

CHAPTER 6
CONCLUSIONS

6.1 Summary

Two strategies, PEGylation and cell encapsulation, are employed in this dissertation to overcome the stability and immunogenicity issues of CocE. Using PEGylation or cell encapsulation, CocE can be protected from deactivation by proteases and antibodies in circulation, and therefore extending its plasma half-life and reducing the triggered immune response.

PEGylation of CocE was successfully carried out and characterized. The PEG-CocE conjugates prepared in this study showed a purity of greater than 93.5%. Attachment of PEG to CocE apparently inhibited the binding of anti-CocE antibodies to the conjugate, as demonstrated by the ELISA assay. In addition, PEGylation yielded protection to CocE against thermal degradation and protease digestion. Furthermore, preliminary *in vivo* results suggested that, similarly to native CocE, the PEG-CocE conjugates were able to protect animals from cocaine-induced lethality.

Cell encapsulation of CocE was accomplished by creating a cell permeable form of CocE, which was achieved by linking CocE and CPP via covalent bond. Two model CPPs, Tat and LMWP, were linked to CocE through chemical conjugation or genetic recombination strategies, generating six CPP-CocE variants. All these CPP-CocE constructs possessed cocaine hydrolysis activity and cell permeability, and their *in vitro* characteristics and cellular uptake behaviors are summarized in Table 8. Among these six CPP-CocE variants, the chemical conjugate LMWP-S-S-DMCocE showed a high level of cellular internalization, homogenous cytoplasmic distribution, as well as the

highest cocaine-hydrolyzing activity. However, its low production yield (3.9 mg per batch) is needed to be further optimized. In comparison, the fusion protein DMCocE-C-Tat also showed a decent cellular internalization and homogenous cytoplasmic distribution. Although it cocaine-hydrolyzing activity ranked the second highest (lower than LWMP-S-S-DMCocE), it had the largest production yield (73 mg per batch), which was approximately 20-fold compared with LMWP-S-S-DMCocE. Another worthy-noting CPP-CocE variant is Tat-N-DMCocE, which showed the longest *in vitro* half-life (5.76 hr) compared with any known CocE variants.

Table 8 *In vitro* characteristics and cellular uptake behaviors of CPP-DMCocE variants.

	Cellular Uptake Behavior		Yield in Mass Quantity Per Batch** (mg)	% Efficiency Compared with DMCocE	*In Vitro* $t_{1/2}$ at 37 ^{o}C (hr)
	Uptake Level	Cytoplasmic Distribution			
Chemical Protein Conjugates					
Tat-S-S-DMCocE	√	Condensed	1.1	n/a	n/a
LMWP-S-S-DMCocE	√√	Homogenous	3.9	77-85	n/a
Recombinant Fusion Proteins					
Tat-N-DMCocE	√	Condensed	32.7	53	5.76
LMWP-N-DMCocE	√	Condensed	10.3	45	4.83
DMCocE-C-Tat	√√	Homogenous	73.3	50	1.66
DMCocE-C-LMWP	√√	Homogenous	7.3	49	2.98

*Assessed by the intracellular fluorescence intensity after FITC labeling.

** Based on current facility in our lab.

By using DMCocE-C-Tat and Tat-N-DMCocE as models, CPP-mediated internalization was found to be dependent upon incubation time and concentration. Similar cellular internalization behaviors were also observed in the RBC and nasal epithelial cells, which were used to evaluate the potential for a non-disruptive RBC

encapsulation, as well as for the epithelial-cell-involving olfactory delivery from nose to the CNS, of CPP-DMCocE variants. Moreover, the nasal epithelial cells transduced with CPP-DMCocEs showed the ability to hydrolyze cocaine, indicating that the internalized CPP-DMCocE maintains its enzymatic activity.

Overall, this dissertation research provides the evidence that PEGylation may serve as a tool to prolong CocE functionality in the circulation and reduce its potential immunogenicity. Also, this research demonstrates that the attachment of CPP groups enables CocE to be cell permeable and meanwhile maintains CocE's enzymatic activity. More importantly, as the first research to systemically compare the *in vitro* properties of different CPP-protein variants, this dissertation also provides some interesting observations about how the CPP attachment could influence the cellular uptake extent and phenotype of CPP-protein constructs. These observations would not be only useful for developing other new CPP-CocE constructs, but also valuable for modifying other therapeutic proteins and making them cell permeable by CPP attachment.

6.2 Future Studies

Based on the promising results of preliminary *in vivo* results, further investigations of the efficacy and safety of PEGylated CocE in animal models are currently proceeding in our laboratory, with the goal of bringing this project to a successful clinical translation. Regarding the future studies for CPP-CocE variants, a more comprehensive comparison to address different ways in CPP attachment, *i.e.* different numbers, location, and orientations of CPP groups, would provide insightful information of the CPP-mediated intracellular delivery for CocE. Furthermore, for further development of CPP-CocE variants, complete in vitro characterizations, as well as preliminary in vivo studies of cell encapsulation or nasal delivery, are essential to evaluate their possibilities in clinical applications.

BIBLIOGRAPHY

1. United Nations Office on Drugs and Crime (UNODC). World Drug Report 2010. 2010.
2. Substance Abuse and Mental Health Services Administration. Results from the 2009 National Survey on Drug Use and Health: Volume I. Summary of National Findings. Rockville, MD: Office of Applied Studies, U.S. Department of Health and Human Services; 2010.
3. Boghdadi MS, Henning RJ. Cocaine: pathophysiology and clinical toxicology. Heart Lung. 1997;26(6):466-83
4. O'Brian C. Drug Addiction and Drug Abuse. In: Hardman JG, Limbird LE, Gilman AG, editors. Goodman & Gilman's The Pharmacological Basis of Therapeutics. 10 ed: McGraw-Hill Professional; 2001. p. 621-42.
5. Knuepfer MM. Cardiovascular disorders associated with cocaine use: myths and truths. Pharmacol Ther. 2003;97(3):181-222
6. Substance Abuse and Mental Health Services Administration. Drug Abuse Warning Network, 2007: National Estimates of Drug-Related Emergency Department Visits. Rockville, MD: Office of Applied Studies, U.S. Department of Health and Human Services; 2010.
7. Jupp B, Lawrence AJ. New horizons for therapeutics in drug and alcohol abuse. Pharmacology & Therapeutics. 2010;125(1):138-68
8. Gorelick DA, Gardner EL, Xi ZX. Agents in development for the management of cocaine abuse. Drugs. 2004;64(14):1547-73
9. Mattes CE, Lynch TJ, Singh A, Bradley RM, Kellaris PA, Brady RO, et al. Therapeutic use of butyrylcholinesterase for cocaine intoxication. Toxicol Appl Pharmacol. 1997;145(2):372-80
10. Cooper ZD, Narasimhan D, Sunahara RK, Mierzejewski P, Jutkiewicz EM, Larsen NA, et al. Rapid and Robust Protection against Cocaine-Induced Lethality in Rats by the Bacterial Cocaine Esterase. Molecular Pharmacology. 2006;70(6):1885-91
11. Bresler MM, Rosser SJ, Basran A, Bruce NC. Gene cloning and nucleotide sequencing and properties of a cocaine esterase from Rhodococcus sp. strain MB1. Appl Environ Microbiol. 2000;66(3):904-8
12. Larsen NA, Turner JM, Stevens J, Rosser SJ, Basran A, Lerner RA, et al. Crystal structure of a bacterial cocaine esterase. Nat Struct Biol. 2002;9(1):17-21
13. Turner JM, Larsen NA, Basran A, Barbas CF, 3rd, Bruce NC, Wilson IA, et al. Biochemical characterization and structural analysis of a highly proficient cocaine esterase. Biochemistry. 2002;41(41):12297-307
14. Inaba T. Cocaine: pharmacokinetics and biotransformation in man. Can J Physiol Pharmacol. 1989;67(9):1154-7
15. Pindel EV, Kedishvili NY, Abraham TL, Brzezinski MR, Zhang J, Dean RA, et al. Purification and cloning of a broad substrate specificity human liver carboxylesterase that catalyzes the hydrolysis of cocaine and heroin. J Biol Chem. 1997;272(23):14769-75
16. Sun H, Pang YP, Lockridge O, Brimijoin S. Re-engineering butyrylcholinesterase as a cocaine hydrolase. Mol Pharmacol. 2002;62(2):220-4

17. Landry DW, Zhao K, Yang GX, Glickman M, Georgiadis TM. Antibody-catalyzed degradation of cocaine. Science. 1993;259(5103):1899-901
18. Ko MC, Bowen LD, Narasimhan D, Berlin AA, Lukacs NW, Sunahara RK, et al. Cocaine Esterase: Interactions with Cocaine and Immune Responses in Mice. Journal of Pharmacology and Experimental Therapeutics. 2006;320(2):926-33
19. Jutkiewicz EM, Baladi MG, Cooper ZD, Narasimhan D, Sunahara RK, Woods JH. A Bacterial Cocaine Esterase Protects Against Cocaine-Induced Epileptogenic Activity and Lethality. Ann Emerg Med. 2009;54(3):409-20
20. Wood SK, Narasimhan D, Cooper Z, Sunahara RK, Woods JH. Prevention and reversal by cocaine esterase of cocaine-induced cardiovascular effects in rats. Drug and Alcohol Dependence. 2010;106(2-3):219-29
21. Gao D, Narasimhan DL, Macdonald J, Brim R, Ko MC, Landry DW, et al. Thermostable Variants of Cocaine Esterase for Long-Time Protection against Cocaine Toxicity. Mol Pharmacol. 2008;75(2):318-23
22. Brim RL, Nance MR, Youngstrom DW, Narasimhan D, Zhan CG, Tesmer JJG, et al. A Thermally Stable Form of Bacterial Cocaine Esterase: A Potential Therapeutic Agent for Treatment of Cocaine Abuse. Molecular Pharmacology. 2010;77(4):593-600
23. Caliceti P, Veronese FM. Pharmacokinetic and biodistribution properties of poly(ethylene glycol)-protein conjugates. Adv Drug Deliv Rev. 2003;55(10):1261-77
24. Harris JM, Chess RB. Effect of pegylation on pharmaceuticals. Nature Reviews Drug Discovery. 2003;2(3):214-21
25. Lipinski CA, Lombardo F, Dominy BW, Feeney PJ. Experimental and computational approaches to estimate solubility and permeability in drug discovery and development settings. Adv Drug Deliv Rev. 2001;46(1-3):3-26
26. Zorko M, Langel U. Cell-penetrating peptides: mechanism and kinetics of cargo delivery. Advanced Drug Delivery Reviews. 2005;57(4):529-45
27. Rousselle C, Clair P, Lefauconnier JM, Kaczorek M, Scherrmann JM, Temsamani J. New advances in the transport of doxorubicin through the blood-brain barrier by a peptide vector-mediated strategy. Mol Pharmacol. 2000;57(4):679-86
28. Lindgren M, Rosenthal-Aizman K, Saar K, Eiriksdottir E, Jiang Y, Sassian M, et al. Overcoming methotrexate resistance in breast cancer tumour cells by the use of a new cell-penetrating peptide. Biochem Pharmacol. 2006;71(4):416-25
29. Fawell S, Seery J, Daikh Y, Moore C, Chen LL, Pepinsky B, et al. Tat-mediated delivery of heterologous proteins into cells. Proc Natl Acad Sci U S A. 1994;91(2):664-8
30. Liang JF, Yang VC. Insulin-cell penetrating peptide hybrids with improved intestinal absorption efficiency. Biochem Biophys Res Commun. 2005;335(3):734-8
31. Rothbard JB, Garlington S, Lin Q, Kirschberg T, Kreider E, McGrane PL, et al. Conjugation of arginine oligomers to cyclosporin A facilitates topical delivery and inhibition of inflammation. Nat Med. 2000;6(11):1253-7
32. Fulda S, Wick W, Weller M, Debatin KM. Smac agonists sensitize for Apo2L/TRAIL- or anticancer drug-induced apoptosis and induce regression of malignant glioma in vivo. Nat Med. 2002;8(8):808-15
33. Park YS, Huang Y, Park YJ, David AE, White L, He H, et al. Specific down regulation of 3T3-L1 adipocyte differentiation by cell-permeable antisense HIF1α-oligonucleotide. J Control Release. 2010;144(1):82-90
34. Simeoni F, Morris MC, Heitz F, Divita G. Insight into the mechanism of the peptide-based gene delivery system MPG: implications for delivery of siRNA into mammalian cells. Nucleic Acids Res. 2003;31(11):2717-24
35. Ignatovich IA, Dizhe EB, Pavlotskaya AV, Akifiev BN, Burov SV, Orlov SV, et al. Complexes of plasmid DNA with basic domain 47-57 of the HIV-1 Tat protein are

transferred to mammalian cells by endocytosis-mediated pathways. J Biol Chem. 2003;278(43):42625-36
36. de la Fuente JM, Berry CC. Tat peptide as an efficient molecule to translocate gold nanoparticles into the cell nucleus. Bioconjug Chem. 2005;16(5):1176-80
37. Lewin M, Carlesso N, Tung CH, Tang XW, Cory D, Scadden DT, et al. Tat peptide-derivatized magnetic nanoparticles allow in vivo tracking and recovery of progenitor cells. Nat Biotechnol. 2000;18(4):410-4
38. Dietz GP, Bahr M. Delivery of bioactive molecules into the cell: the Trojan horse approach. Mol Cell Neurosci. 2004;27(2):85-131
39. Fonseca SB, Pereira MP, Kelley SO. Recent advances in the use of cell-penetrating peptides for medical and biological applications. Advanced Drug Delivery Reviews. 2009;61(11):953-64
40. Patel LN, Zaro JL, Shen WC. Cell penetrating peptides: intracellular pathways and pharmaceutical perspectives. Pharm Res. 2007;24(11):1977-92
41. Heitz F, Morris MC, Divita G. Twenty years of cell-penetrating peptides: from molecular mechanisms to therapeutics. Br J Pharmacol. 2009;
42. Belting M. Heparan sulfate proteoglycan as a plasma membrane carrier. Trends Biochem Sci. 2003;28(3):145-51
43. Jarver P, Mager I, Langel U. In vivo biodistribution and efficacy of peptide mediated delivery. Trends Pharmacol Sci. 2010;
44. Wadia JS, Stan RV, Dowdy SF. Transducible TAT-HA fusogenic peptide enhances escape of TAT-fusion proteins after lipid raft macropinocytosis. Nat Med. 2004;10(3):310-5
45. Guyton AG, Hall JE. Red blood cells, anemia and polycytemica. Textbook of Medical Physiology. Philadelphia: W.B. Saunders; 1996. p. 425-33.
46. Javaid JI, Dekirmenjian H, Davis JM, Schuster CR. Determination of cocaine in human urine, plasma and red blood cells by gas-liquid chromatography. J Chromatogr. 1978;152(1):105-13
47. Marsden NV, Ostling SG. Accumulation of dextran in human red cells after haemolysis. Nature. 1959;184(Suppl 10):723-4
48. Hamidi M, Tajerzadeh H. Carrier erythrocytes: an overview. Drug Deliv. 2003;10(1):9-20
49. Kravtzoff R, Desbois I, Lamagnere JP, Muh JP, Valat C, Chassaigne M, et al. Improved pharmacodynamics of L-asparaginase-loaded in human red blood cells. Eur J Clin Pharmacol. 1996;49(6):465-70
50. Beutler E, Dale GL, Guinto DE, Kuhl W. Enzyme replacement therapy in Gaucher's disease: preliminary clinical trial of a new enzyme preparation. Proc Natl Acad Sci U S A. 1977;74(10):4620-3
51. Magnani M, Laguerre M, Rossi L, Bianchi M, Ninfali P, Mangani F, et al. Acetaldehyde dehydrogenase-loaded erythrocytes as bioreactors for the removal of blood acetaldehyde. Alcohol Clin Exp Res. 1989;13(6):849
52. Muthuvel A, Rajamani R, Manikandan S, Sheeladevi R. Detoxification of formate by formate dehydrogenase-loaded erythrocytes and carbicarb in folate-deficient methanol-intoxicated rats. Clin Chim Acta. 2006;367(1-2):162-9
53. Gutierrez Millan C, Marinero ML, Castaneda AZ, Lanao JM. Drug, enzyme and peptide delivery using erythrocytes as carriers. J Control Release. 2004;95(1):27-49
54. Li YT, Yang VC, Liang JF. The use of a transduction peptide as a possible means for enzyme rod blood cell encapsulation. American Pharmaceutical Review2003. p. 22-7.
55. Kwon YM, Li YT, Liang JF, Park YJ, Chang LC, Yang VC. PTD-modified ATTEMPTS system for enhanced asparaginase therapy: a proof-of-concept investigation. J Control Release. 2008;130(3):252-8

56. Ascenzi P, Clementi E, Polticelli F. The Rhodococcus sp. cocaine esterase: a bacterial candidate for novel pharmacokinetic-based therapies for cocaine abuse. IUBMB Life. 2003;55(7):397-402
57. Rogers CJ, Mee JM, Kaufmann GF, Dickerson TJ, Janda KD. Toward cocaine esterase therapeutics. J Am Chem Soc. 2005;127(28):10016-7
58. Kim SH, Jeong JH, Lee SH, Kim SW, Park TG. PEG conjugated VEGF siRNA for anti-angiogenic gene therapy. J Control Release. 2006;116(2):123-9
59. Graham ML. Pegaspargase: a review of clinical studies. Adv Drug Deliv Rev. 2003;55(10):1293-302
60. Kozlowski A, Harris JM. Improvements in protein PEGylation: pegylated interferons for treatment of hepatitis C. J Control Release. 2001;72(1-3):217-24
61. Bailon P, Palleroni A, Schaffer CA, Spence CL, Fung WJ, Porter JE, et al. Rational design of a potent, long-lasting form of interferon: a 40 kDa branched polyethylene glycol-conjugated interferon alpha-2a for the treatment of hepatitis C. Bioconjug Chem. 2001;12(2):195-202
62. Wroblewski JJ, Wells JA, 3rd, Adamis AP, Buggage RR, Cunningham ET, Jr., Goldbaum M, et al. Pegaptanib sodium for macular edema secondary to central retinal vein occlusion. Arch Ophthalmol. 2009;127(4):374-80
63. Preclinical and phase 1A clinical evaluation of an anti-VEGF pegylated aptamer (EYE001) for the treatment of exudative age-related macular degeneration. Retina. 2002;22(2):143-52
64. Veronese FM, Pasut G. PEGylation, successful approach to drug delivery. Drug Discov Today. 2005;10(21):1451-8
65. Veronese FM. Peptide and protein PEGylation: a review of problems and solutions. Biomaterials. 2001;22(5):405-17
66. Wang JH, Tam SC, Huang H, Ouyang DY, Wang YY, Zheng YT. Site-directed PEGylation of trichosanthin retained its anti-HIV activity with reduced potency in vitro. Biochem Biophys Res Commun. 2004;317(4):965-71
67. Li W, Wang Y, Zhu X, Li M, Su Z. Preparation and characterization of PEGylated adducts of recombinant human tumor necrosis factor-alpha from Escherichia coli. J Biotechnol. 2002;92(3):251-8
68. Ramon J, Saez V, Baez R, Aldana R, Hardy E. PEGylated interferon-alpha2b: a branched 40K polyethylene glycol derivative. Pharm Res. 2005;22(8):1374-86
69. Rodriguez-Martinez JA, Rivera-Rivera I, Sola RJ, Griebenow K. Enzymatic activity and thermal stability of PEG-alpha-chymotrypsin conjugates. Biotechnol Lett. 2009;31(6):883-7
70. Rodriguez-Martinez JA, Sola RJ, Castillo B, Cintron-Colon HR, Rivera-Rivera I, Barletta G, et al. Stabilization of alpha-chymotrypsin upon PEGylation correlates with reduced structural dynamics. Biotechnol Bioeng. 2008;101(6):1142-9
71. Greenwald RB. PEG drugs: an overview. J Control Release. 2001;74(1-3):159-71
72. Choe YH, Conover CD, Wu D, Royzen M, Gervacio Y, Borowski V, et al. Anticancer drug delivery systems: multi-loaded N4-acyl poly(ethylene glycol) prodrugs of ara-C. II. Efficacy in ascites and solid tumors. J Control Release. 2002;79(1-3):55-70
73. Lee H, Jang IH, Ryu SH, Park TG. N-terminal site-specific mono-PEGylation of epidermal growth factor. Pharm Res. 2003;20(5):818-25
74. Pasut G, Canal F, Dalla Via L, Arpicco S, Veronese FM, Schiavon O. Antitumoral activity of PEG-gemcitabine prodrugs targeted by folic acid. J Control Release. 2008;127(3):239-48
75. Ko M-C, Narasimhan D, Berlin AA, Lukacs NW, Sunahara RK, Woods JH. Effects of cocaine esterase following its repeated administration with cocaine in mice. Drug and Alcohol Dependence. 2009;101(3):202-9

76. He XH, Shaw PC, Tam SC. Reducing the immunogenicity and improving the in vivo activity of trichosanthin by site-directed pegylation. Life Sci. 1999;65(4):355-68
77. Clark R, Olson K, Fuh G, Marian M, Mortensen D, Teshima G, et al. Long-acting growth hormones produced by conjugation with polyethylene glycol. J Biol Chem. 1996;271(36):21969-77
78. Cox GN, Rosendahl MS, Chlipala EA, Smith DJ, Carlson SJ, Doherty DH. A long-acting, mono-PEGylated human growth hormone analog is a potent stimulator of weight gain and bone growth in hypophysectomized rats. Endocrinology. 2007;148(4):1590-7
79. Takagi A, Yamashita N, Yoshioka T, Takaishi Y, Sano K, Yamaguchi H, et al. Enhanced pharmacological activity of recombinant human interleukin-11 (rhIL11) by chemical modification with polyethylene glycol. J Control Release. 2007;119(3):271-8
80. Youn YS, Kwon MJ, Na DH, Chae SY, Lee S, Lee KC. Improved intrapulmonary delivery of site-specific PEGylated salmon calcitonin: optimization by PEG size selection. J Control Release. 2008;125(1):68-75
81. Frankel AD, Pabo CO. Cellular uptake of the tat protein from human immunodeficiency virus. Cell. 1988;55(6):1189-93
82. Brooks H, Lebleu B, Vives E. Tat peptide-mediated cellular delivery: back to basics. Advanced Drug Delivery Reviews. 2005;57(4):559-77
83. Vives E, Brodin P, Lebleu B. A truncated HIV-1 Tat protein basic domain rapidly translocates through the plasma membrane and accumulates in the cell nucleus. J Biol Chem. 1997;272(25):16010-7
84. Noguchi H, Matsumoto S. Protein transduction technology: a novel therapeutic perspective. Acta Med Okayama. 2006;60(1):1-11
85. Hallbrink M, Floren A, Elmquist A, Pooga M, Bartfai T, Langel U. Cargo delivery kinetics of cell-penetrating peptides. Biochim Biophys Acta. 2001;1515(2):101-9
86. Schwarze SR, Ho A, Vocero-Akbani A, Dowdy SF. In vivo protein transduction: delivery of a biologically active protein into the mouse. Science. 1999;285(5433):1569-72
87. Chen L, Harrison SD. Cell-penetrating peptides in drug development: enabling intracellular targets. Biochem Soc Trans. 2007;35(Pt 4):821-5
88. Byun Y, Singh VK, Yang VC. Low molecular weight protamine: a potential nontoxic heparin antagonist. Thromb Res. 1999;94(1):53-61
89. Park YJ, Liang JF, Ko KS, Kim SW, Yang VC. Low molecular weight protamine as an efficient and nontoxic gene carrier: in vitro study. J Gene Med. 2003;5(8):700-11
90. Liang JF, Yang VC. Synthesis of doxorubicin-peptide conjugate with multidrug resistant tumor cell killing activity. Bioorg Med Chem Lett. 2005;15(22):5071-5
91. Yu F, Huang Y, Cole AJ, Yang VC. The artificial peroxidase activity of magnetic iron oxide nanoparticles and its application to glucose detection. Biomaterials. 2009;30(27):4716-22
92. Park YJ, Chang LC, Liang JF, Moon C, Chung CP, Yang VC. Nontoxic membrane translocation peptide from protamine, low molecular weight protamine (LMWP), for enhanced intracellular protein delivery: in vitro and in vivo study. Faseb J. 2005;19(11):1555-7
93. Chang LC, Lee HF, Yang Z, Yang VC. Low molecular weight protamine (LMWP) as nontoxic heparin/low molecular weight heparin antidote (I): preparation and characterization. AAPS PharmSci. 2001;3(3):E17
94. Lee LM, Chang LC, Wrobleski S, Wakefield TW, Yang VC. Low molecular weight protamine as nontoxic heparin/low molecular weight heparin antidote (III): preliminary in vivo evaluation of efficacy and toxicity using a canine model. AAPS PharmSci. 2001;3(3):E19

95. Narasimhan D, Nance MR, Gao D, Ko MC, Macdonald J, Tamburi P, et al. Structural analysis of thermostabilizing mutations of cocaine esterase. Protein Engineering Design and Selection. 2010;23(7):537-47
96. Gatley SJ. Activities of the enantiomers of cocaine and some related compounds as substrates and inhibitors of plasma butyrylcholinesterase. Biochem Pharmacol. 1991;41(8):1249-54
97. Koshland DE. The application and usefulness of the ratio k(cat)/K(M). Bioorg Chem. 2002;30(3):211-3
98. Park J-B, Kwon YM, Lee T-Y, Brim R, Ko M-C, Sunahara RK, et al. PEGylation of bacterial cocaine esterase for protection against protease digestion and immunogenicity. J Control Release. 2010;142(2):174-9
99. Kane JF. Effects of rare codon clusters on high-level expression of heterologous proteins in Escherichia coli. Curr Opin Biotechnol. 1995;6(5):494-500
100. Sorensen H, Mortensen K. Advanced genetic strategies for recombinant protein expression in. Journal of Biotechnology. 2005;115(2):113-28
101. Terpe K. Overview of bacterial expression systems for heterologous protein production: from molecular and biochemical fundamentals to commercial systems. Applied Microbiology and Biotechnology. 2006;72(2):211-22
102. Goldman E, Rosenberg AH, Zubay G, Studier FW. Consecutive low-usage leucine codons block translation only when near the 5' end of a message in Escherichia coli. J Mol Biol. 1995;245(5):467-73
103. Becker-Hapak M, Dowdy S. Protein transduction: generation of full-length transducible proteins using the TAT system. Current Protocols in Cell Biology2003. p. 20.2.01-25.
104. Richard JP, Melikov K, Vives E, Ramos C, Verbeure B, Gait MJ, et al. Cell-penetrating peptides. A reevaluation of the mechanism of cellular uptake. J Biol Chem. 2003;278(1):585-90
105. Duchardt F, Fotin-Mleczek M, Schwarz H, Fischer R, Brock R. A Comprehensive Model for the Cellular Uptake of Cationic Cell-penetrating Peptides. Traffic. 2007;8(7):848-66
106. Zhang X, Jin Y, Plummer M, Pooyan S, Gunaseelan S, Sinko P. Endocytosis and membrane potential are required for HeLa cell uptake of R.I.-CKTat9, a retro inverso Tat cell penetrating peptide. Mol Pharm. 2009;
107. Rothe R, Liguori L, Villegas-Mendez A, Marques B, Grunwald D, Drouet E, et al. Characterization of the Cell-penetrating Properties of the Epstein-Barr Virus ZEBRA trans-Activator. Journal of Biological Chemistry. 2010;285(26):20224-33
108. Ziegler A, Seelig J. High affinity of the cell-penetrating peptide HIV-1 Tat-PTD for DNA. Biochemistry. 2007;46(27):8138-45
109. Kharidia R, Friedman KA, Liang JF. Improved gene expression using low molecular weight peptides produced from protamine sulfate. Biochemistry (Mosc). 2008;73(10):1162-8
110. Lo SL, Wang S. An endosomolytic Tat peptide produced by incorporation of histidine and cysteine residues as a nonviral vector for DNA transfection. Biomaterials. 2008;29(15):2408-14
111. Booze RM, Lehner AF, Wallace DR, Welch MA, Mactutus CF. Dose-response cocaine pharmacokinetics and metabolite profile following intravenous administration and arterial sampling in unanesthetized, freely moving male rats. Neurotoxicol Teratol. 1997;19(1):7-15
112. Benuck M, Lajtha A, Reith ME. Pharmacokinetics of systemically administered cocaine and locomotor stimulation in mice. J Pharmacol Exp Ther. 1987;243(1):144-9
113. Ma F, Falk JL, Lau CE. Cocaine pharmacodynamics after intravenous and oral administration in rats: relation to pharmacokinetics. Psychopharmacology. 1999;144(4):323-32

114. Loike JD, Silverstein SC. A fluorescence quenching technique using trypan blue to differentiate between attached and ingested glutaraldehyde-fixed red blood cells in phagocytosing murine macrophages. J Immunol Methods. 1983;57(1-3):373-9
115. Alberts B. Molecular biology of the cell. 4th ed. New York: Garland Science; 2002.
116. Pardridge WM. The blood-brain barrier: bottleneck in brain drug development. NeuroRx. 2005;2(1):3-14
117. Cao G, Pei W, Ge H, Liang Q, Luo Y, Sharp FR, et al. In Vivo Delivery of a Bcl-xL Fusion Protein Containing the TAT Protein Transduction Domain Protects against Ischemic Brain Injury and Neuronal Apoptosis. J Neurosci. 2002;22(13):5423-31
118. Bright R, Steinberg GK, Mochly-Rosen D. DeltaPKC mediates microcerebrovascular dysfunction in acute ischemia and in chronic hypertensive stress in vivo. Brain Res. 2007;1144:146-55
119. Choi HS, Lee SH, Kim SY, An JJ, Hwang SI, Kim DW, et al. Transduced Tat-alpha-synuclein protects against oxidative stress in vitro and in vivo. J Biochem Mol Biol. 2006;39(3):253-62
120. Illum L. Is nose-to-brain transport of drugs in man a reality? J Pharm Pharmacol. 2004;56(1):3-17
121. Gozes I, Bardea A, Reshef A, Zamostiano R, Zhukovsky S, Rubinraut S, et al. Neuroprotective strategy for Alzheimer disease: intranasal administration of a fatty neuropeptide. Proc Natl Acad Sci U S A. 1996;93(1):427-32
122. Gizurarson S, Thorvaldsson T, Sigurdsson P, Gunnarsson E. Selective delivery of insulin into the brain: Intraolfactory absorption. International Journal of Pharmaceutics. 1996;140(1):77-83
123. Thorne RG, Frey WH, 2nd. Delivery of neurotrophic factors to the central nervous system: pharmacokinetic considerations. Clin Pharmacokinet. 2001;40(12):907-46
124. Shipley MT, Halloran FJ, de la Torre J. Surprisingly rich projection from locus coeruleus to the olfactory bulb in the rat. Brain Res. 1985;329(1-2):294-9
125. Thorne RG, Emory CR, Ala TA, Frey WH, 2nd. Quantitative analysis of the olfactory pathway for drug delivery to the brain. Brain Res. 1995;692(1-2):278-82